PROPERTIES OF THE DISCRETELY STRATIFIED MICROSTRUCTURE IN THE ARCTIC OCEAN

William Clifford Barney

United States
Naval Postgraduate School

THESIS

PROPERTIES OF THE DISCRETELY STRATIFIED

MICROSTRUCTURE IN THE ARCTIC OCEAN

by

William Clifford Barney

Thesis Advisor: Warren W. Denner

September 1971

Properties of the Discretely Stratified Microstructure in the Arctic Ocean

by

William Clifford Barney
Lieutenant Commander, United States Navy
B.S., United States Naval Academy, 1963

Submitted in partial fulfillment of the
requirements for the degree of

MASTER OF SCIENCE IN OCEANOGRAPHY

from the

NAVAL POSTGRADUATE SCHOOL
September 1971

ABSTRACT

The layered microstructure in the Arctic Ocean is examined from long time-series of high-resolution temperature profiles and concurrent digital salinity data. The motion within the layers is found to be turbulent, while the flow within the interface sheets is laminar. The structure is stable for long periods of time, and is coherent for a considerable horizontal extent. It is suggested that the initial formation of the layers is due to the energy dissipation of higher modes of locally generated internal waves. The layers may be sustained for long periods by weak shear produced by geostrophic density currents. The distribution of salinity and temperature differences between layers indicates that the layers are in a state of dynamic equilibrium, the differing diffusion characteristics of heat and salt accounting for the transfer of these properties across the interface sheets.

TABLE OF CONTENTS

I. INTRODUCTION

Recent measurements reveal a stratified microstructure in the Arctic Ocean between the depths of 175 and 375 meters. The discretely layered nature of this microstructure first became evident from data collected with a high-resolution continuous temperature profiling system [Denner 1969]. In contrast to the smooth gradient inferred from classical Nansen bottle analysis, a structure was observed which consisted of layers of negligible gradient, separated by thin sheets of very high gradient (Figure 1). A similar salinity structure has become manifest from subsequent Arctic experiments [Neshyba et al 1971a].

Stratified microstructure is not a feature unique to the Arctic Ocean; there is strong evidence that it is a phenomenon common to all oceans, and that the occurrence of layering may be expected in a variety of oceanic environments. Such structure was first described by Woods and Fosberry [1966] from measurements in the summer thermocline of the Mediterranean Sea near Malta, a region in which salinity increases with depth while temperature decreases with depth. Using dye tracers it was found that the motion in the layers was weakly turbulent and three-dimensional, while the motion in the interface sheets was generally laminar with a shear in the velocity across them. It was concluded that this velocity shear, coupled with the disturbance of internal gravity waves, may induce instabilities of the Kelvin-Helmholtz type which may cause the formation of new

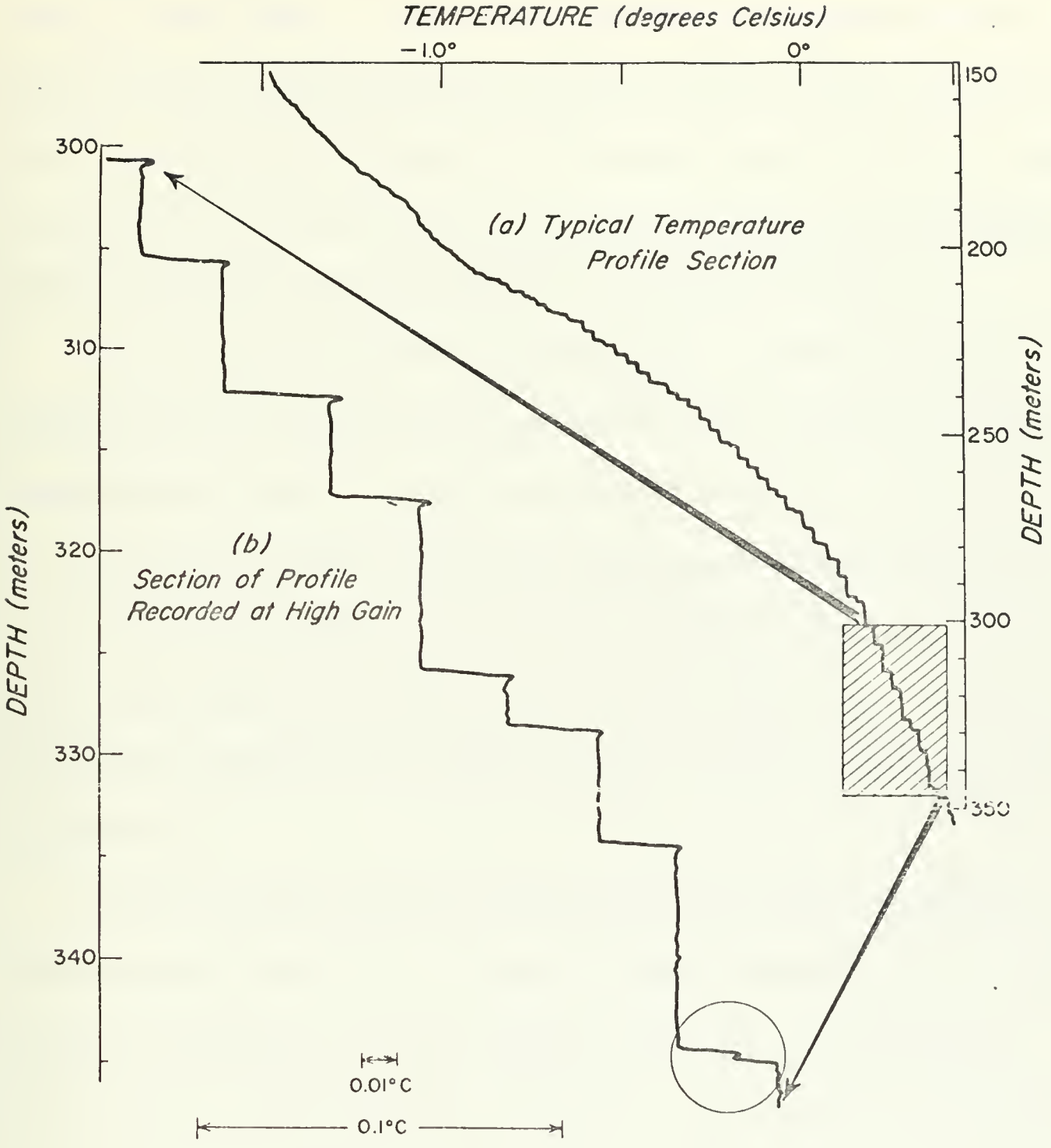

Figure 1. High-resolution temperature profile collected in March 1969 beneath the Arctic Ice Station T-3 (84-38N; 128-22W). Shaded section of profile (a) is displayed at expanded resolution in profile (b). [Denner 1969]

layers [Woods 1968] . Stratified microstructure was also identified in a similar oceanic environment beneath the mixed surface layer in the Western Pacific near Timor and Mindanao by Stommel and Fedorov [1967]. They concluded that turbulent mixing and molecular diffusion could be important mechanisms involved in the formation and sustention of layers.

High-resolution measurements obtained by Cooper and Stommel [1968] in the main thermocline of the Atlantic Ocean near Bermuda, and by Tait and Howe [1968] in the Eastern Atlantic, disclose stratification in an environment where both salinity and temperature decrease with depth. Laboratory studies by Turner [1967] have indicated that layering may occur in this environment as a result of the differing diffusion rates of heat and salt as these properties are carried downward by narrow convective cells (salt fingers).

Based on earlier laboratory experiments of the molecular diffusive characteristics of heat and salt across a density interface, Turner [1965] predicted stratification in a third oceanic environment in which both temperature and salinity increase with depth. Such a unique environment is formed by the circulation of warm, salty Atlantic water at 200-900 m beneath cold, less saline Arctic water [Coachman 1962] . It is in the upper 200 m of the Atlantic water that discrete stratification has been observed.

It is certain that the double-diffusion mechanism proposed by Turner does not completely account for the observed microstructure in the Arctic. Clearly, in a complex oceanic environment the interactions of many

processes must be examined. The purpose of this investigation is to describe the microstructure in detail, and to determine the most probable combination of mechanisms involved in its formation and sustention.

Experiments were conducted from the Arctic Ice Station T-3 (85-20N; 89-50W) in March and April 1971 with the following objectives:

(1) To determine the lifetime and spatial stability of the strata by obtaining a long time-series of temperature profiles with high-resolution temperature measuring equipment.

(2) To investigate the velocity shear across layer interfaces by measuring the current velocity within discrete layers with an experimental photographic current meter.

(3) To determine the density distribution by employing a digital-recording salinity-temperature-depth instrument (STD).

II. HIGH-RESOLUTION TEMPERATURE PROFILING

A. RECORDING SYSTEM

A modified General Motors prototype expendable bathythermograph (XBT) was used to obtain the temperature profiles. Denner et al [1971] showed that the XBT could be utilized for microstructure studies by decreasing the descent rate and increasing the amplification of the thermistor bridge null circuit to provide a temperature resolution of better than 0.002°C.

The temperature signal from the XBT thermistor was supplied to one arm of a dc Wheatstone bridge specifically designed to operate in the resistance-temperature ranges expected in the Arctic (Figure 2). The bridge was a modified version of that described by Denner et al [op. cit.], allowing greater flexibility of balancing and more convenient field calibration. The bridge was supplied with a constant 6.75 V from a Digitec model 201 dc voltmeter. The bridge input voltage was critical to stable operation and ultimate resolution since its value determined the temperature sensitivity and heat dissipation characteristics of the thermistor. The bridge output voltage was proportional to the thermistor resistance corresponding to the water temperature at the thermistor depth. This output voltage was amplified by a Preston model 8300XWB high-gain, low-noise amplifier, and the amplified signal recorded on one axis of a Honeywell model 540 X-Y plotter.

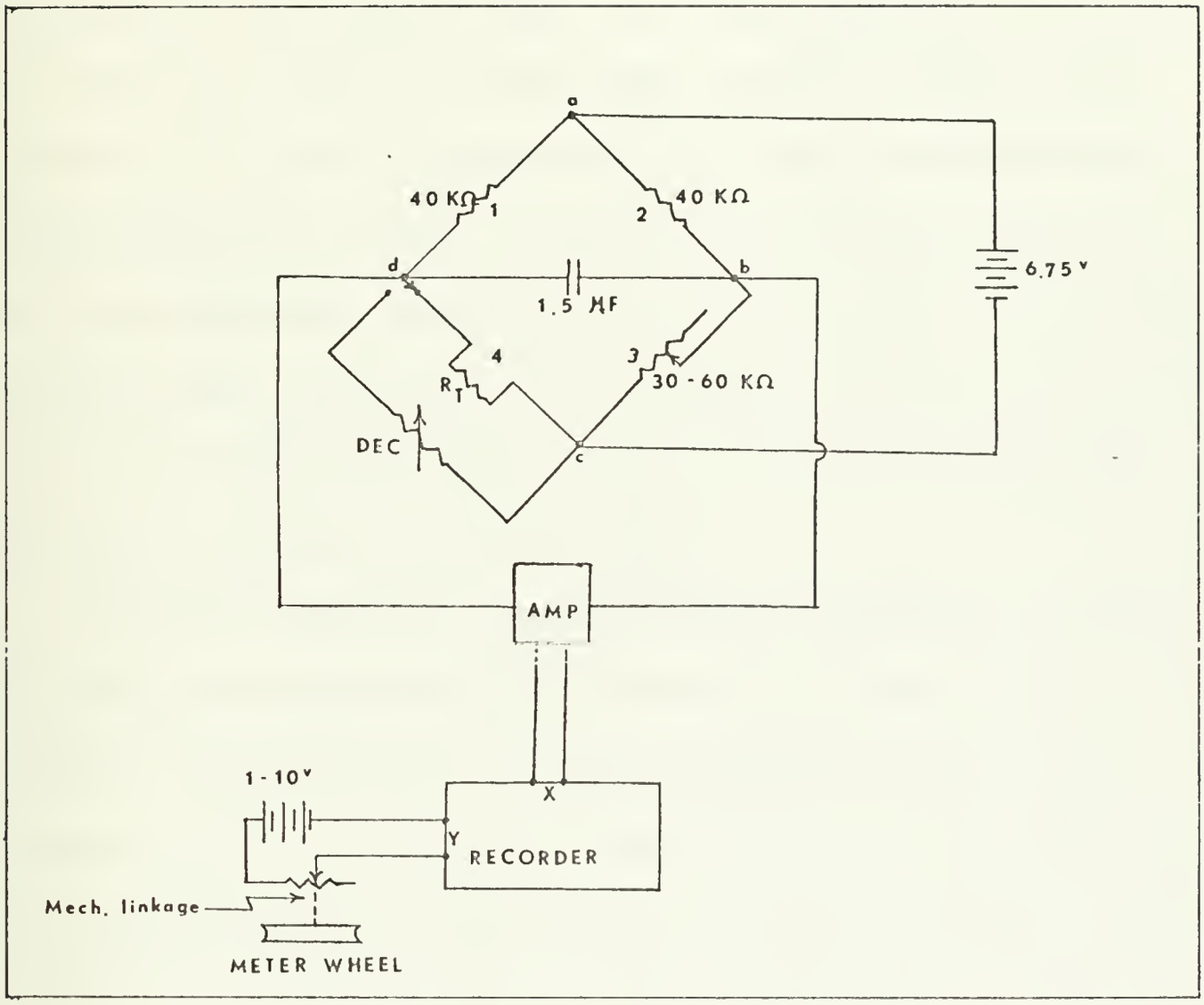

Figure 2. Thermistor resistance bridge null circuit used for Arctic measurements. All resistors are accurate to 5%, the decade box is adjustable to 1 Ω (±5%). The 1.5 μF capacitor between terminals b and d was included to eliminate instrument noise and transient electrical interference.

The depth signal, recorded on the other plotter axis, was generated by a modified hydrographic wire metering wheel (Figure 3). A recording range of 100 m/15 in was achieved by mechanically linking a ten-turn potentiometer to the tens dial of the meter wheel, supplying the potentiometer with 1.5 V, and recording the output voltage at 0.1 V/in recorder sensitivity. A narrower recording range was possible by increasing the potentiometer supply voltage. In order to avoid accidental slippage of the potentiometer shaft, the winch was stopped three meters short of full recording range. A tape mark on the hydrographic wire was aligned with a fixed surface reference mark to zero the potentiometer and recalibrate the meter wheel while the XBT was at depth.

Laboratory calibration of the equipment was conducted in a water-glycerine tank, with the temperature monitored by a quartz-crystal thermometer, accurate to .001°C. A linear calibration curve for a 2.5°C temperature range was produced by determining the thermistor resistance for each temperature from the balancing resistance of the decade box when substituted for the thermistor in arm 4 of the bridge (Figure 4). With the decade box adjusted to the resistance of the desired temperature range the field calibrations were accomplished by positioning the recorder pen at mid-scale with the bridge balance resistor (arm 3), and amplifying the bridge output voltage to achieve the maximum resolution.

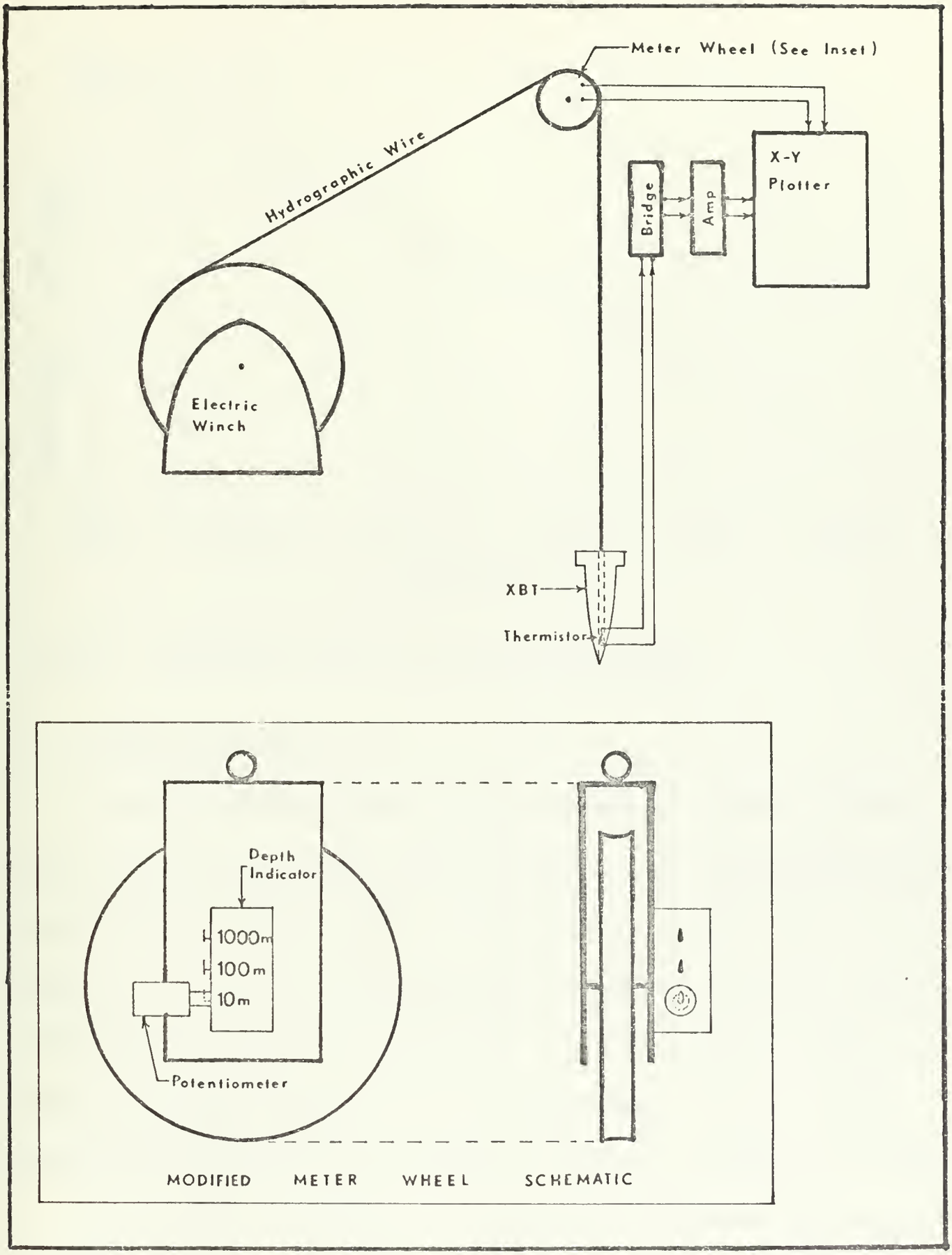

Figure 3. XBT profiling system with detail of metering wheel depth indicator.

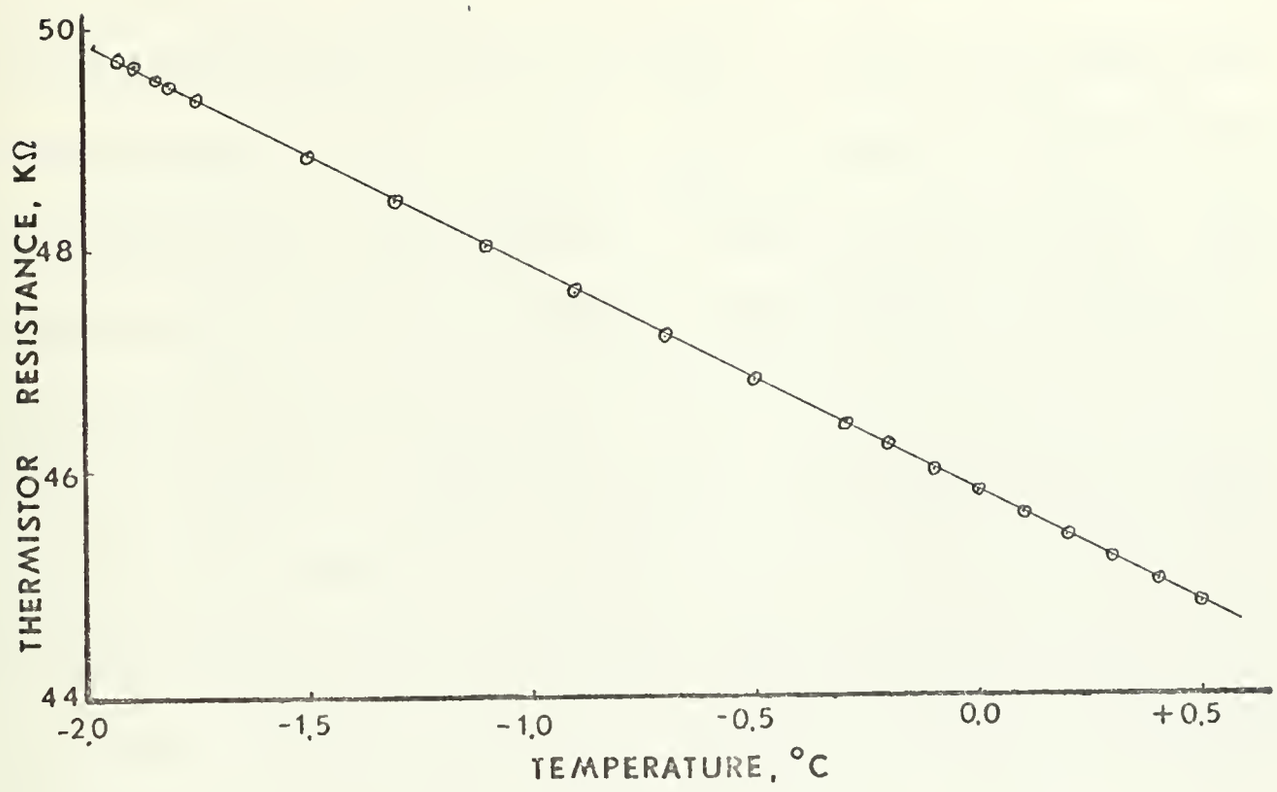

Figure 4. Calibration curve for XBT profiling system.

B. DATA COLLECTION

Several individual profiles from the surface to the core of Atlantic water at 400 m were collected from 3-5 March. Layered microstructure was well defined from 185 m to 330 m, with the best examples occurring between 200 m and 300 m. It was decided to conduct the continuous time-series within this interval. Between 200 m and 300 m the temperature increases from approximately -0.7°C to approximately +0.3°C, with the mean gradient decreasing from .025°C/m at 200 m to .006°C/m at 300 m.

For recording the profiles, the bridge null circuit was balanced at -0.2°C and the output voltage was amplified ten times, providing a temperature scale of .1475°C/in on the Y-axis (1.0°C = 6.75 in) with a resolution of .003°C. Depth was recorded at .667m/in (100 m = 15 in) at a

resolution of 20 cm. The time-series was begun at 2000 5 March and was conducted continuously until 2000 7 March. A total of 265 profiles was collected during this 48-hour period, with an average repetition rate of 5.52 profiles/hour, or approximately 11 minutes between profiles. The lowering rate was .2 m/sec, differing substantially from the 6 m/sec lowering rate for the unmodified XBT. With a sensor response time-constant of 100 msec [Denner et al 1971] the modified XBT traversed 2 cm in one time-constant compared with 60 cm for the unmodified XBT. Four XBTs were used for the experiment, thirty minutes being required for replacement. A failure of the main power supply system at T-3 interrupted the experiment for twenty minutes at 0730 7 March.

Two shorter time-series were collected immediately following the 48-hour experiment. The objectives of these measurements were to increase the recording resolution and to determine the accuracy of the recording system for positioning instruments within specific layers. The first of the short time-series was conducted during the two-hour period 2020 to 2220 7 March. Twenty-six profiles, four minutes apart, were collected within a depth interval from 245 m to 270 m. The temperature signal was recorded at .0735°C/in on the X-axis, with a resolution of .0015°C. The depth signal was recorded at 2.5 m/in on the Y-axis, with a resolution of 5 cm.

From 2235 7 March until 0015 9 March, 48 profiles were collected from the interval 252.5 m to 262.5 m, with an average of 90 seconds between profiles during the latter part of the series. The bridge output voltage was amplified 50 times, providing a temperature resolution of .0006°C.

With a potentiometer input voltage of 10 V the depth signal was recorded at 1 m/in, with a resolution of 2 cm.

C. DESCRIPTION AND ANALYSIS OF DATA

1. General Description

The high-resolution profiles obtained during the 48-hour time-series are presented in Figure 5(a-o). The discretely layered nature of the temperature microstructure is readily ascertained from these profiles. Thirty-seven layers can be consistently identified in each profile throughout the series, having an average thickness of 2.58 m with a standard deviation of 1.34 m. The largest observed layers are 6 m thick, and the smallest observed layers are only 40 cm thick, occurring at several depths. These small layers are termed "half-steps" when they occur between two large layers, and have a temperature increase of about half the total increase between the two larger layers. Half-steps occur on each profile and provide excellent reference features for correlating one profile to the next. The gradient within the layers is negligible, most of the layers appearing to be isothermal within .003°C.

Each layer is separated by a thin sheet, averaging 15 cm in thickness, across which a very high temperature gradient exists. The average temperature gradient across the interface sheets is .15°C/m which is many times larger than the mean gradient. The largest observed temperature "step" across an interface is 0.0233°C with a standard deviation of 0.0077°C.

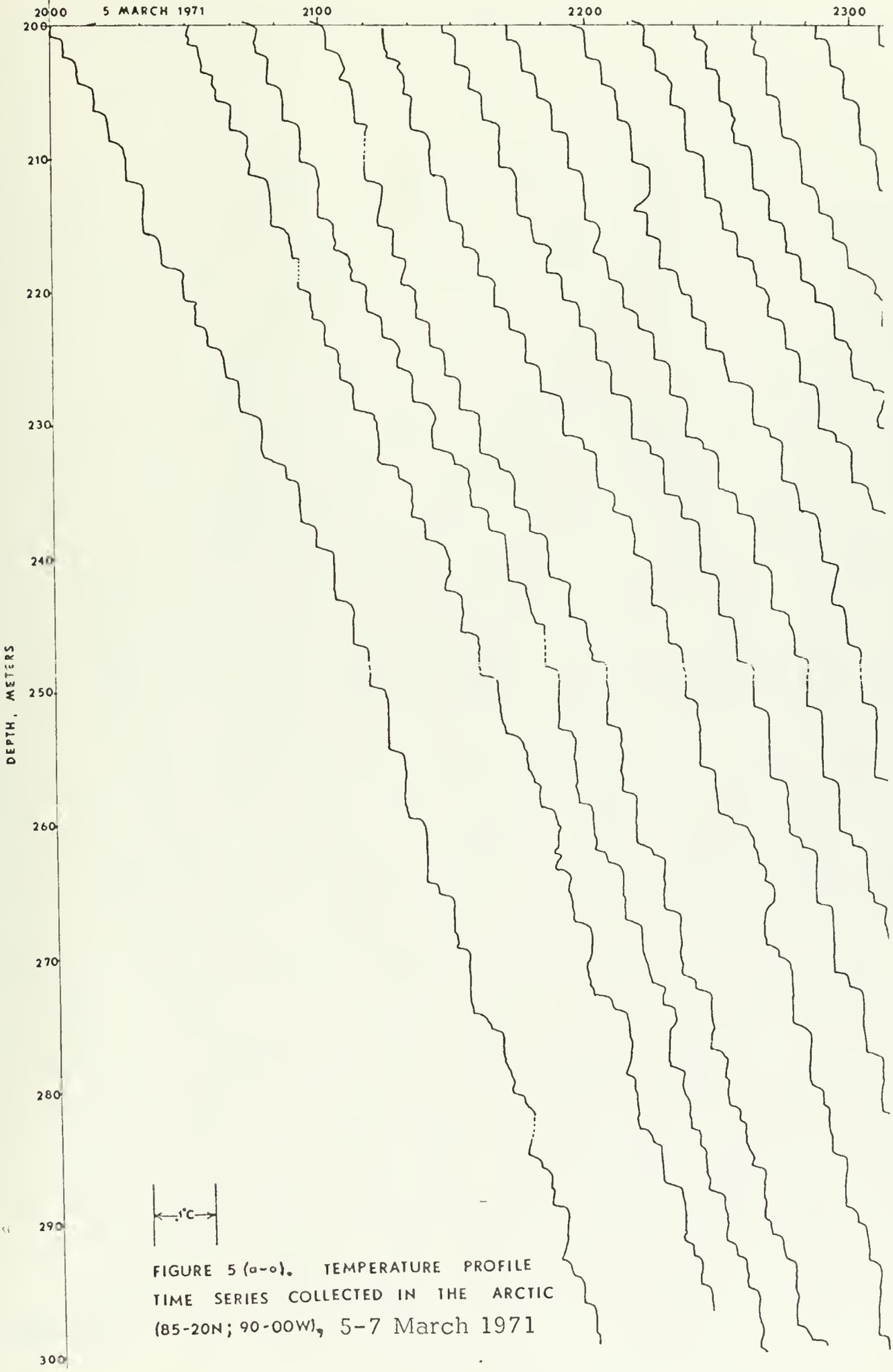

FIGURE 5 (a-o). TEMPERATURE PROFILE TIME SERIES COLLECTED IN THE ARCTIC (85-20N; 90-00W), 5-7 March 1971

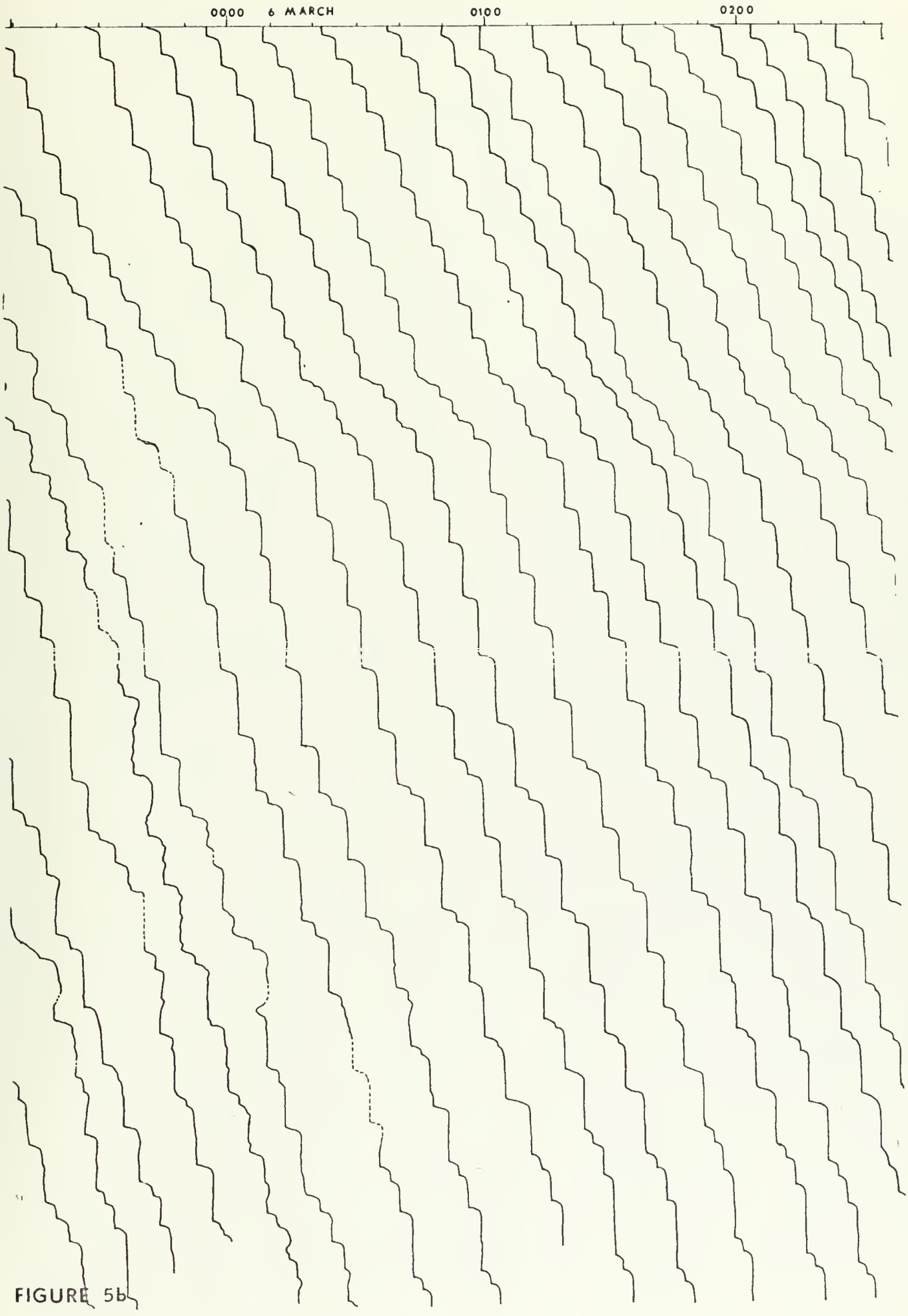

FIGURE 5b

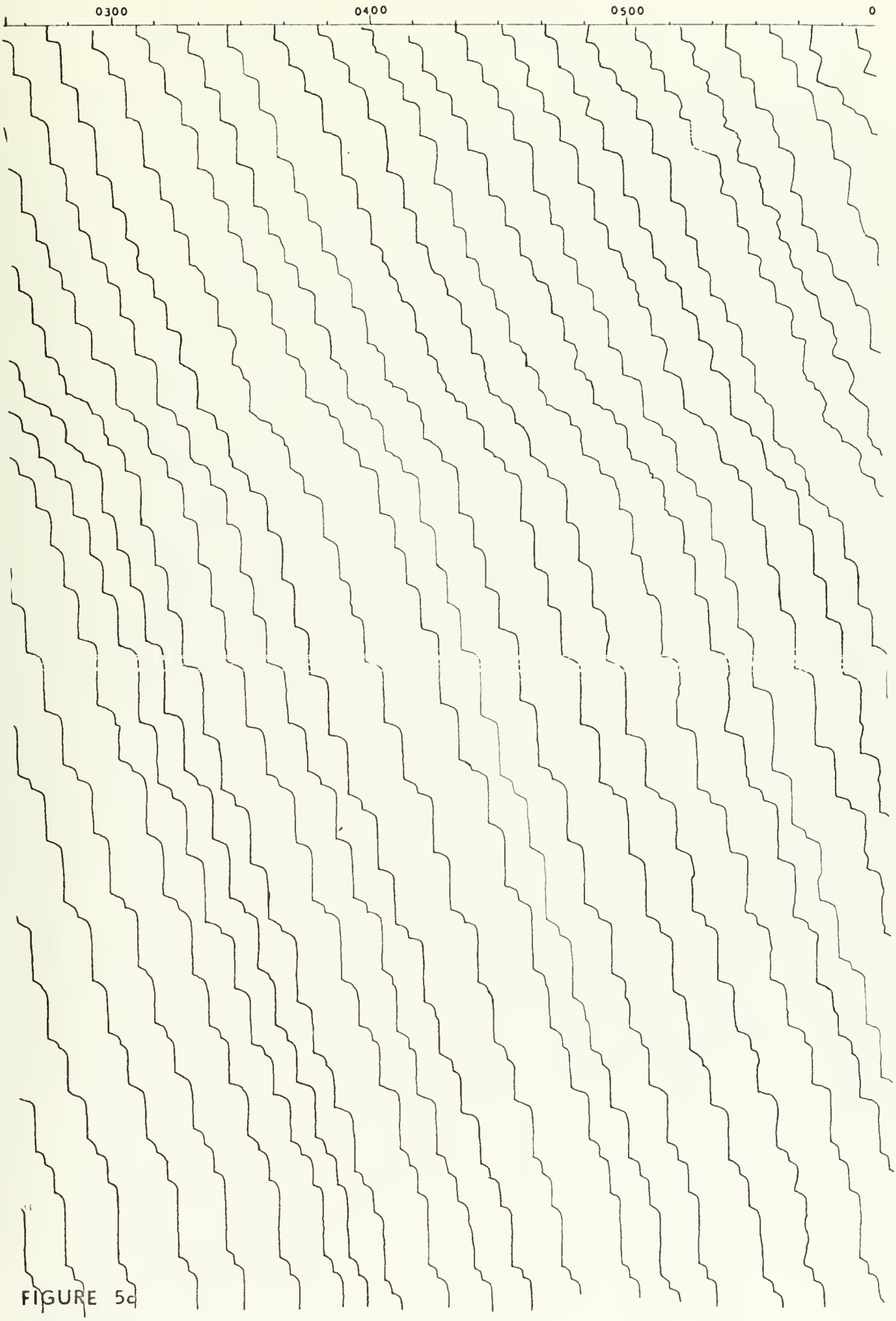

FIGURE 5c

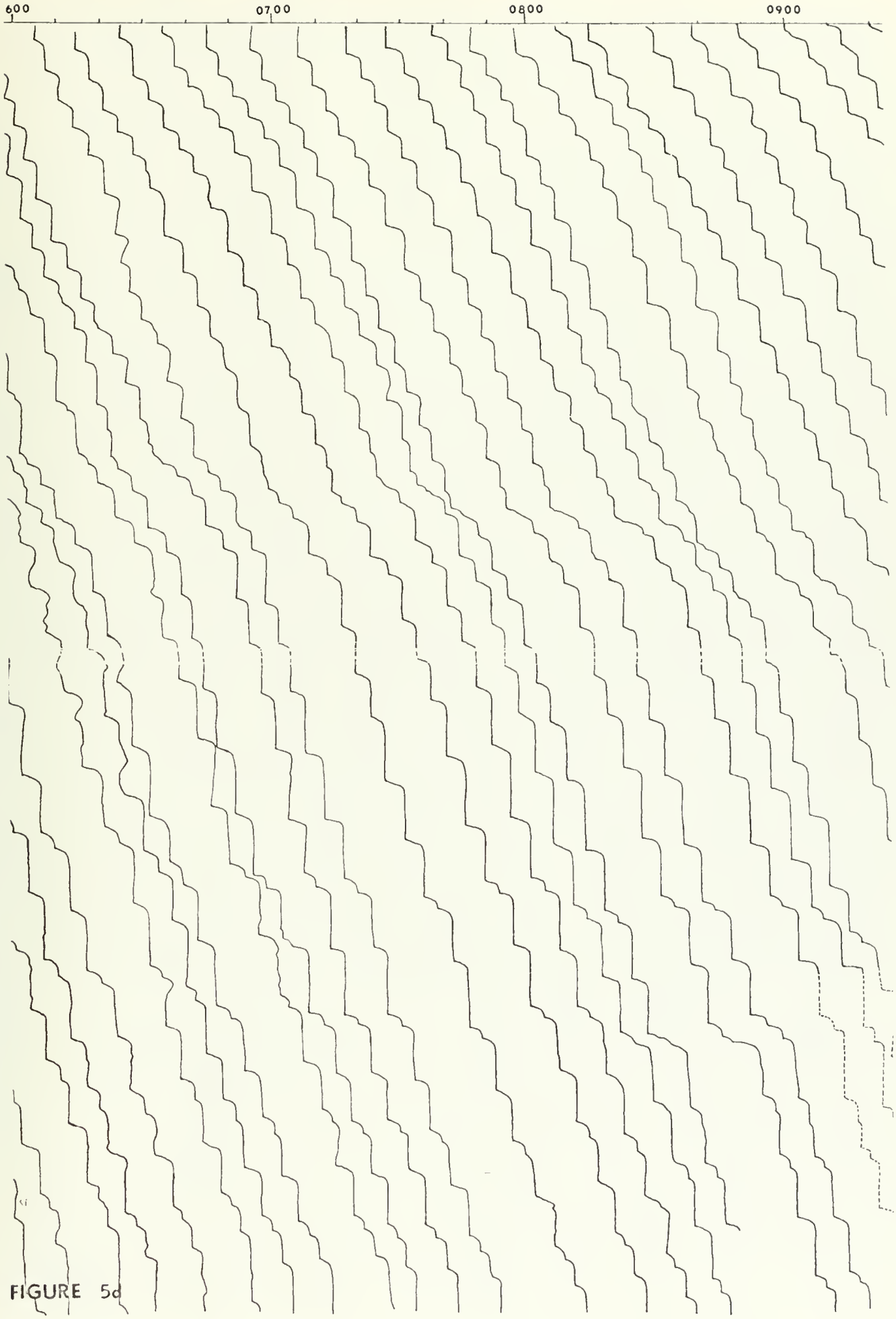

FIGURE 5d

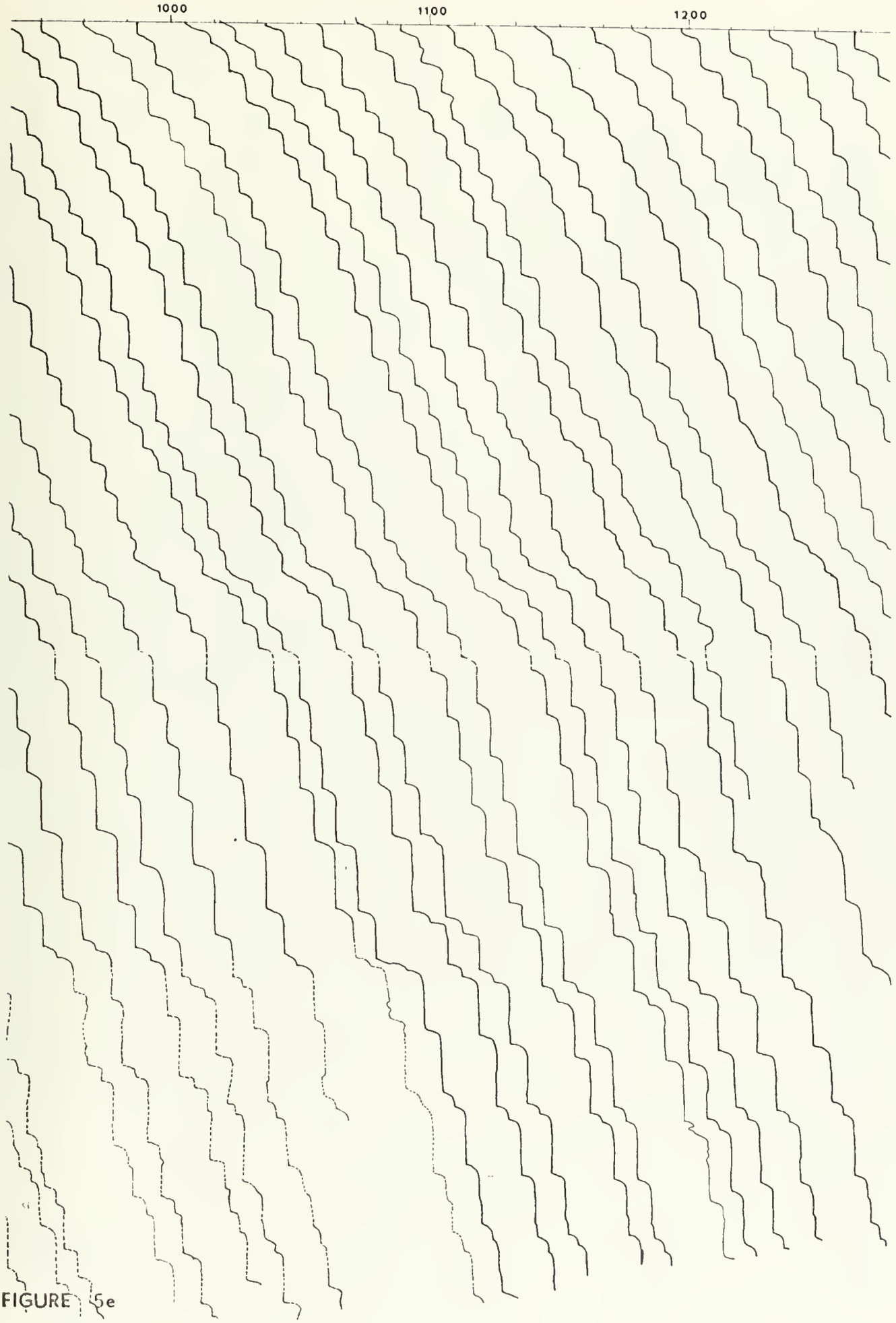

FIGURE 5e

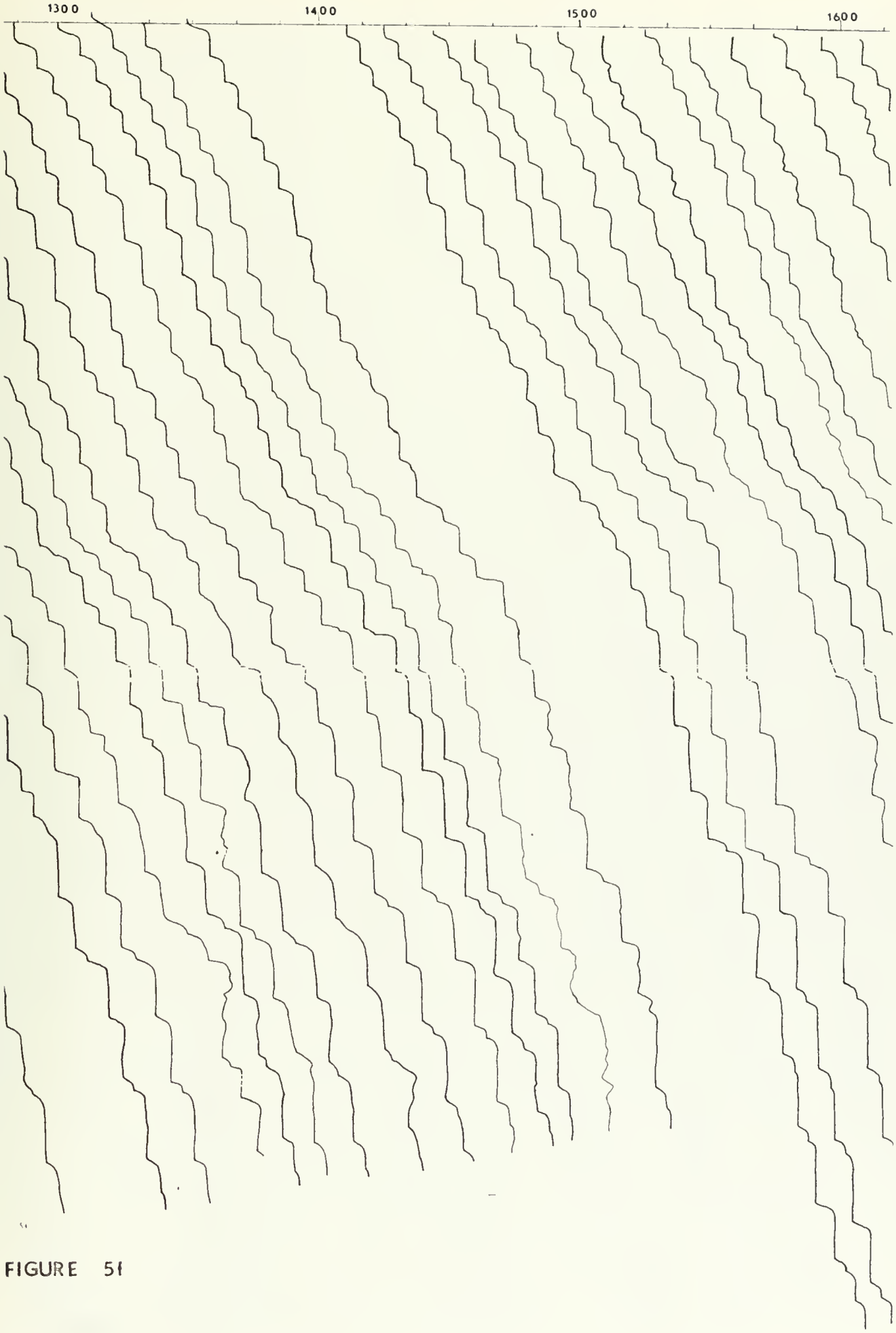

FIGURE 5f

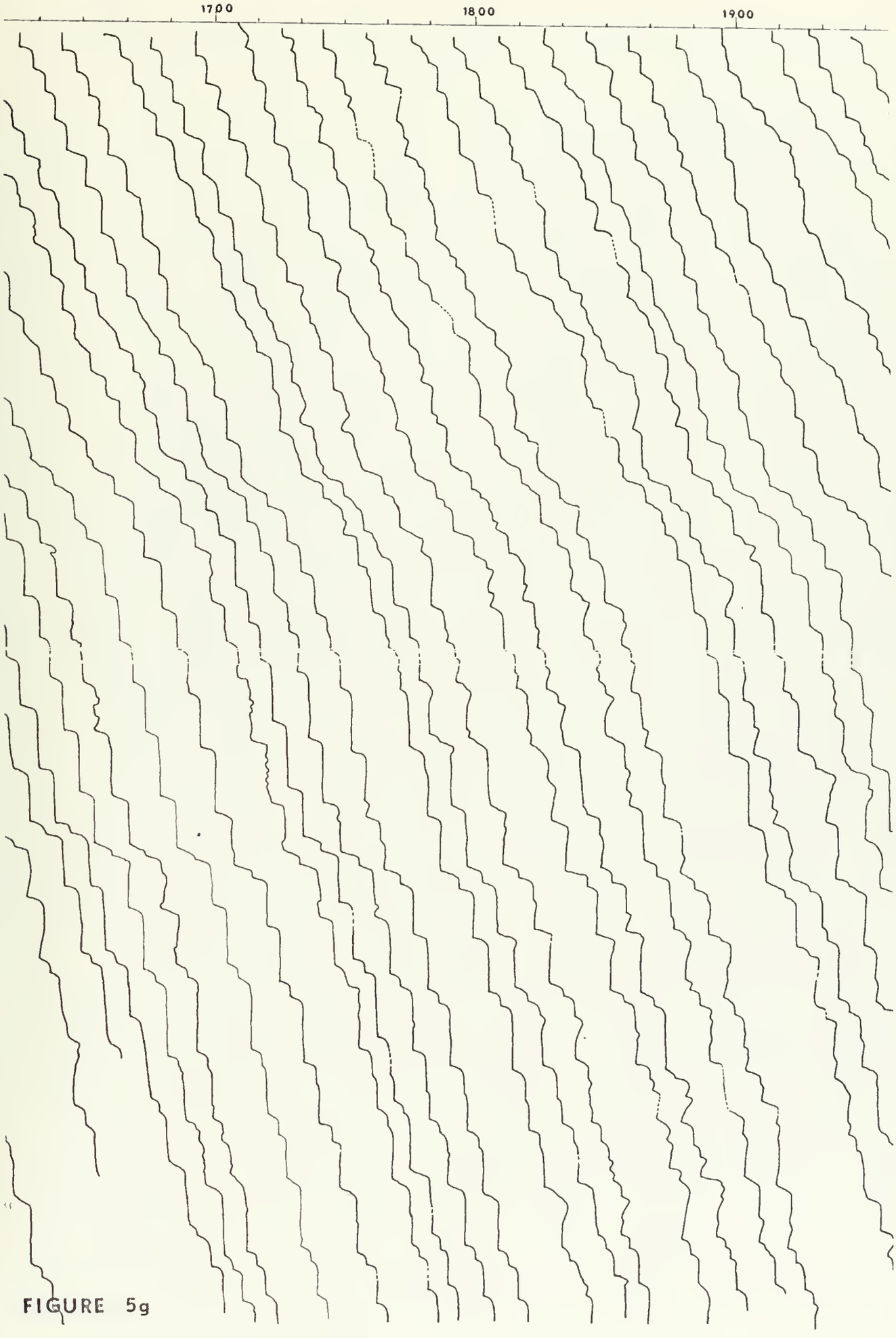

FIGURE 5g

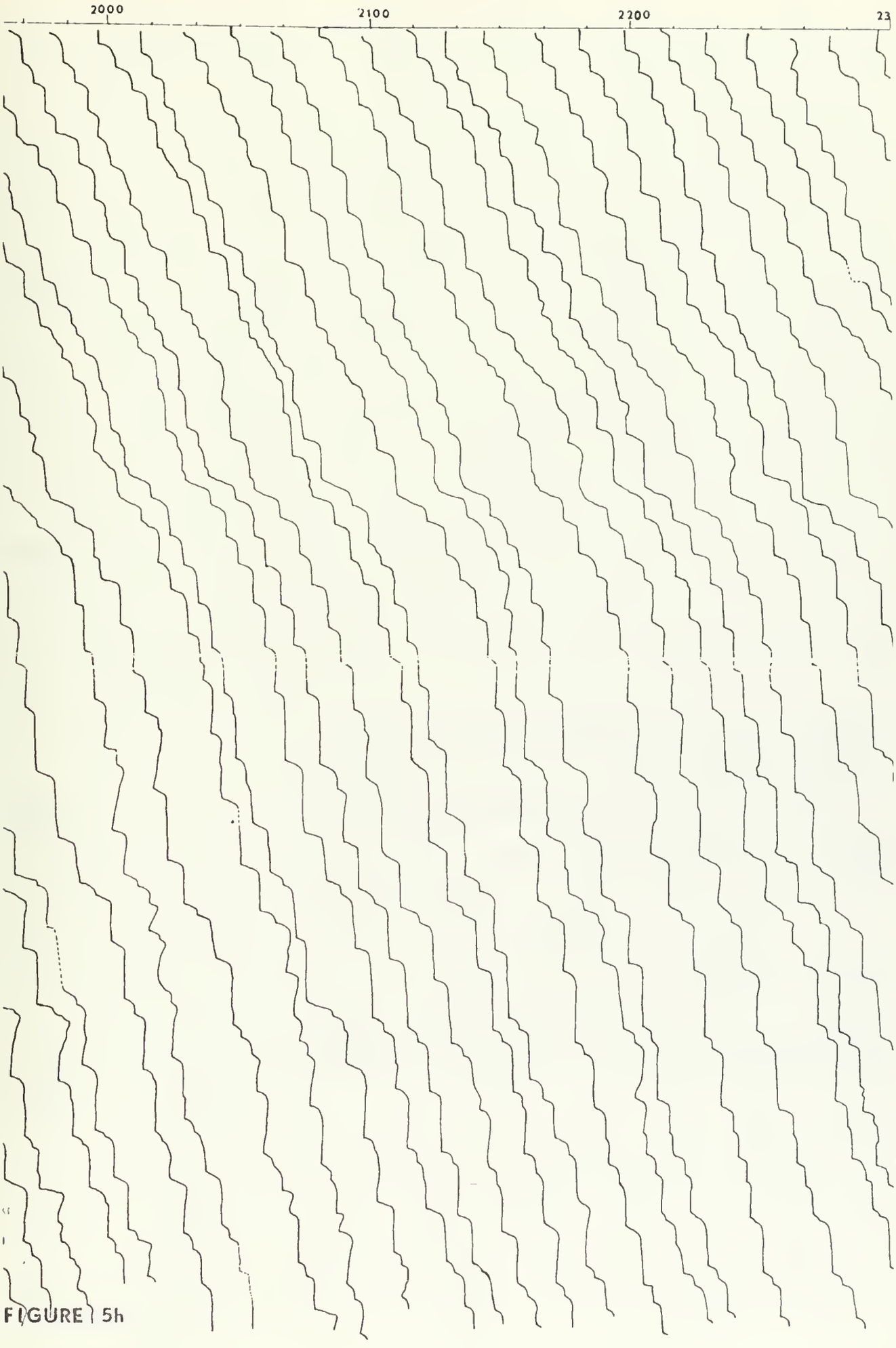

FIGURE 5h

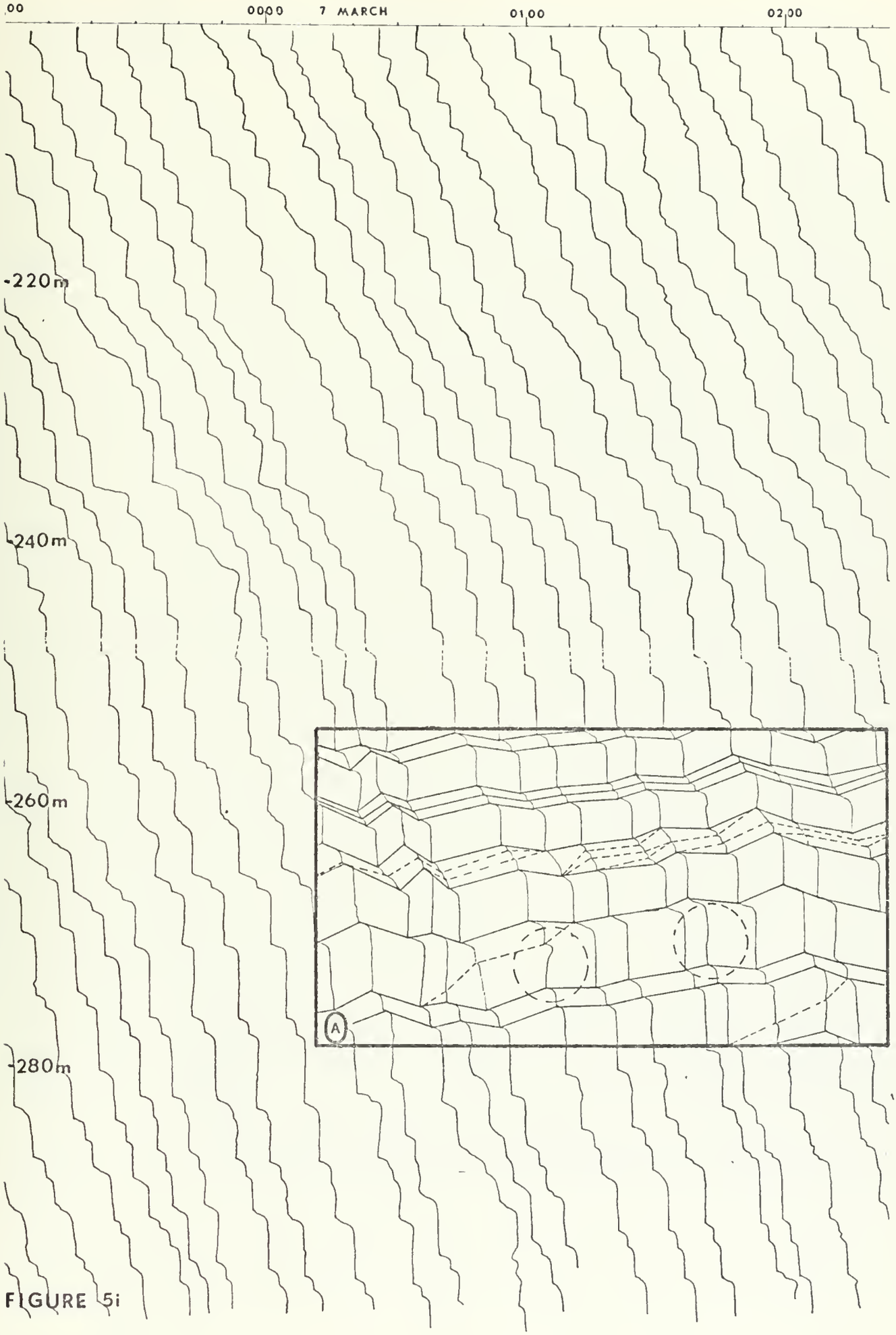

FIGURE 5i

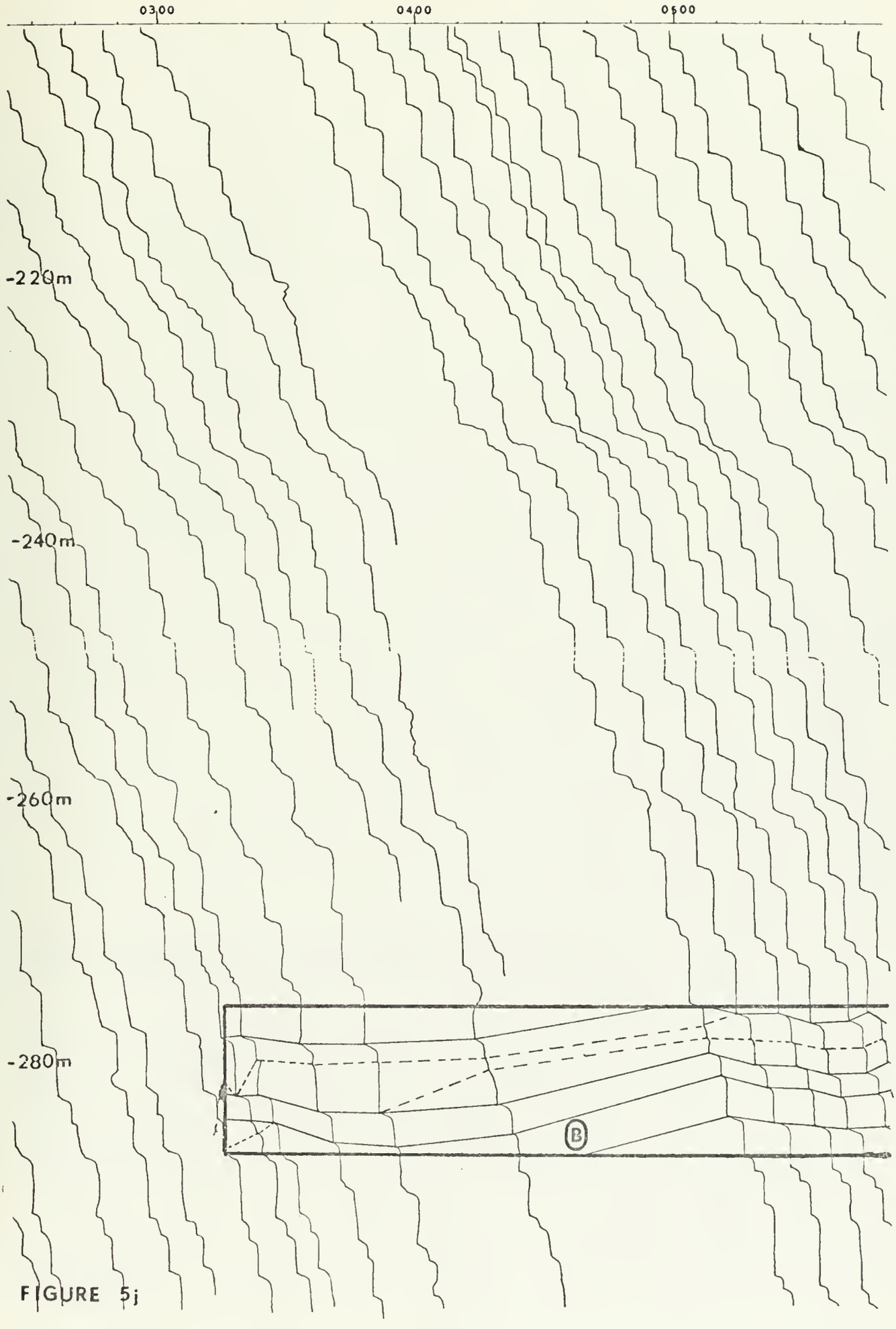

FIGURE 5j

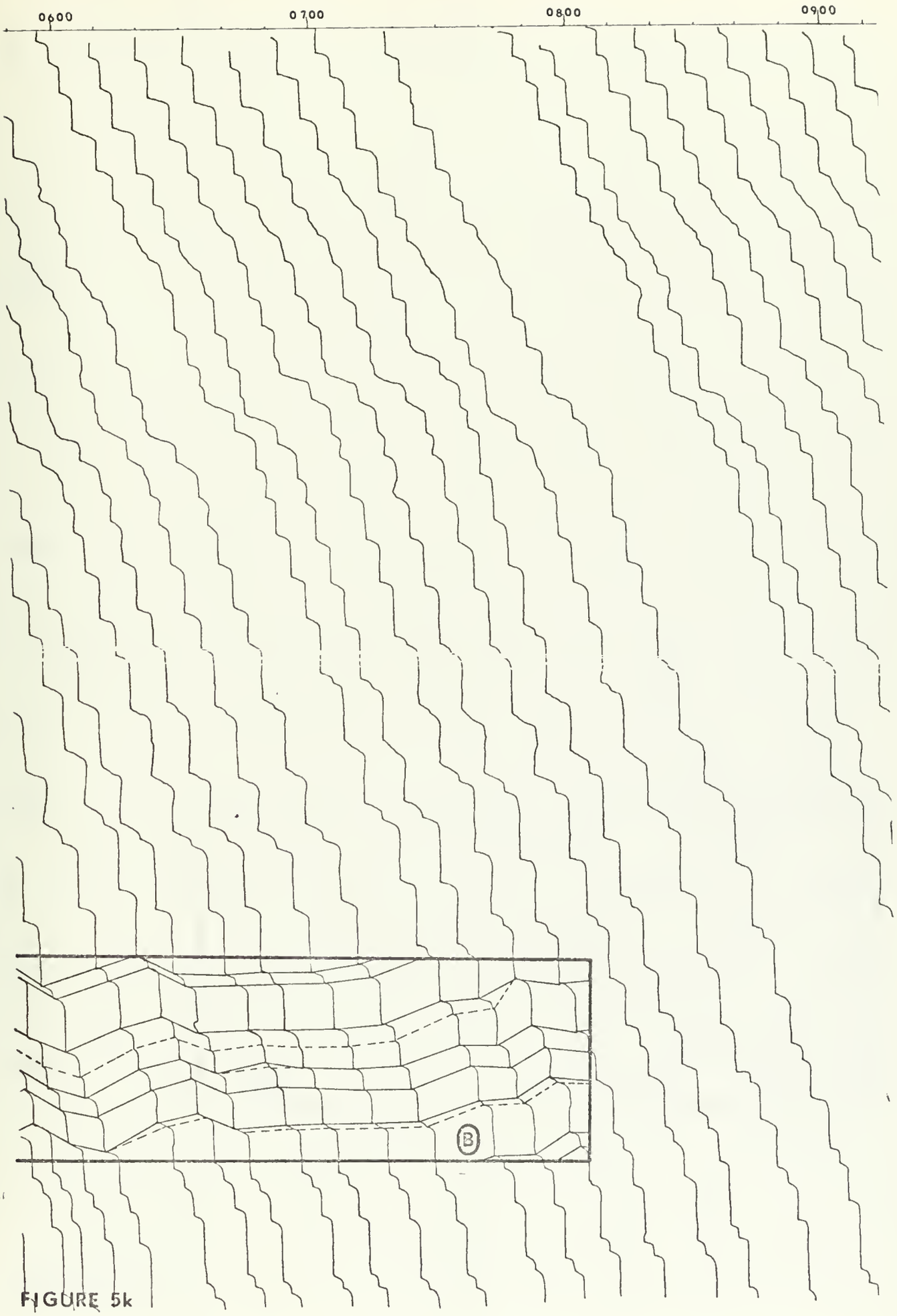

FIGURE 5k

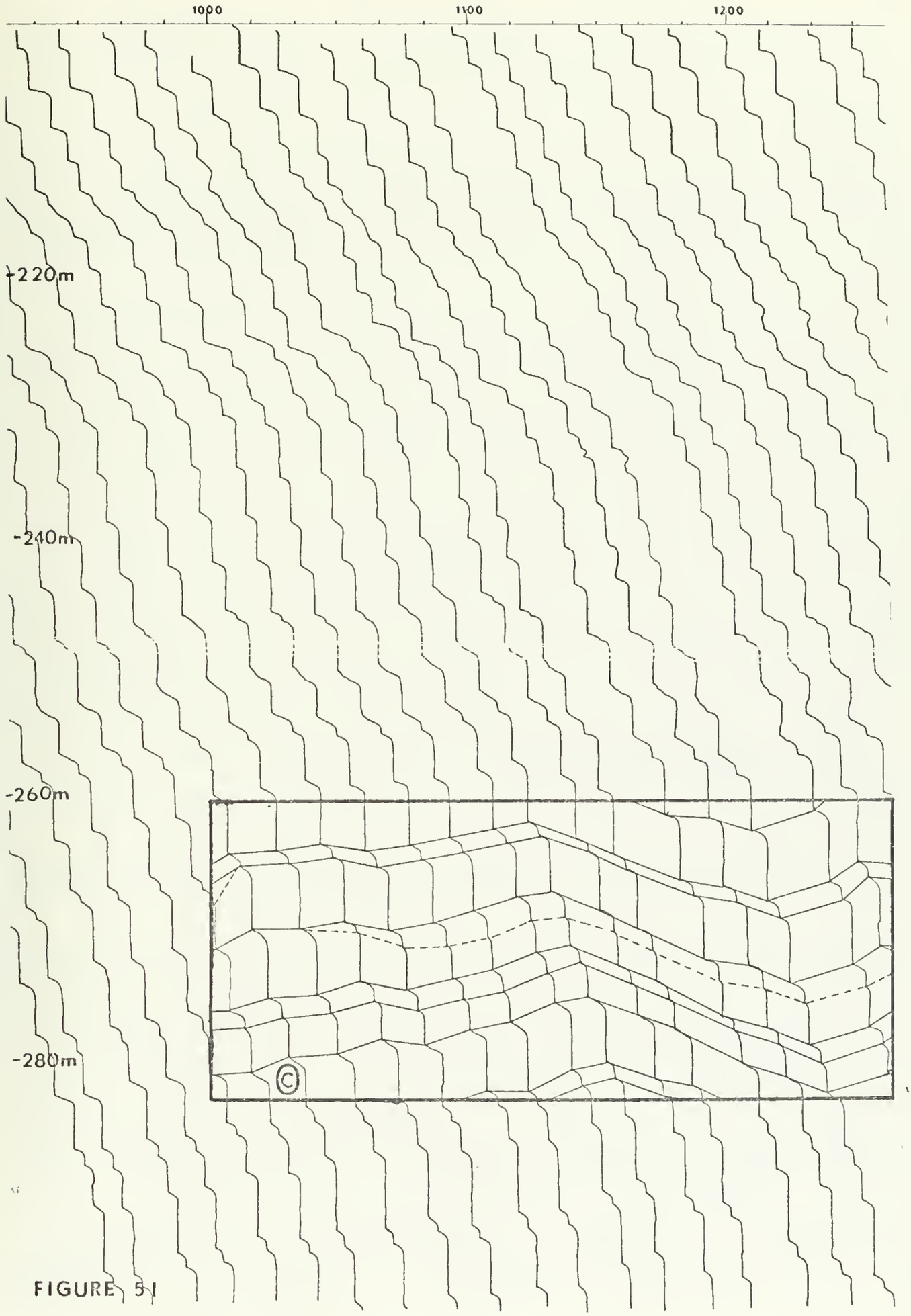

FIGURE 5-1

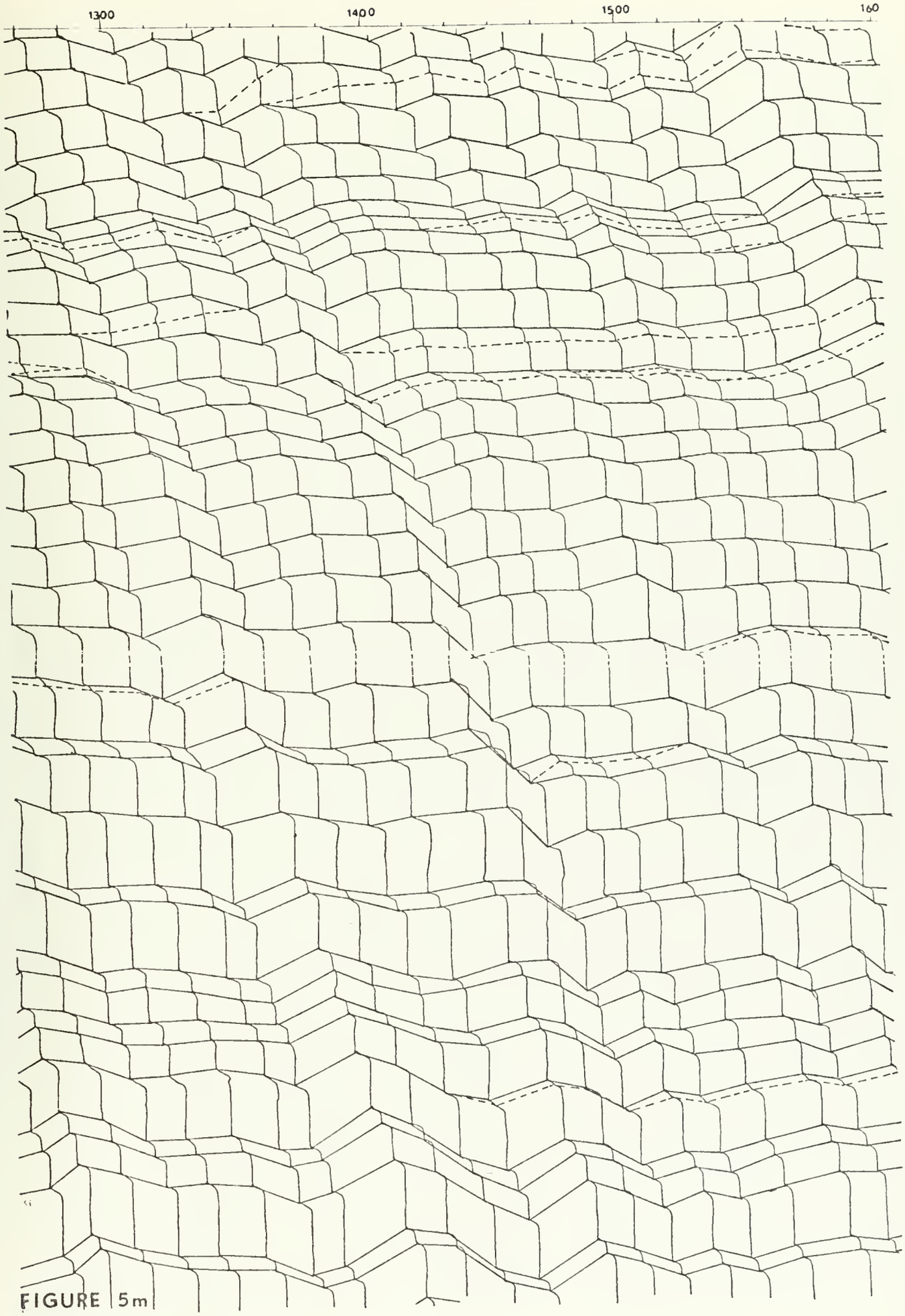

FIGURE 5m

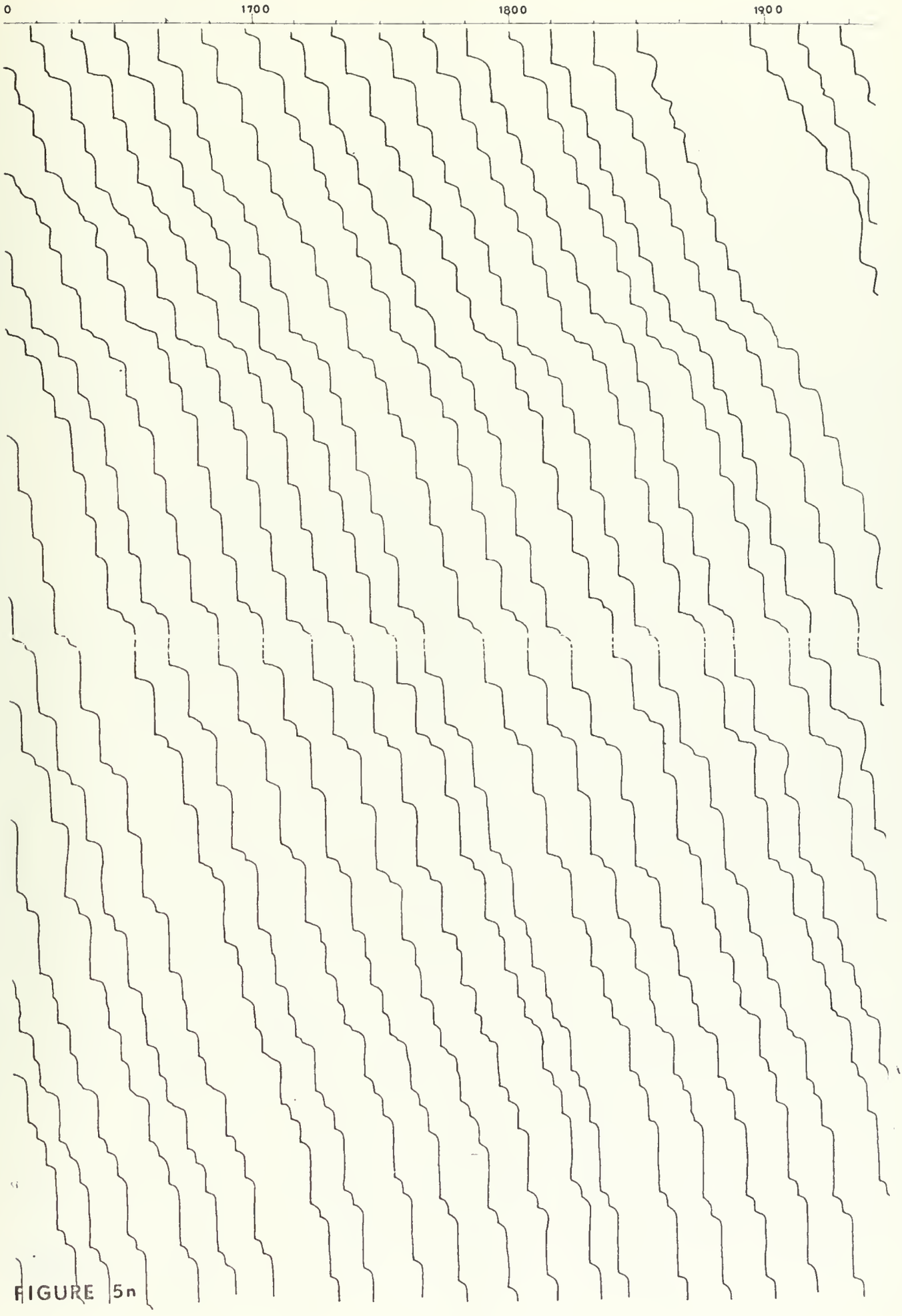

FIGURE 5n

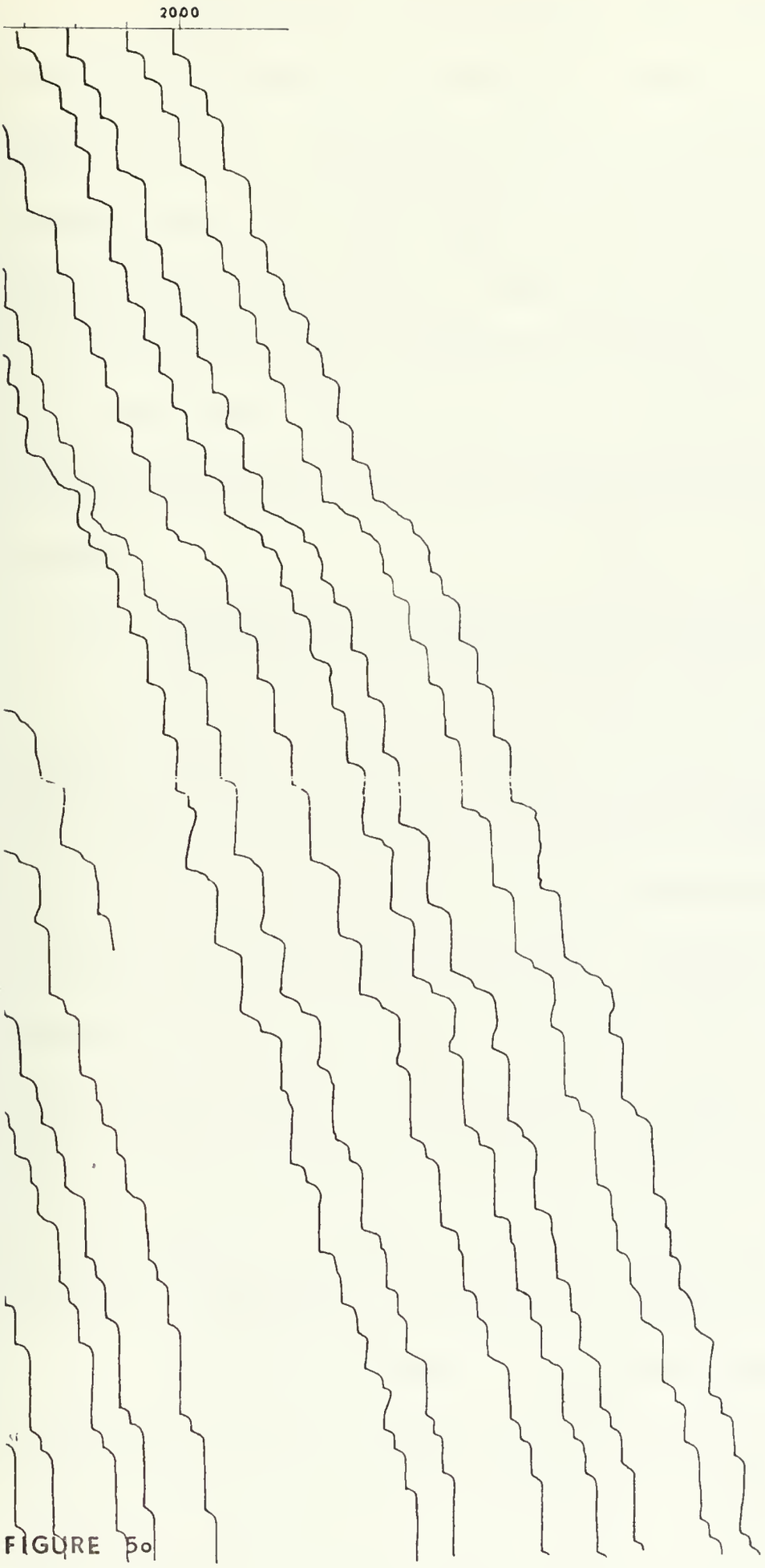

FIGURE 5o

Much of the apparent rounding of the temperature gradient within the interface sheets can be attributed to the 1.5 μF capacitor across the bridge null circuit. This capacitor acted as a low-pass filter to eliminate equipment noise and transient electrical interference, but also slowed the response of the system slightly. Figure 6 is a comparison of recordings of a square-wave signal, demonstrating the effect of the capacitor. Profiles recorded under low-noise conditions, with the capacitor removed, show sharp delineations of both boundaries of the interface sheet (Figure 6 Inset).

2. Stability and Horizontal Extent of Layered Structure

One of the most striking features of the temperature profiles is the nearly absolute stability and integrity of the layers for the entire length of the series. Using the recurring half-steps as references the layers can be connected from one profile to the next, demonstrating conclusively that the layers are stable features (Figure 5m). Profiles obtained by Neal [personal communication] from 28 March to 7 April 1971 show nearly a one-to-one correspondence to those displayed in Figure 5. The lifetime of the layers must then be measured in weeks or months, and cannot be limited by either diffusive or turbulent transfer of heat and salt across the interface sheets as suggested by Stommel and Fedorov [1967].

The horizontal extent of the discrete layers was estimated from the movement of the ice island during the recording interval, assuming the currents at 200 to 300 m were smaller than the surface drift. During the period 5-8 March the island drifted a total of ten nautical miles (Figure 7)

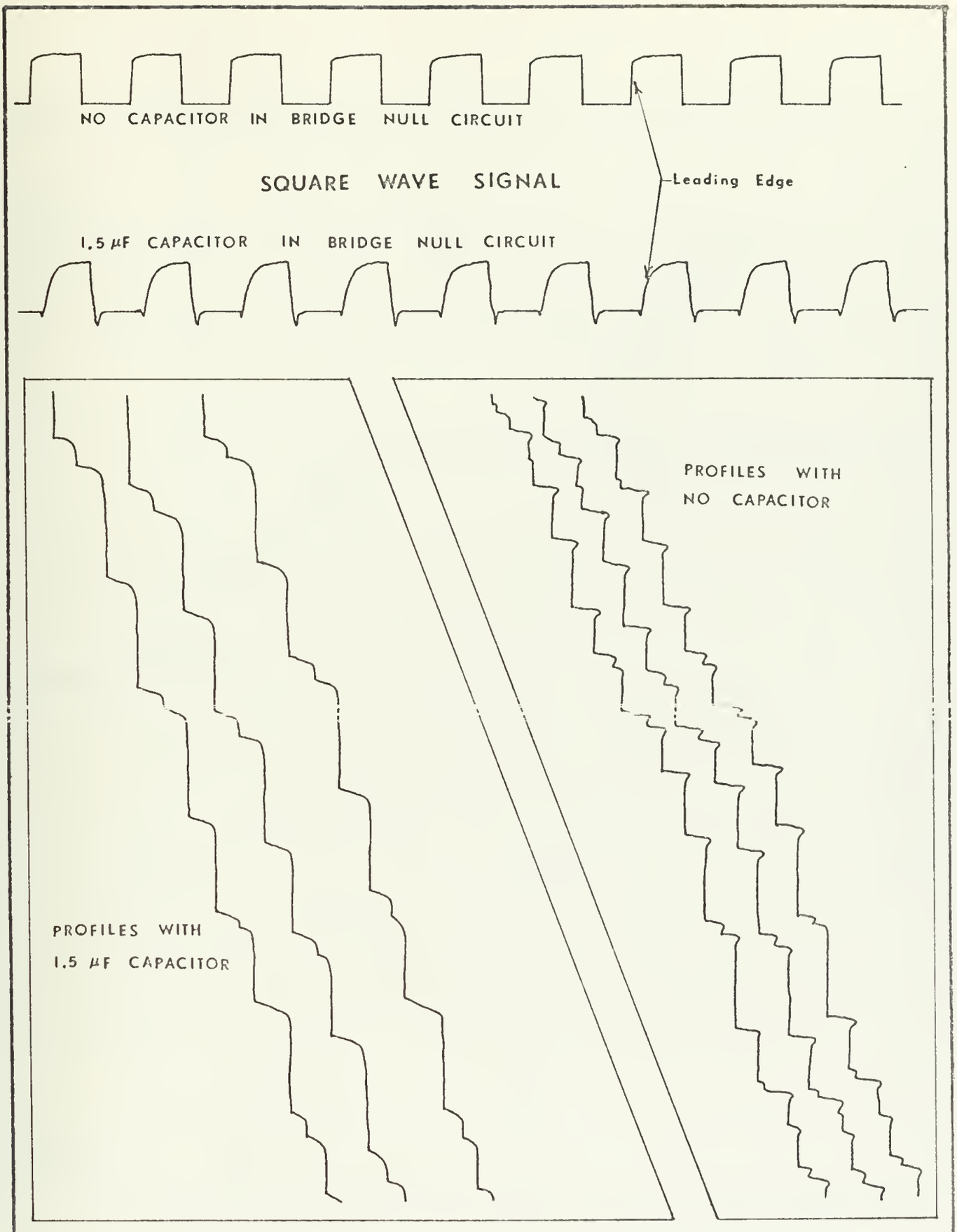

Figure 6. Response damping of capacitor in bridge null circuit.

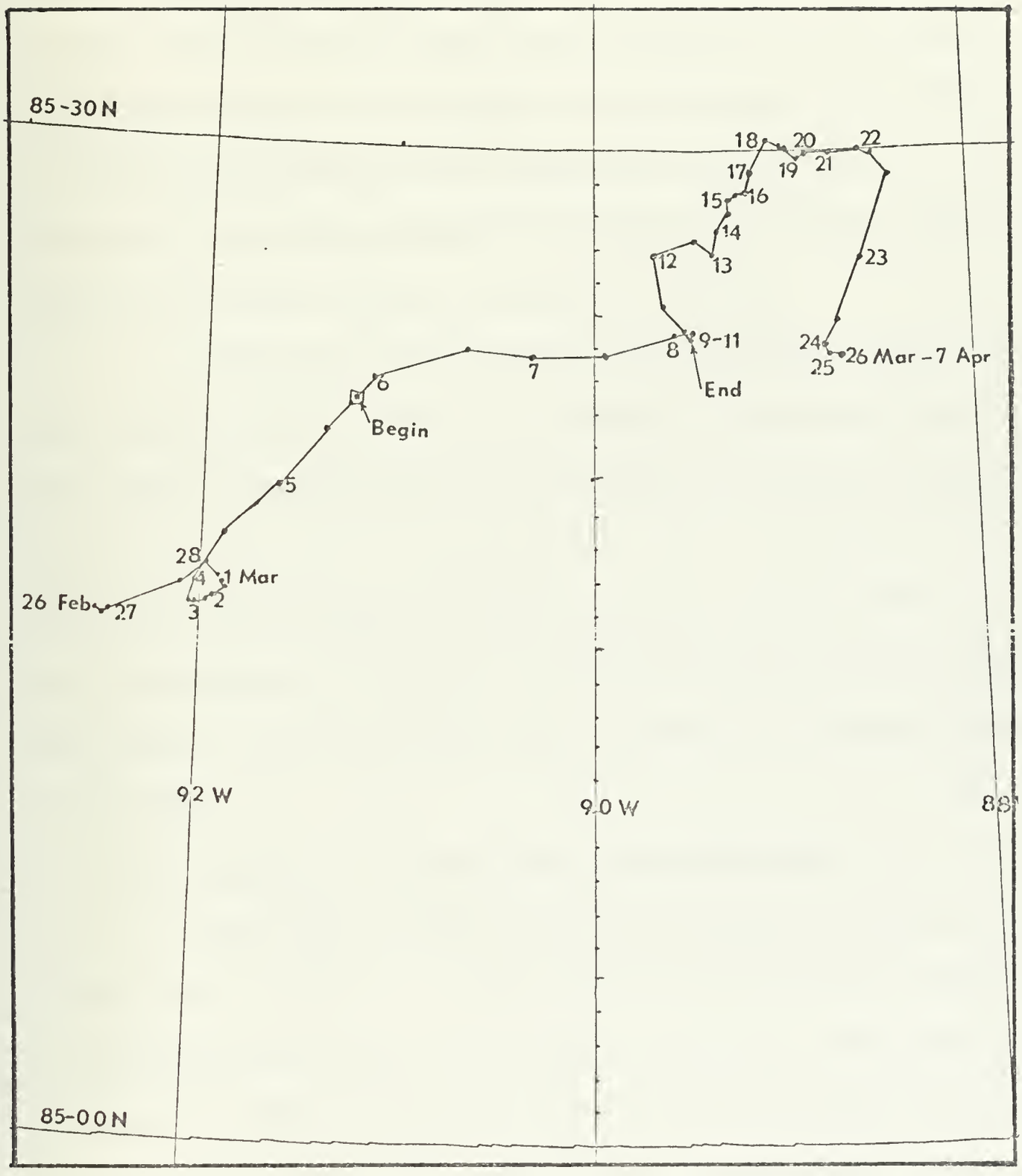

Figure 7. Movement of T-3 from 26 February until 7 April 1971.

based upon positions calculated every half-hour by a satellite navigation system [Lamont Geophysical Observatory, personal communication] . The drift velocity during this period was 4 nmi per day, or .17 knots, and was relatively constant in direction to the east-northeast. From 8 March to 7 April the island drifted 4 nmi to the east in a meandering path. Since the layered structure was coherent from 5 March until 8 April, a horizontal extent of some tens of miles is a conservative estimate.

That the layered structure is highly persistent in time and space indicates that the mechanisms involved are essentially in equilibrium. Since there is a gradual loss of heat and salt from the Atlantic water as it circulates in the Arctic [Coachman 1962], clearly there must be an upward flux of these properties through the layered structure, although no direct measurements are available. Recognizing that these upward fluxes must occur, the layered structure must necessarily be in a state of dynamic equilibrium.

3. Small-scale Changes in the Layered Structure

Even though the form of the layered structure, and the relationships of individual layers, are highly stable in time and space, there are many small-scale changes which can be observed from a close study of the profiles. The most interesting changes involve the formation of new layers or the gradual elimination of existing layers. The formation of new layers can be seen in figure 5i (Inset A). The 2306 6 March profile shows a thick layer at 280 m with a temperature step of .03°C. The next profile shows the formation of a new layer approximately 1 m thick with a temperature

step of .005°C within the original layers. The next two profiles contain the new layer, but it is displaced upward within the original layer, and is nonexistent in the 2346 profile. A similar phenomenon occurs between the 0015 and 0046 7 March profiles, and is suggestive of convective overturning within the original thick layers. A different phenomenon can be observed between the 2246 6 March and 0056 7 March profiles at 264 m. This region is characterized by a mean gradient of .025°C/m, the temperature increasing in a series of small steps which are very small and short lived. Small temperature inversions, indicated by circles at 280 m, are common and support the conclusion that convective turbulent mixing occurs within the layers.

A particularly interesting example of layer formation is observed between the 0208 and 0620 7 March profiles (Figure 5j,k Inset B). The 0208 profile shows a thick layer at 280 m which includes a small transient layer. The 0238 profile shows a partial degeneration of this layer resulting in a 25% decrease in the temperature step at the top of the layer, and the formation of a gradient of .003°C/m within the layer which now contains two transient layers. The next profile at 0238 (the time lapse was incurred while changing the XBT) shows three layers in which there is negligible gradient. The following profile shows only two layers which are well defined, and can be identified until the 0620 profile, the lower layer becoming progressively larger and the upper layer becoming progressively smaller. The original degeneration cannot be explained in terms of convective overturning, but the formation of transient layers and the gradual reformation of the original layer is similar to the phenomenon discussed in Inset A.

A slightly different phenomenon can be observed beginning with the 0906 7 March profile (Figure 5 I Inset C). This profile shows a thick layer at 270 m with a temperature step of .0265°C. The next profile shows two layers, the upper having a temperature step of .019°C and the lower having a temperature step of .0074°C. These two layers can be identified throughout the remainder of the series. It is significant that the total temperature step through the two new layers equals the temperature step of the initial layer. It is evident that some disturbance at the upper interface caused the initial formation of the new layer, which became thicker with time, but was limited in thickness by a stable feature, possibly a density increase.

4. Internal Waves

From Figure 5m it is observed that the entire layered structure moves vertically with respect to a fixed horizontal line. These vertical motions indicate the presence of internal gravity waves propagating through the water column. The apparent changes in layer thickness can be partially accounted for by internal wave propagation, since the profiles do not represent simultaneous measurements of temperature vs. depth. The layers may appear to be expanded or contracted due to phase changes as the XBT was lowered through a propagating internal wave. The cyclic nature of the vertical fluctuations is clearly observed on the expanded resolution profiles collected during the 25 m and 10 m time-series on 7-8 March (Figures 8a,b and 9a-d). The auto-correlation of the depth changes of the half-step at 260 m in the 10 m series discloses periodic fluctuations at phase lags of 12 and 22 minutes (Figure 10).

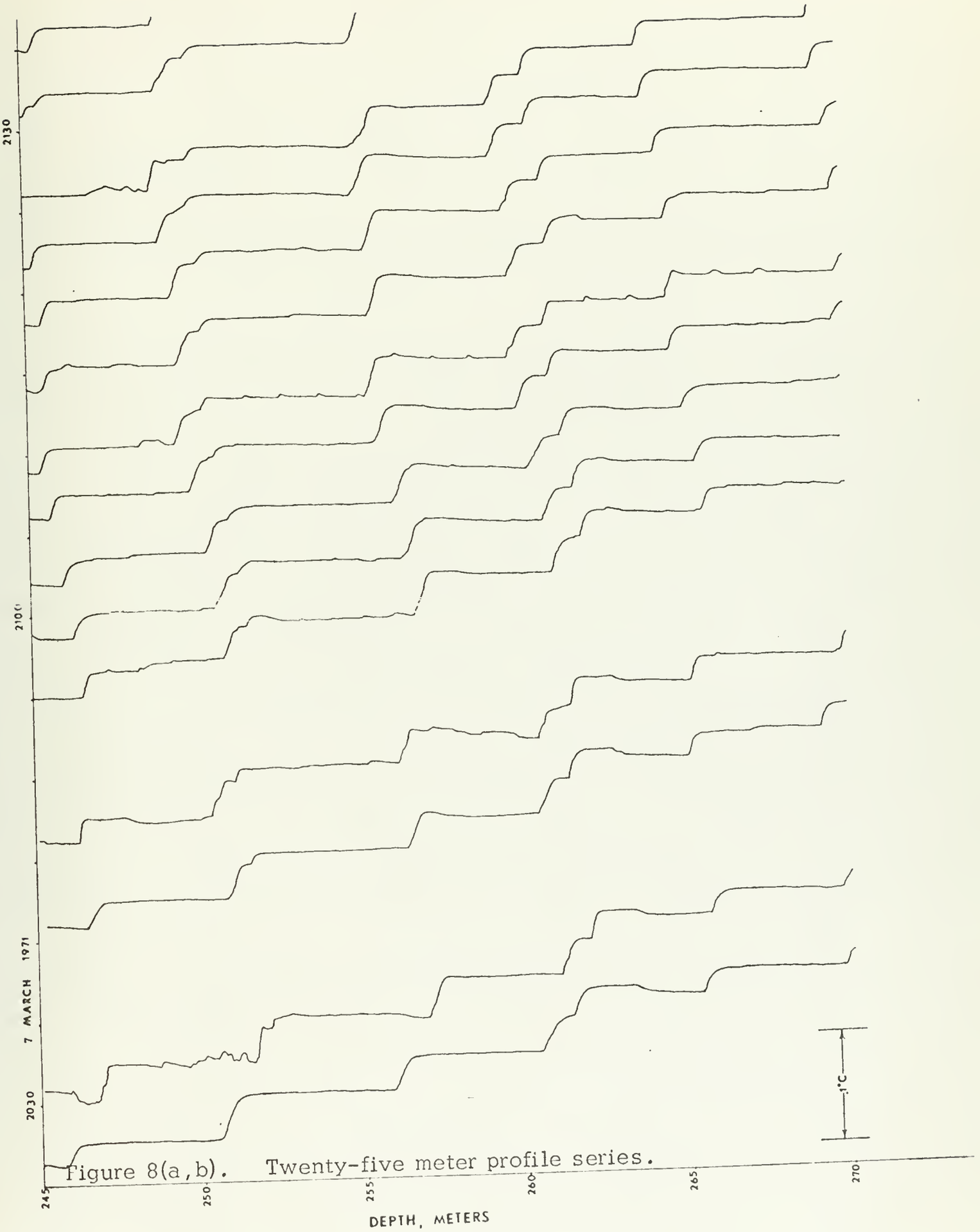

Figure 8(a,b). Twenty-five meter profile series.

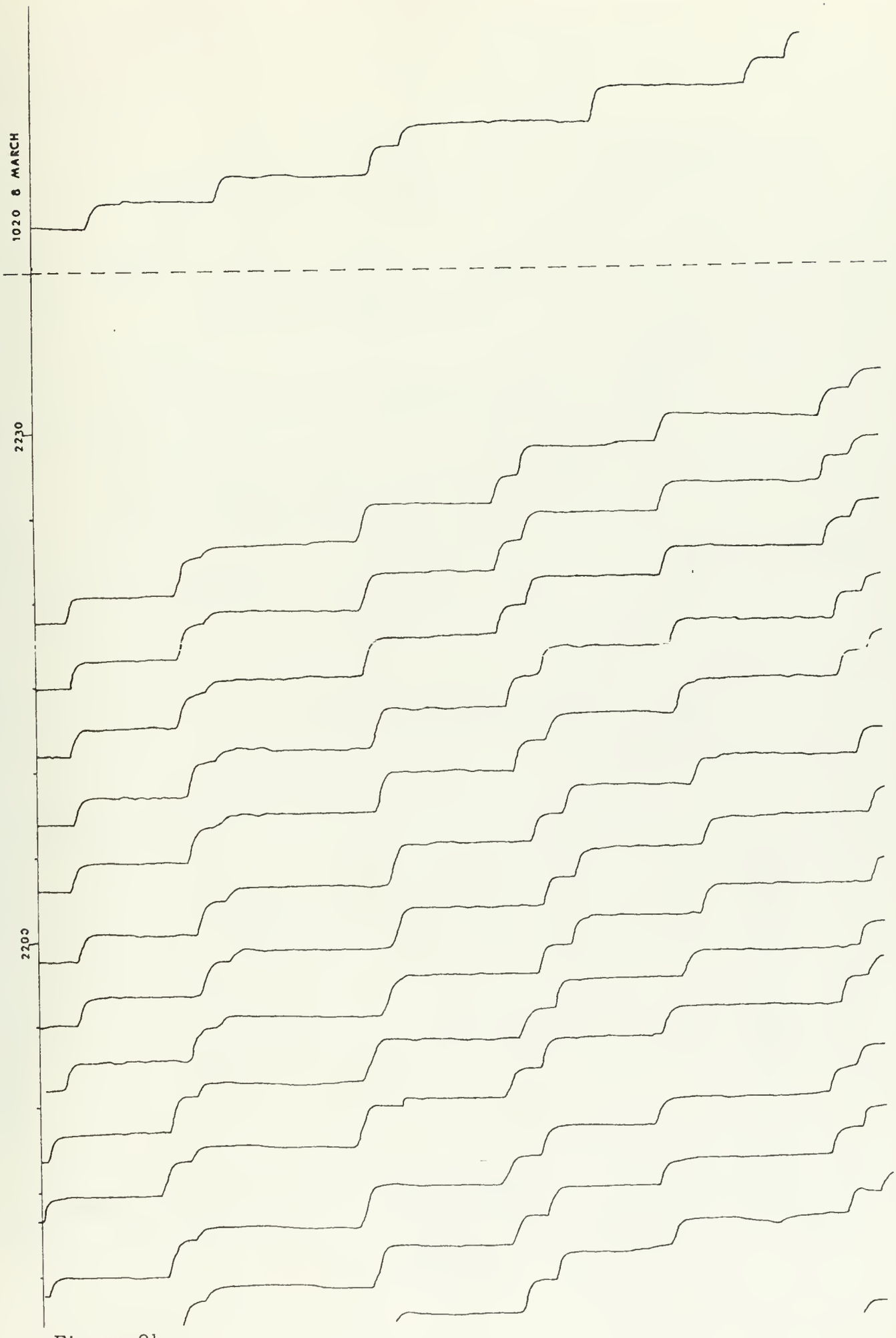

Figure 8b.

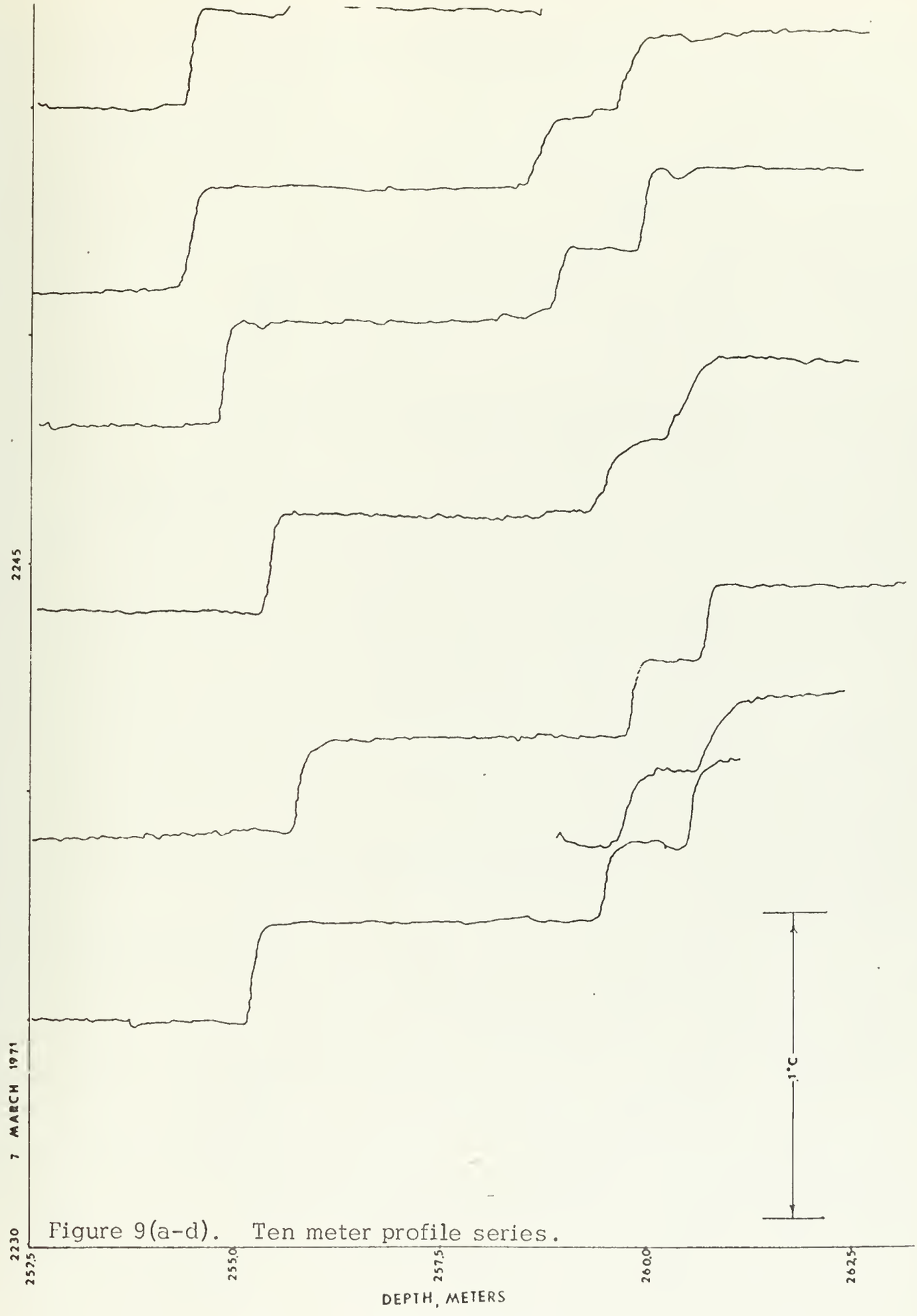

Figure 9(a-d). Ten meter profile series.

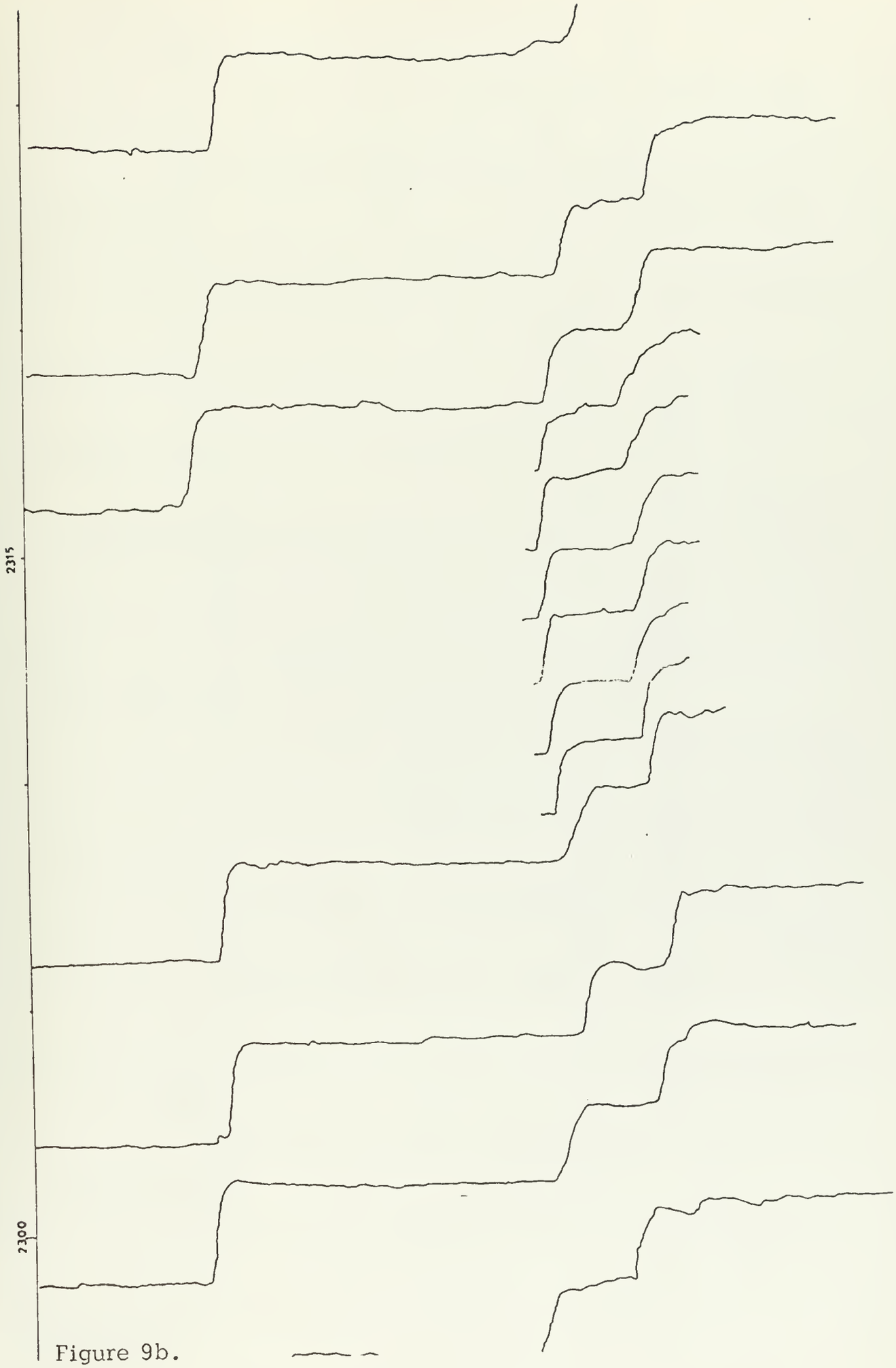

Figure 9b.

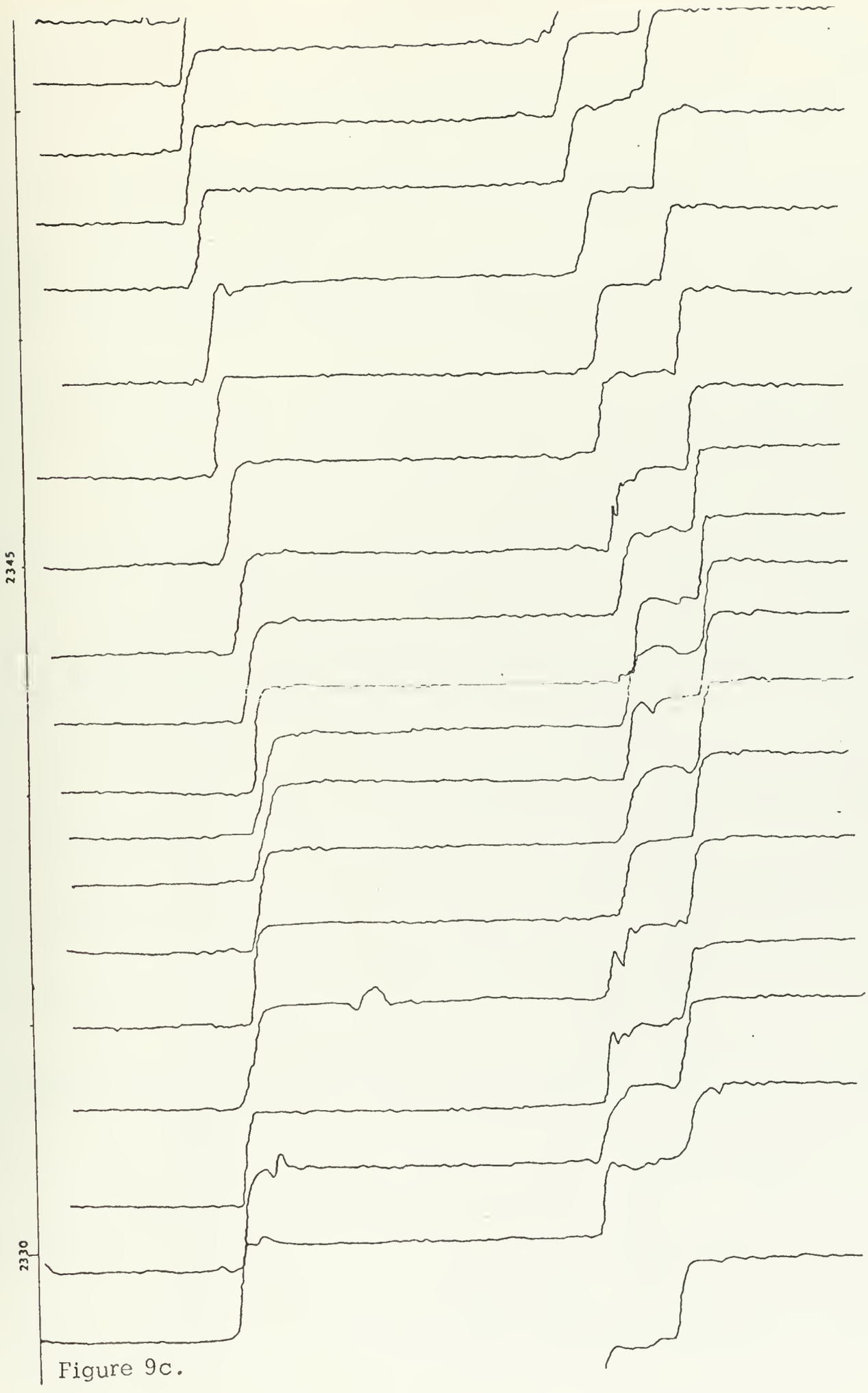

Figure 9c.

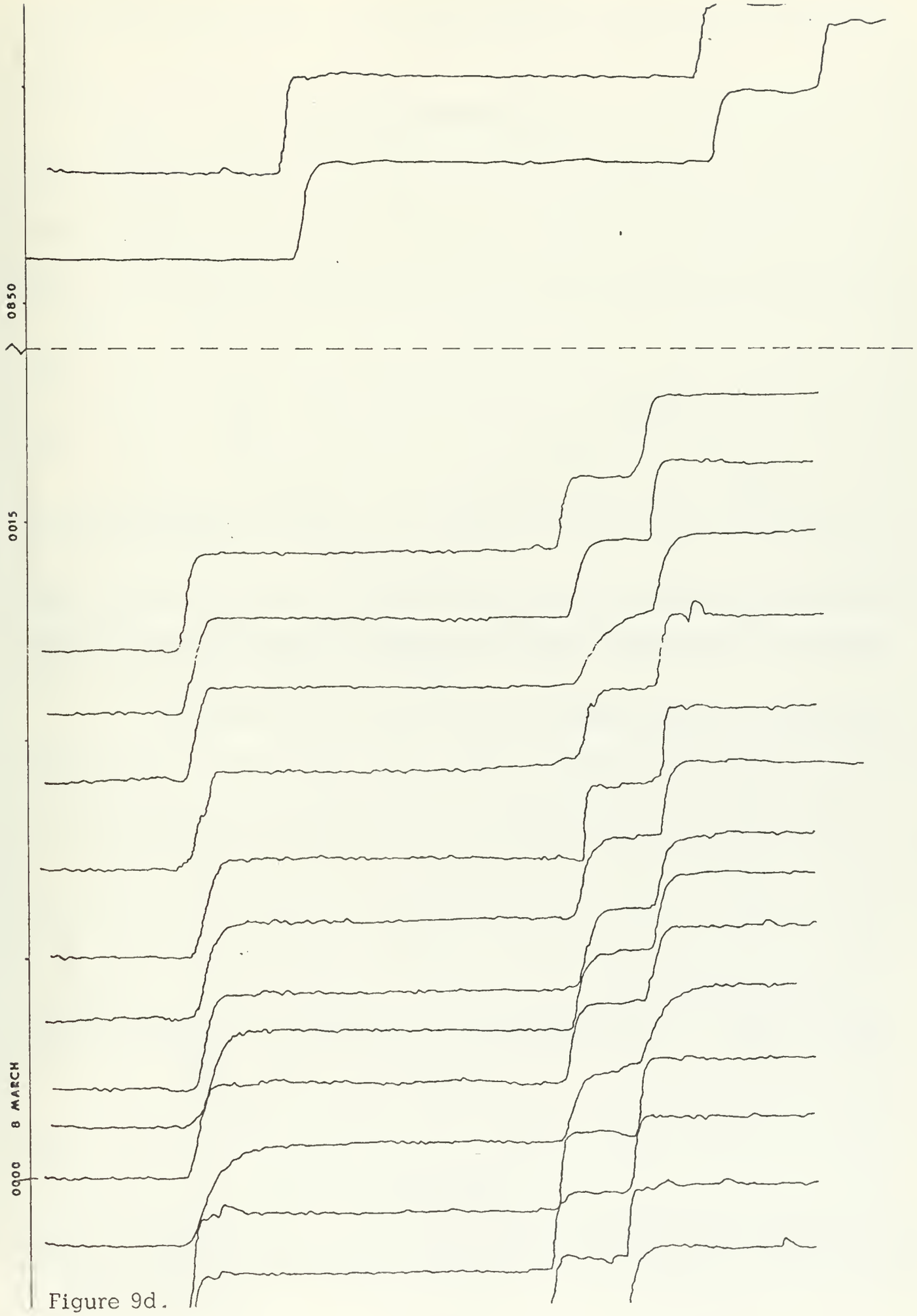

Figure 9d.

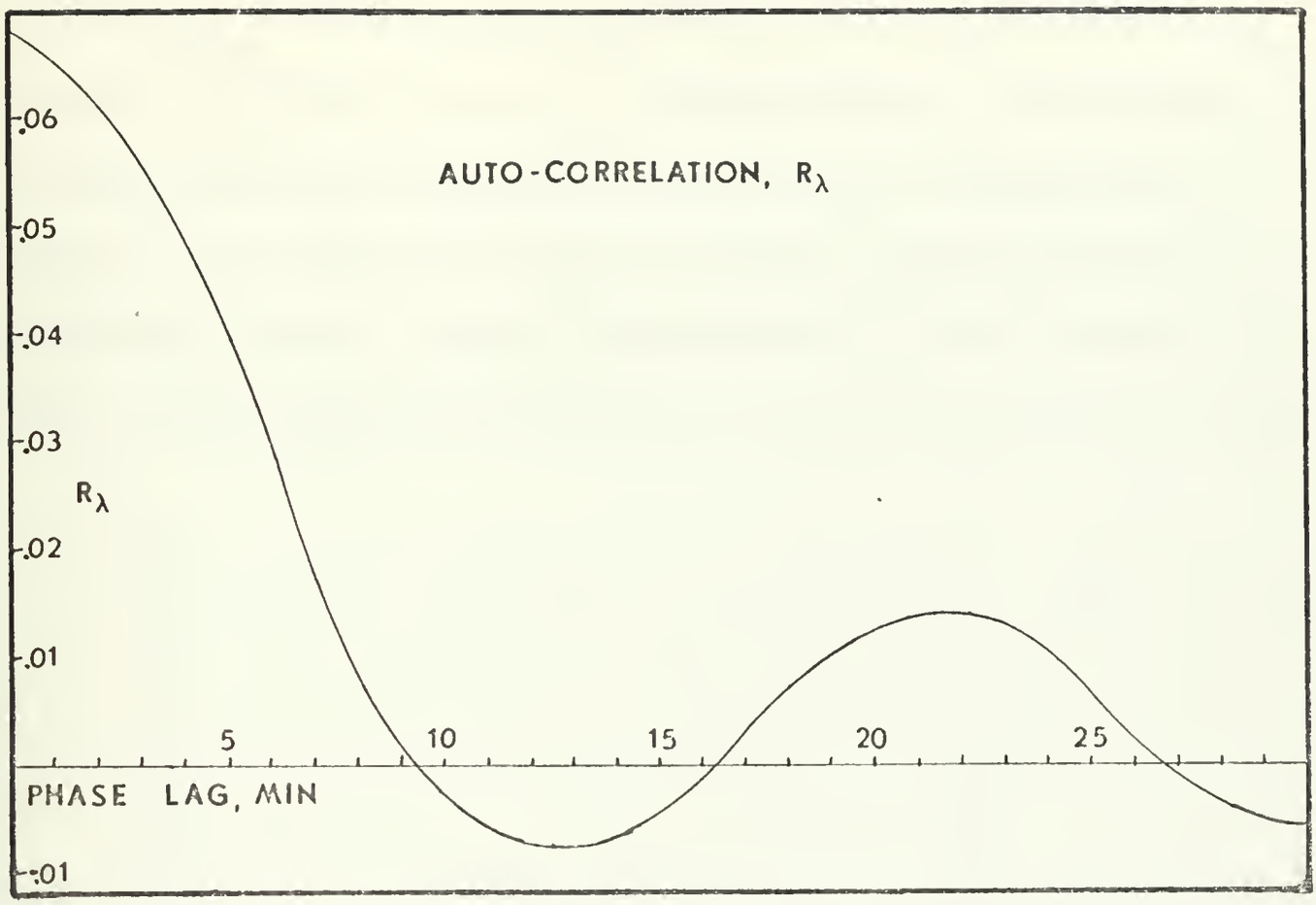

Figure 10. Autocorrelation of depth of half-step feature from 10 m profile series (One minute sampling interval).

An internal wave record was constructed from the vertical fluctuations of the recurring half-step at 260 m. From the constructed record for the 48-hour time-series (Figure 11) the spectral density estimates were

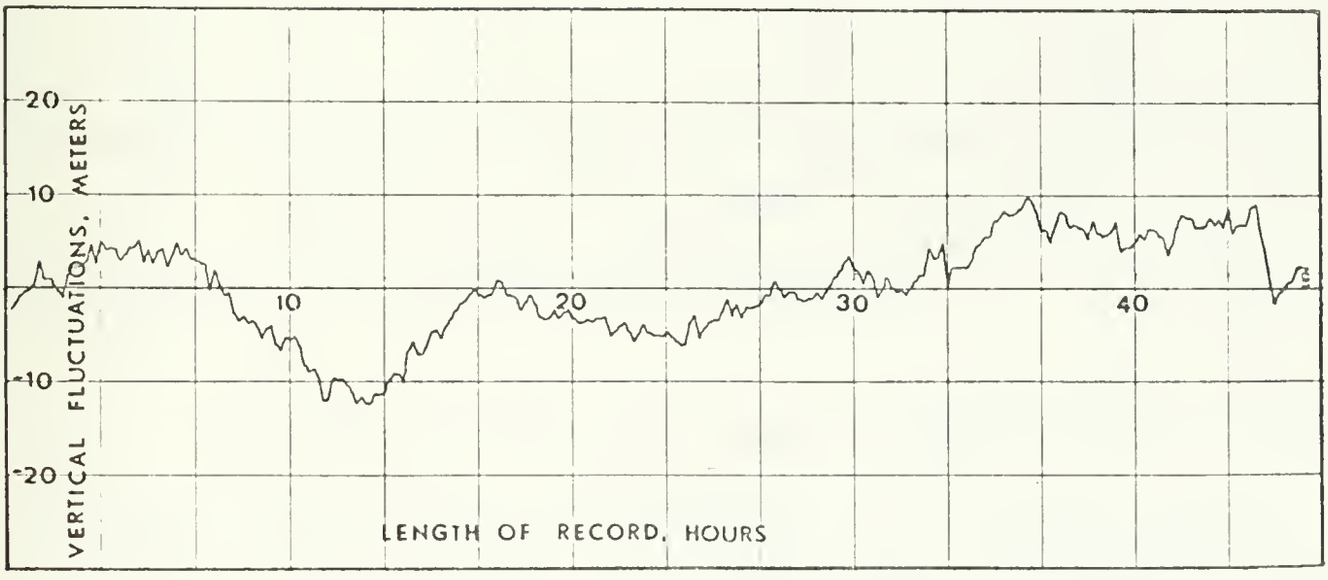

Figure 11. Constructed internal wave record from vertical fluctuations of the half-step feature at approximately 260 m on 48-hour time-series (Ten minute sampling interval).

calculated by conducting a Fourier analysis, assuming the record to be periodic. The Nyquist frequency at 10 minute sampling is 3 cycles/hour, and the lowest frequency extracted from this record was .04 cycles/hour. Figure 12 is the Brunt-Väisälä frequency profile, showing a value of 17 cycles/hour at 260 m. Therefore, the frequencies for which spectral estimates can be computed all lie below the stability frequency at this depth.

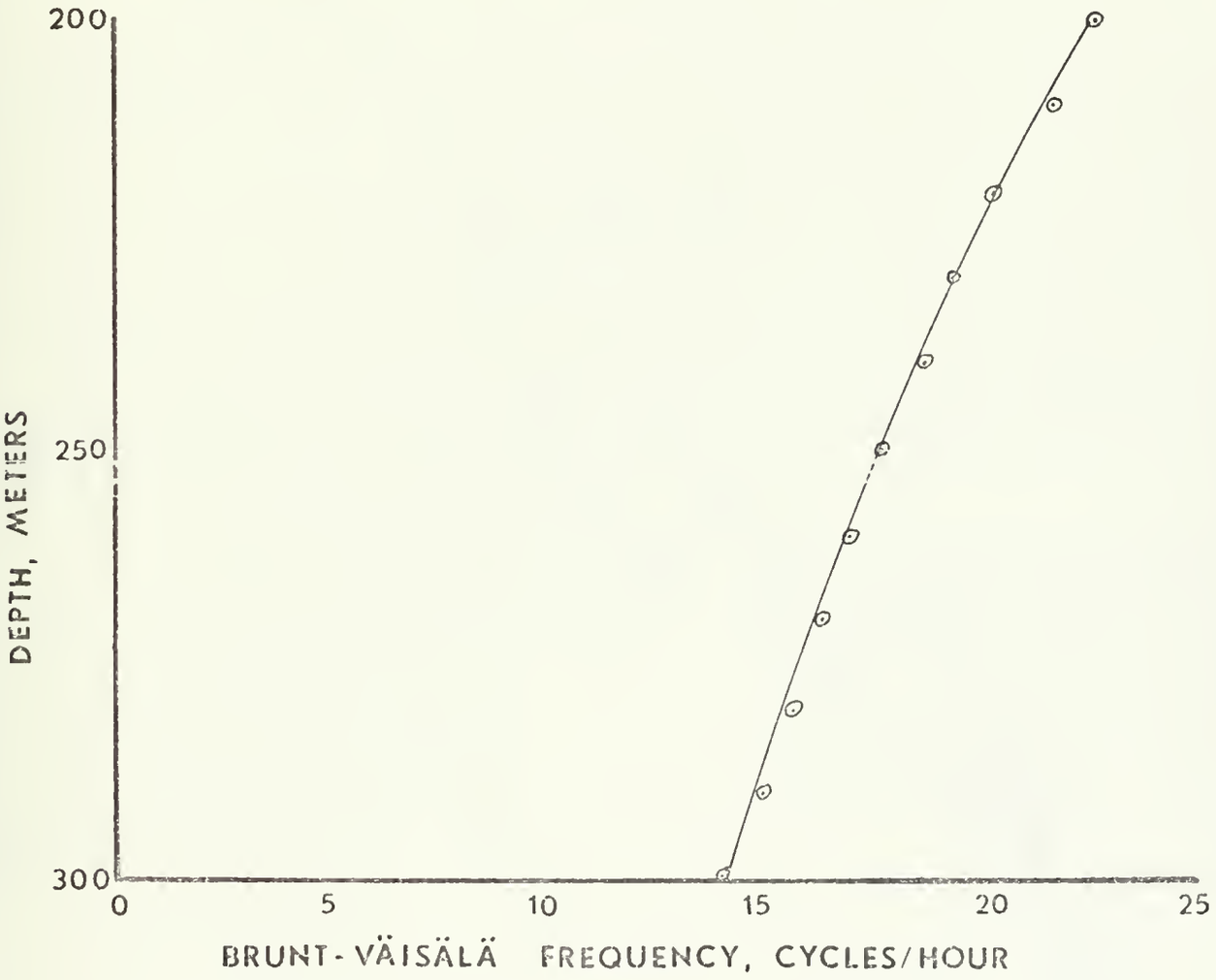

Figure 12. Brunt-Väisälä frequency profile.

The spectral density plot (Figure 13) indicates that the internal wave energy is proportional to $f^{-4/3}$, where f is the frequency. The fit of the -4/3 curve is good for frequencies greater than .2 cycles/hour. The spectral density estimates for the internal wave record constructed from the

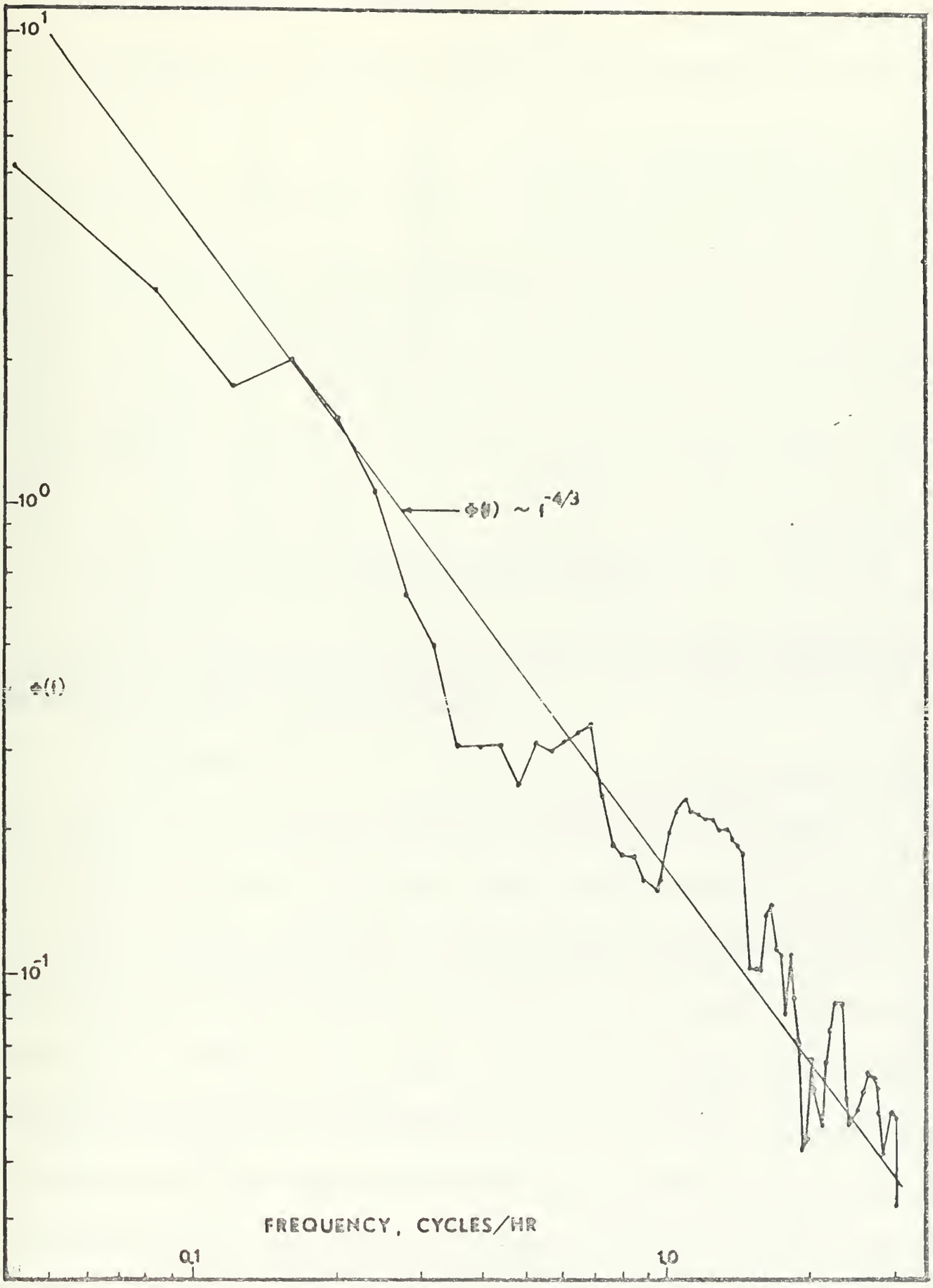

Figure 13. Spectral density of the vertical fluctuations of the 260 m half-step feature for the 48-hour time-series (Ten minute sampling interval).

25 m and 10 m time-series (Figure 14) support the -4/3 relationship of the 48-hour analysis for frequencies between .5 and 8 cycles/hour (Figure 15).

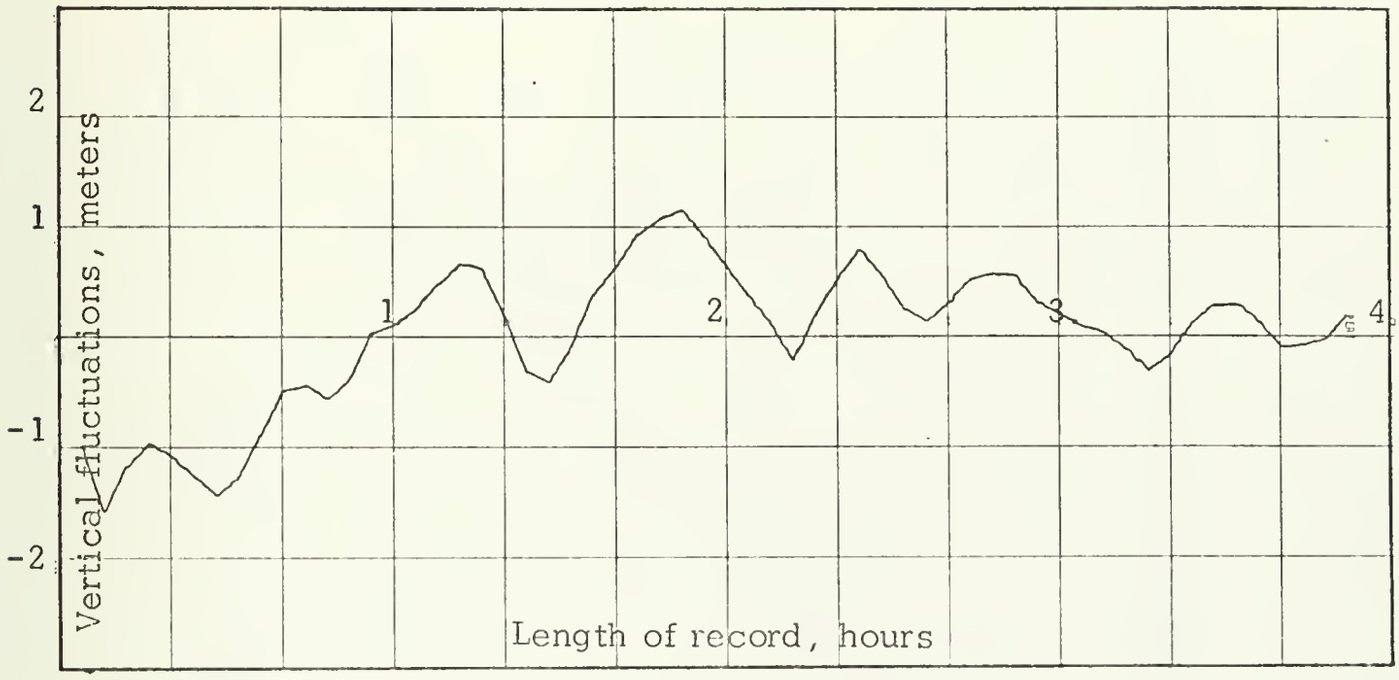

Figure 14. Constructed internal wave record from vertical fluctuations of the half-step feature at approximately 260 m on the 25 m and 10 m time-series (Four minute sampling interval).

Phillips [1971] has shown that in stably stratified regions of the ocean, where the density increases monotonically with depth in a series of homogeneous layers, the motion of this structure relative to a fixed measuring instrument results in a spectral density proportional to (frequency)$^{-2}$, over a range which is not limited by the value of the stability frequency N. Similarly, the spectra obtained by traversing such a structure vertically was found to be proportional to (wave number)$^{-2}$. The turbulent fluctuations of the layers were neglected, the properties within the layers were assumed to be uniform, but vary rapidly across the interface sheets. For temperature the expected spectral estimate is

$$\Phi(f) = \frac{1}{2\pi}\left[\frac{1}{T}\sum_{r}(\Delta\theta)_r^{\,2}\right](2\pi f)^{-2}$$

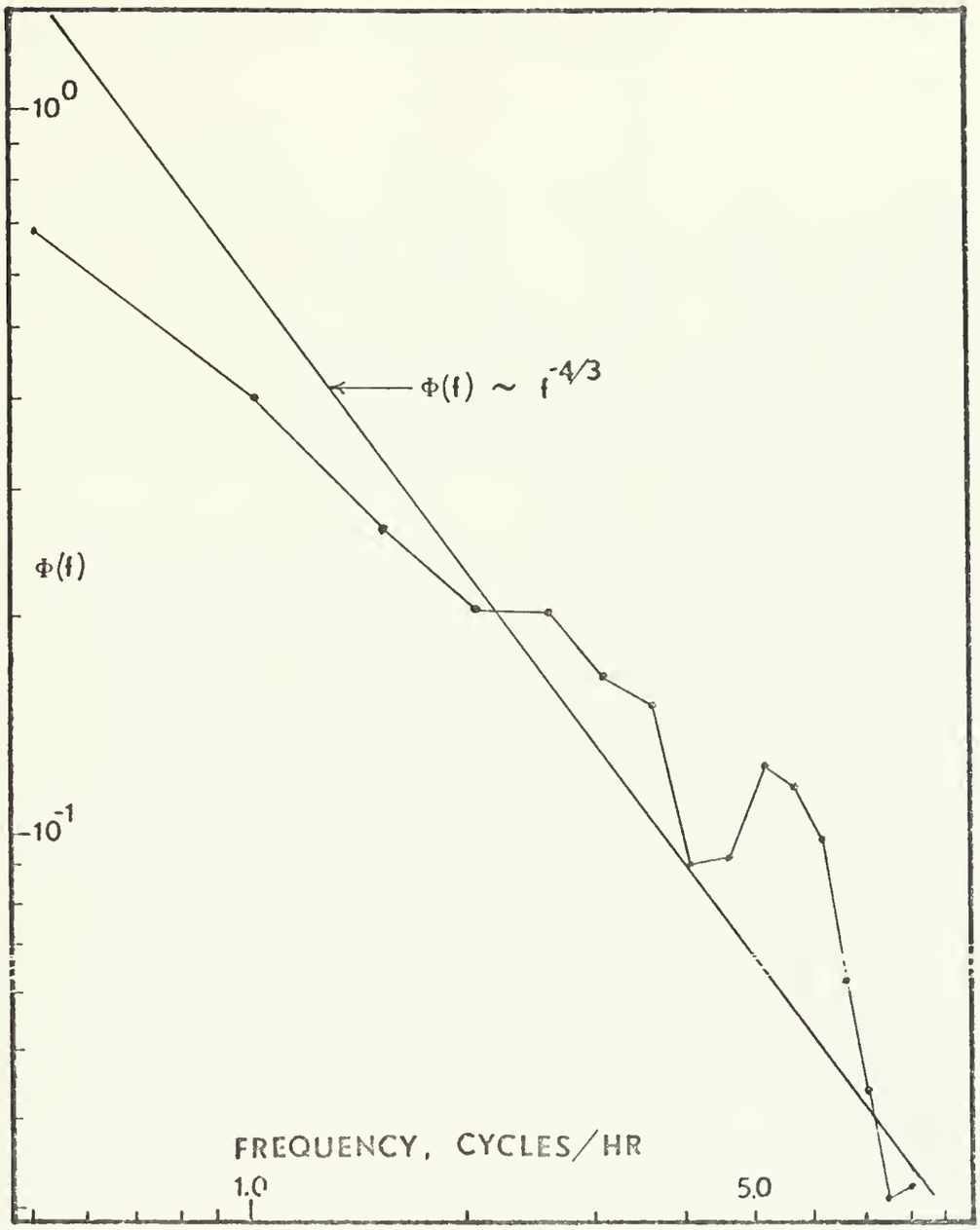

Figure 15. Spectral density for 25 m and 10 m time-series (Four minute sampling interval).

where T is the length of the record and $(\Delta\theta)_r$ is the temperature perturbation which occurs at time t_r. The spectral density of the temperature perturbations at 260 m for the 48-hour time-series (Figure 16) shows good agreement with the -2 decay coefficient for frequencies greater than .2 cycles/hour. Since the thickness of the homogeneous layers is greater

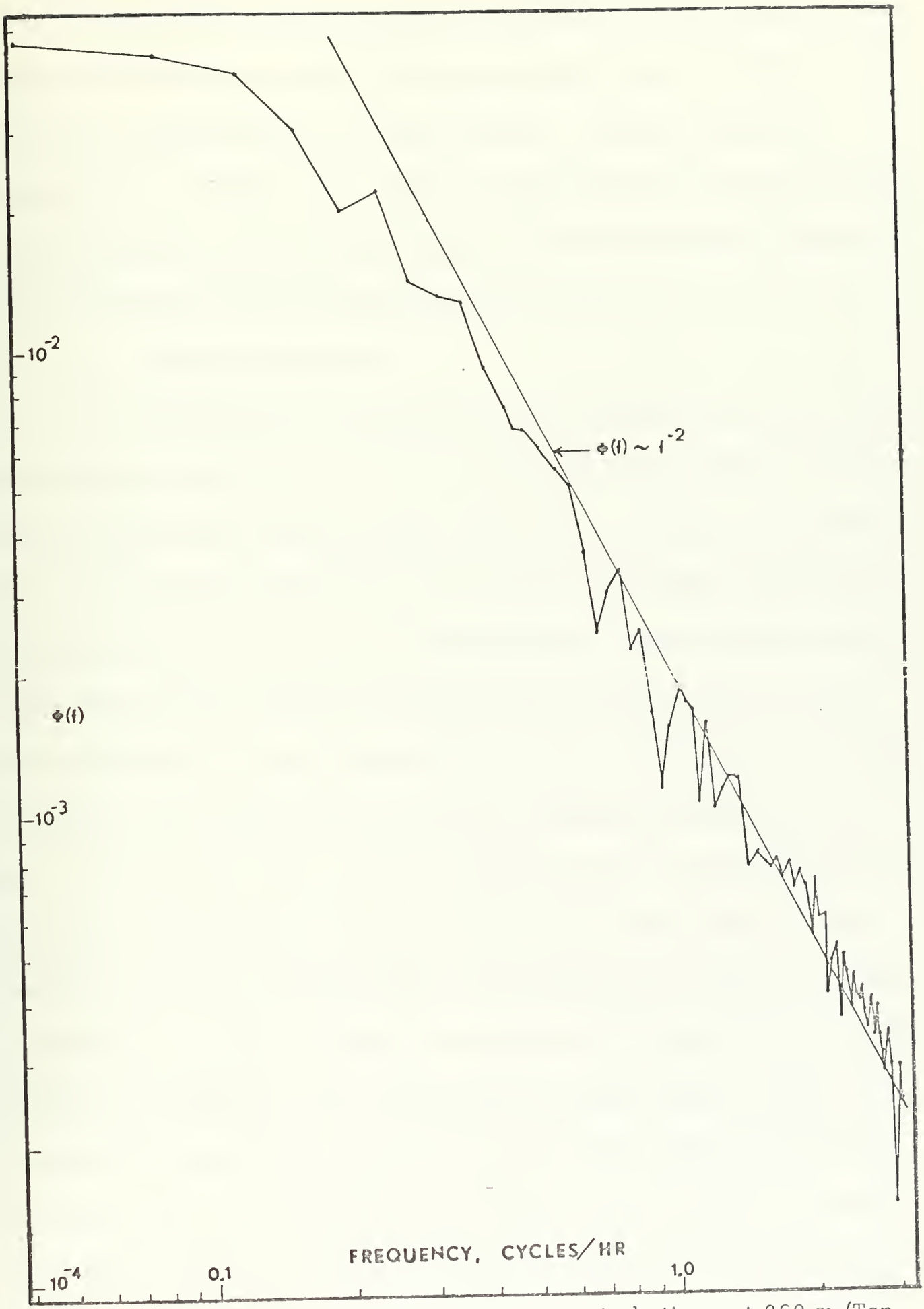

Figure 16. Spectral density of temperature perturbations at 260 m (Ten minute sampling interval).

than the amplitudes of high-frequency internal waves, these spectral forms are not necessarily associated with the spectral density of internal waves, but can be considered to be low-pass filtered. A similar analysis by Neshyba et al [1971b] for a 30-hour record with a four-minute sampling interval resulted in decay coefficients of -2 for the constructed internal wave record, and -3 for the temperature perturbations.

5. Statistical Analysis

Representative profiles selected at intervals of one hour were processed in digital form on the Naval Postgraduate School IBM computer system to determine if relationships between layer thickness, temperature step size, and depth were evident. To convert the profiles from analog to digital form the actual distance to the beginning of each successive temperature step from a horizontal reference line at the top of the X-Y plot was measured to the nearest hundredth of an inch. This measurement corresponded to the depth of each successive temperature interface below 200 m. The distance from a vertical reference line to the temperature in each layer corresponded to the temperature of the layers relative to the temperature at 200 m. The computer was programmed to convert these two measurements to depth in meters and temperature in degrees Celsius. The thickness of each layer and the temperature increase between layers were calculated by subtraction. Three assumptions were made when analyzing the data in this manner: (1) That the interface sheet thickness was negligible; (2) the temperature gradient within the sheets was infinite; and (3) the temperature gradient within the layers was zero. The resulting

profile, with these assumptions, consisted of isothermal layers separated by positive step-discontinuities in temperature.

Linear regression analysis shows that there is a definite tendency for the layers to become thicker with depth, while the temperature step size decreases with depth (Figures 17 and 18). The standard deviation of regression of the layer thickness $\hat{\sigma}_{z\Delta z}$ is 1.412, while that of the temperature step size $\hat{\sigma}_{z\Delta T}$ is 0.0075. Assuming ΔT and ΔZ to be normally distributed the covariance of these quantities yields a correlation coefficient of 0.15 which would suggest little correlation between the thickness of a layer and the corresponding temperature increase from the preceding layer. The pronounced decrease of $\Delta T/\Delta Z$ with depth (Figure 19) was expected from visual examination of the records. Typical half-steps generate a high value for this ratio and fall far to the right of the standard deviation of the regression curve.

The mean gradient is approximated by the relationship

$$T_p = .022\ (Z-200)^{.8}$$

where T_p is the temperature increase from that at 200 m, and is slightly concave down (Figure 20). Linear regression analysis indicates that $\Delta T/\Delta Z$ is strongly dependent on the steepness of the gradient, neglecting the anomalous half-steps (Figure 21). It is obvious from a simple model that, if layered structure is superimposed on a curved mean gradient, the thickness of the layers must necessarily increase, and the size of the temperature steps must necessarily decrease as the gradient becomes small (Figure 22).

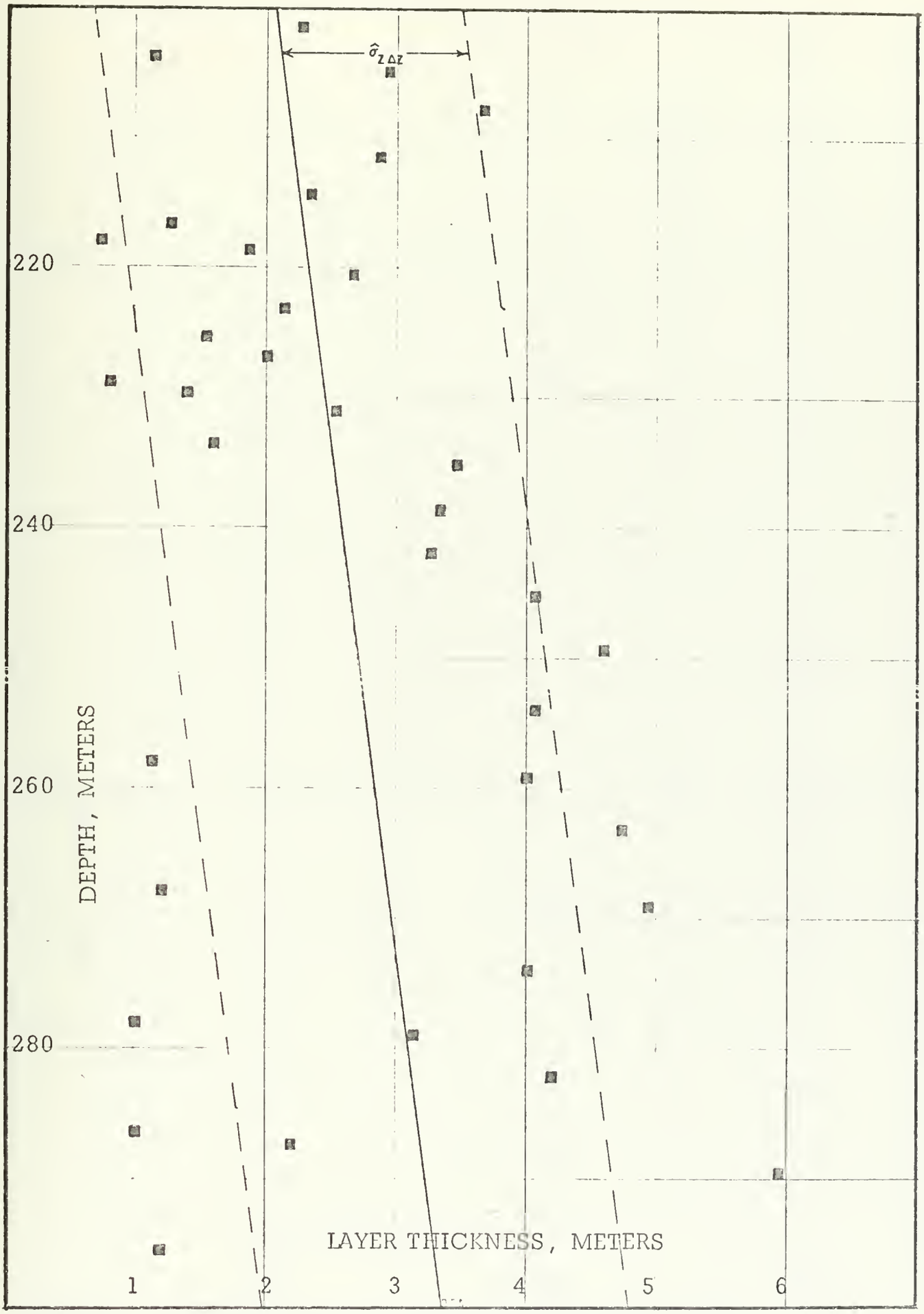

Figure 17. Layer thickness as a function of depth.

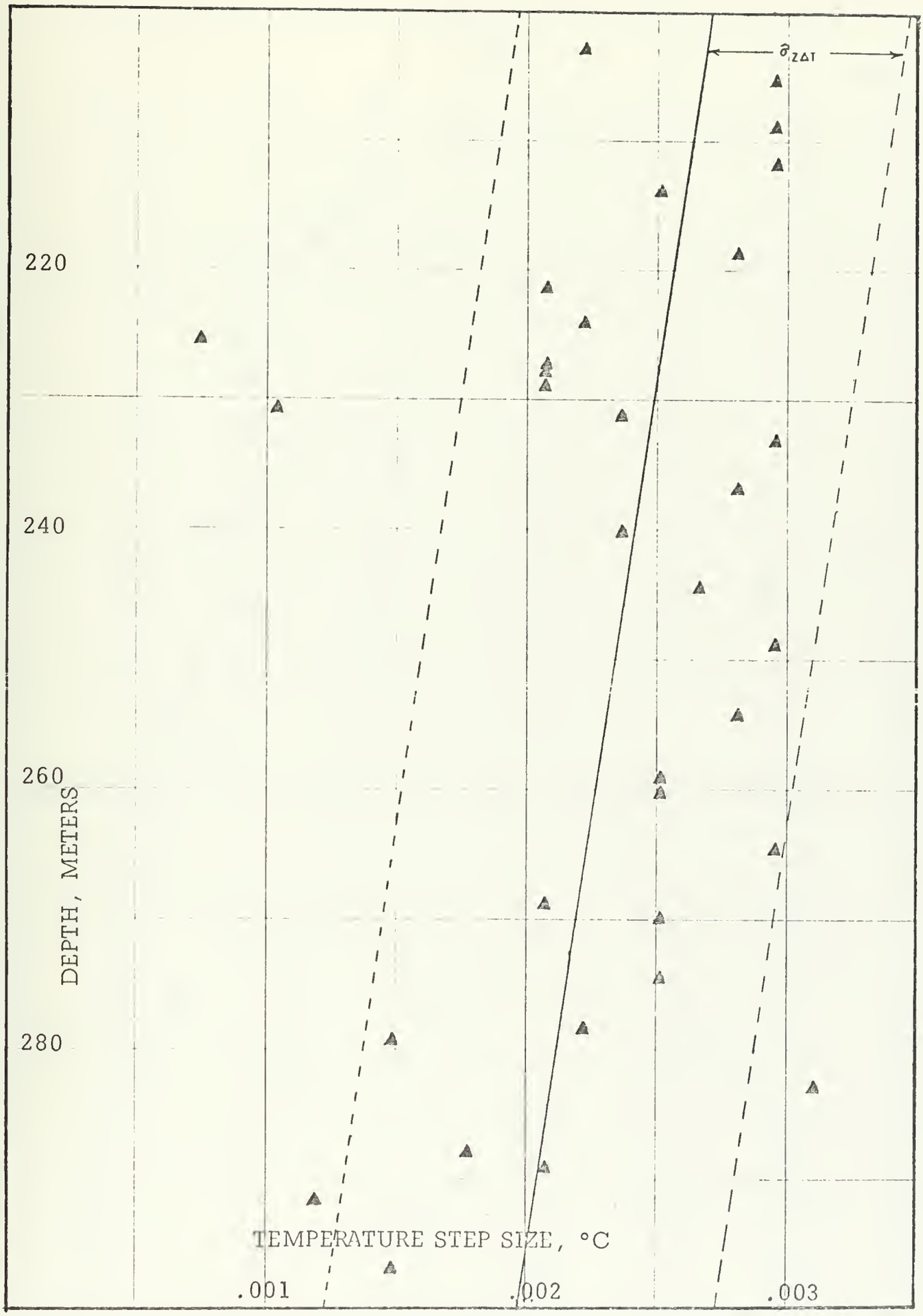

Figure 18. Temperature Step Size as a function of depth.

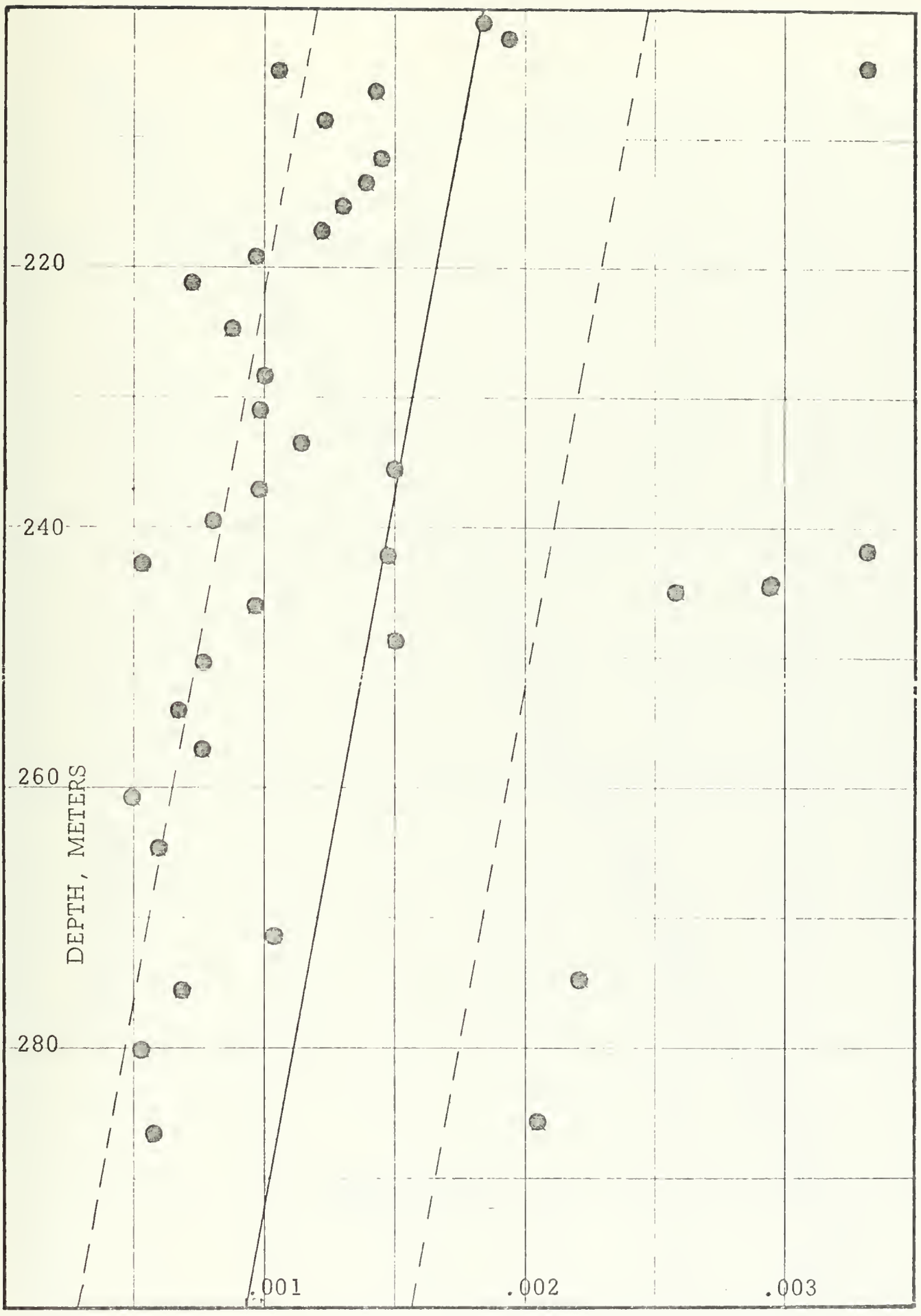

Figure 19. $\Delta T/\Delta Z$ as a function of depth.

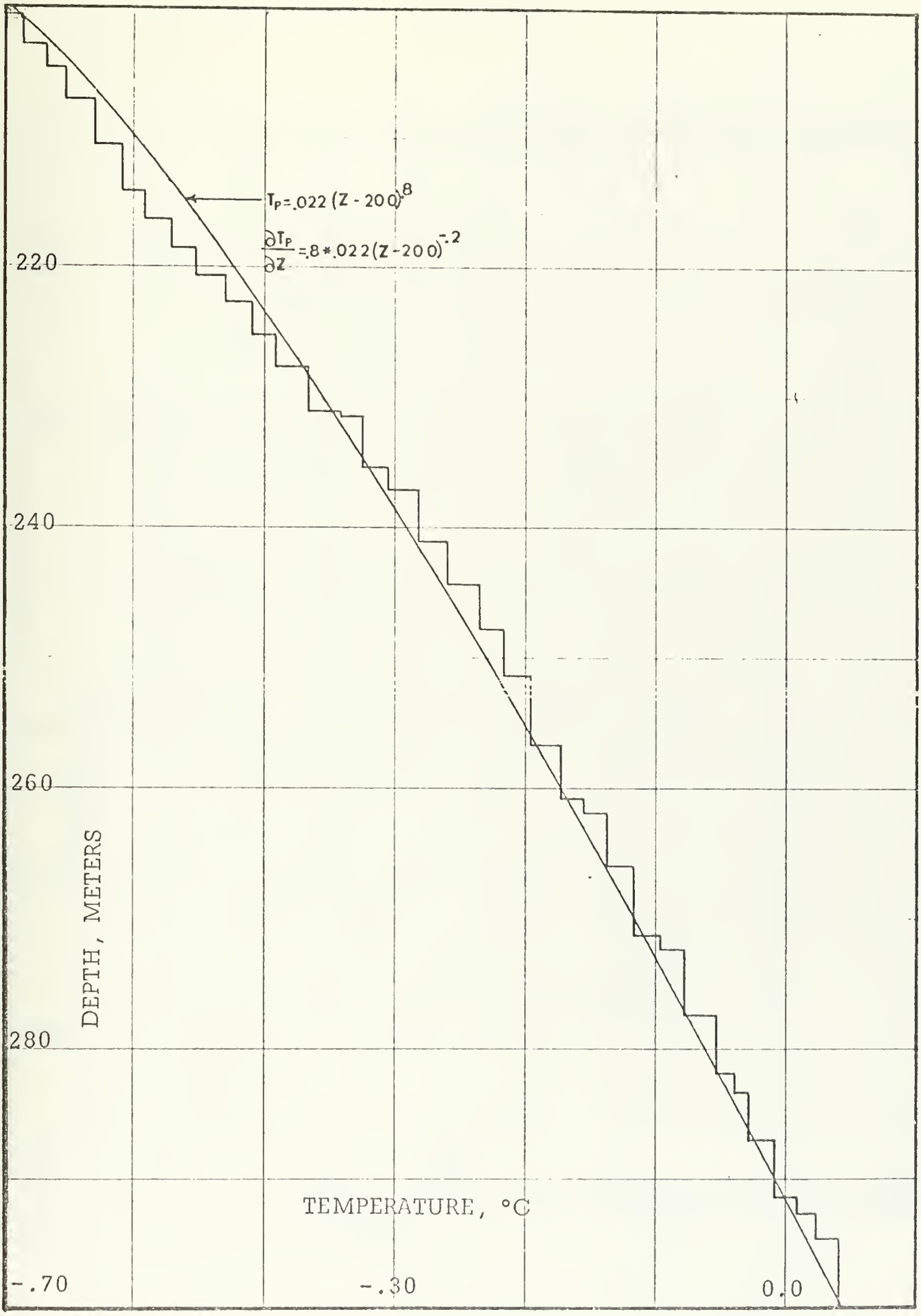

Figure 20. Profile composed of homogeneous layers separated by step-discontinuities in temperature.

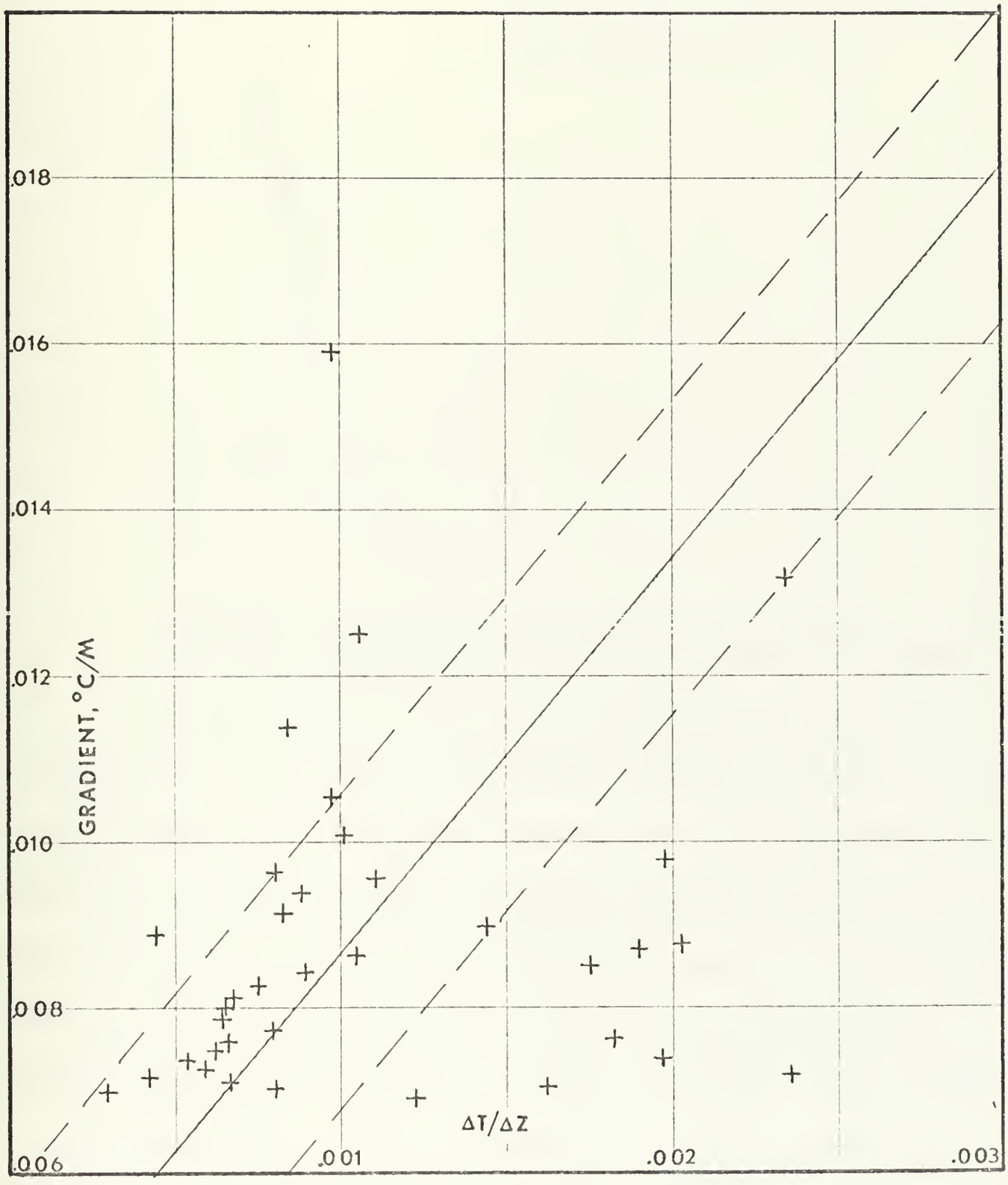

Figure 21. ΔT/ ΔZ vs. Gradient.

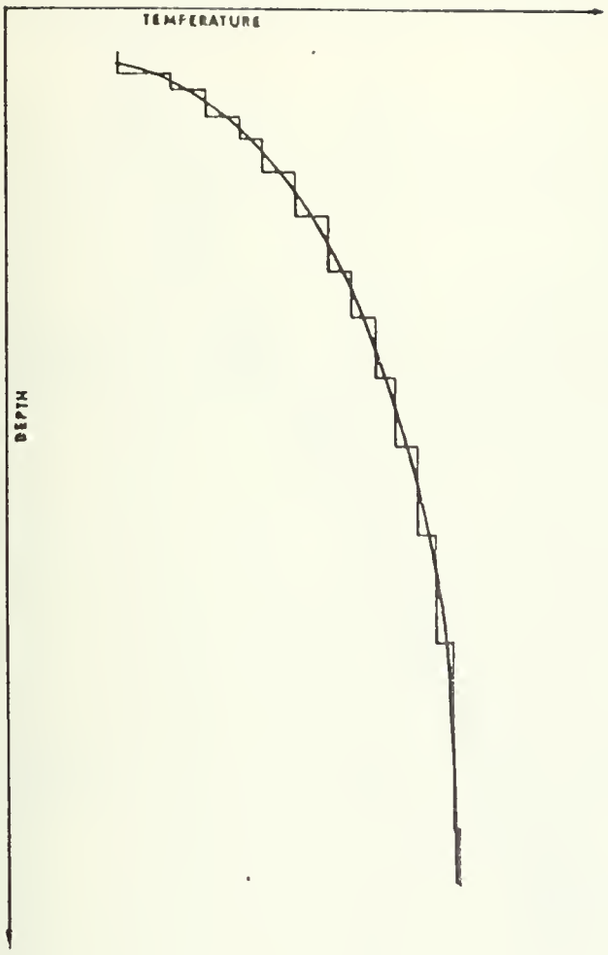

Figure 22. If layered structure is superimposed on a curved gradient, the layers must necessarily become thicker and the temperature steps must necessarily become smaller as the gradient becomes small.

6. Spectrum of Temperature Perturbations in the Depth Domain

The profiles were filtered by a modified binomial filter described by Roden [1971] using 50 cm sampling intervals. The mean profile was subtracted from the original profile resulting in a perturbation profile (Figure 23) which provides an excellent graphical description of the layered structure, and must be considered characteristic for this type of microstructure. The spectral density for the vertical temperature perturbations shows a decay coefficient of about -5/3 for high wave numbers (Figure 24), compared to a decay coefficient of -2 predicted by Phillips [1971] for this type of layered microstructure. Since the stepped structure resembles a square wave, energy from high wave numbers may be "folded back" during the Fourier analysis, resulting in an apparent

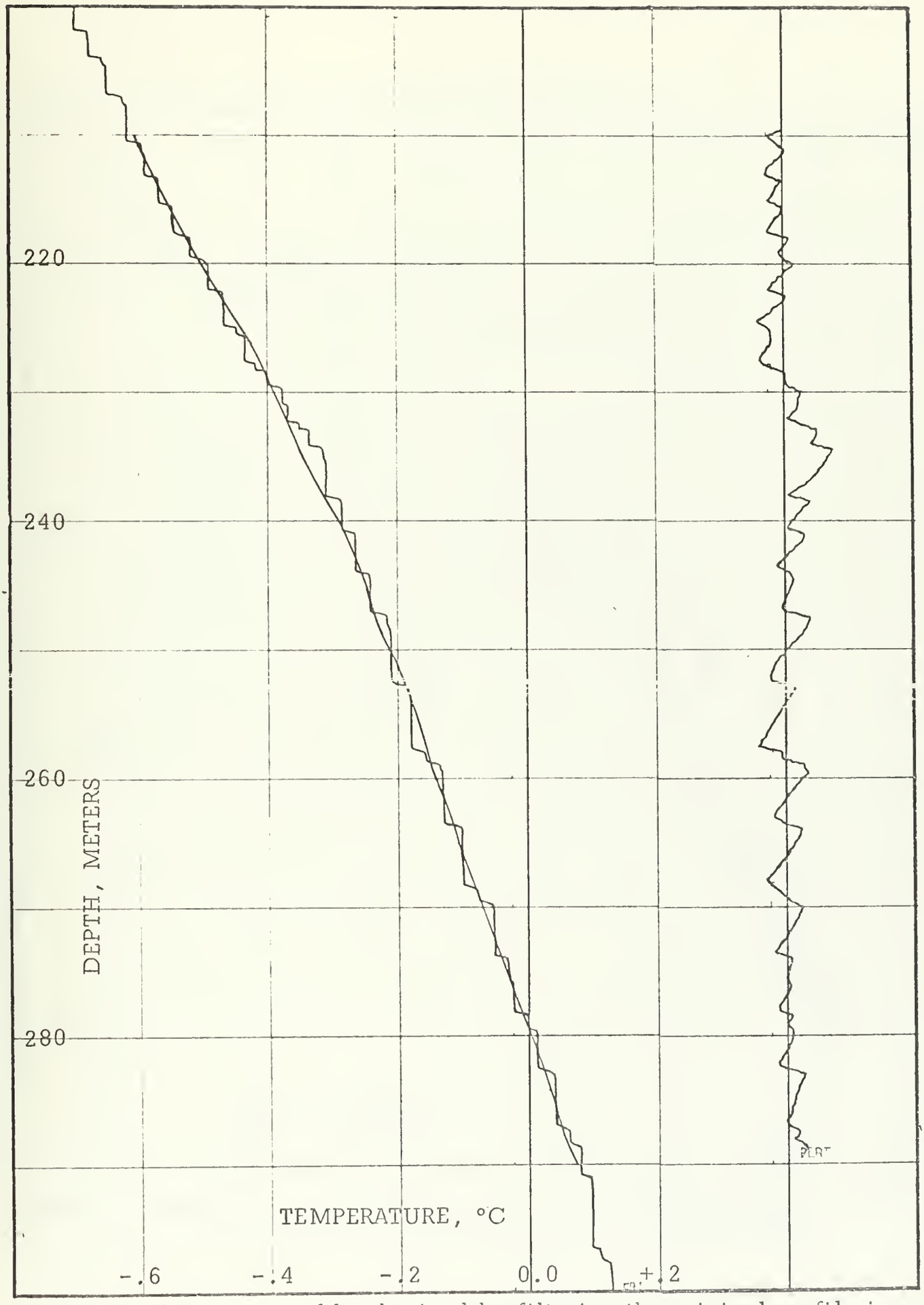

Figure 23. The mean profile obtained by filtering the original profile is subtracted from the original profile, resulting in the perturbation profile, which must be considered characteristic for layered microstructure.

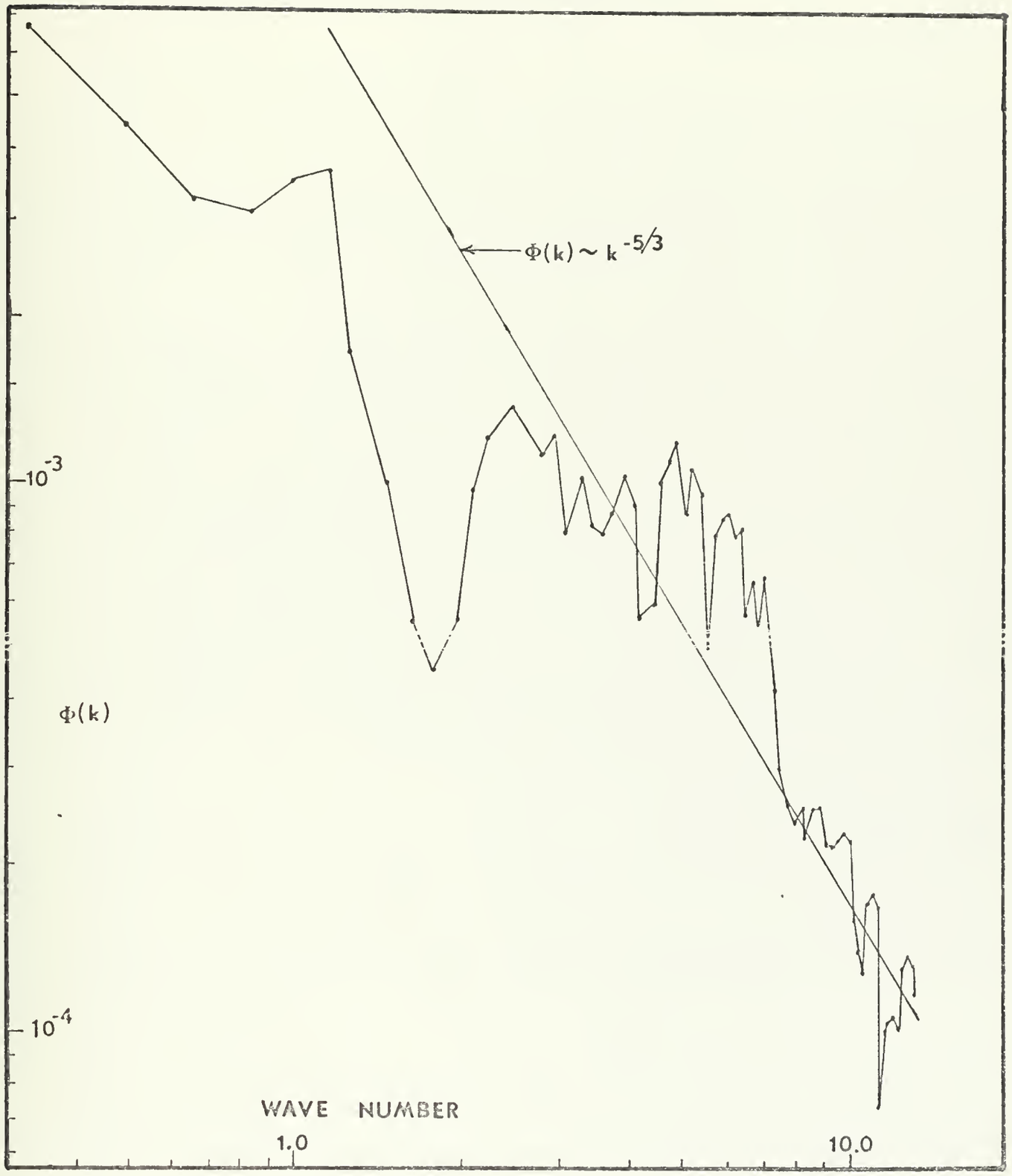

Figure 24. Spectral density of vertical temperature perturbations.

smaller decay coefficient. Roden [1971] observed a decay coefficient of -8/3 for data collected in the central North Pacific.

III. CURRENT MEASUREMENT

A. DESCRIPTION OF EQUIPMENT

The magnitude of the currents within the upper 200 m of the Atlantic water does not generally exceed 10 cm/sec [Neshyba et al 1971a], and it has been theorized that a vertical shear as small as .05 cm/sec/cm could produce Kelvin-Helmholtz instabilities leading to layer formation [op. cit.]. Since the Savonius-rotor type current meter has a nominal threshold velocity of 1.5 cm/sec [Woods Hole Oceanographic Institution 1967], an experimental high-resolution photographic current meter was developed to measure these low velocity currents. A buoyant, fluid-filled ping-pong ball, anchored in the field of an underwater movie camera, was photographed against a calibrated background grid. In the presence of a horizontal flow past the ball it was deflected from its equilibrium position by a distance proportional to the flow velocity. Calculations indicate that the threshold velocity of this current meter could be made substantially lower than the Savonius-rotor type, and good resolution at very low velocities could be obtained.

The current meter assembly is diagrammed in figure 25. Mounted on the background disc were a compass to determine current direction, a dye dispenser to provide observations of turbulence, and a clock. The ping-pong ball was anchored to the center of the disc with 4 lb monofilament line. The shutter mechanism was controlled by an intervalometer which

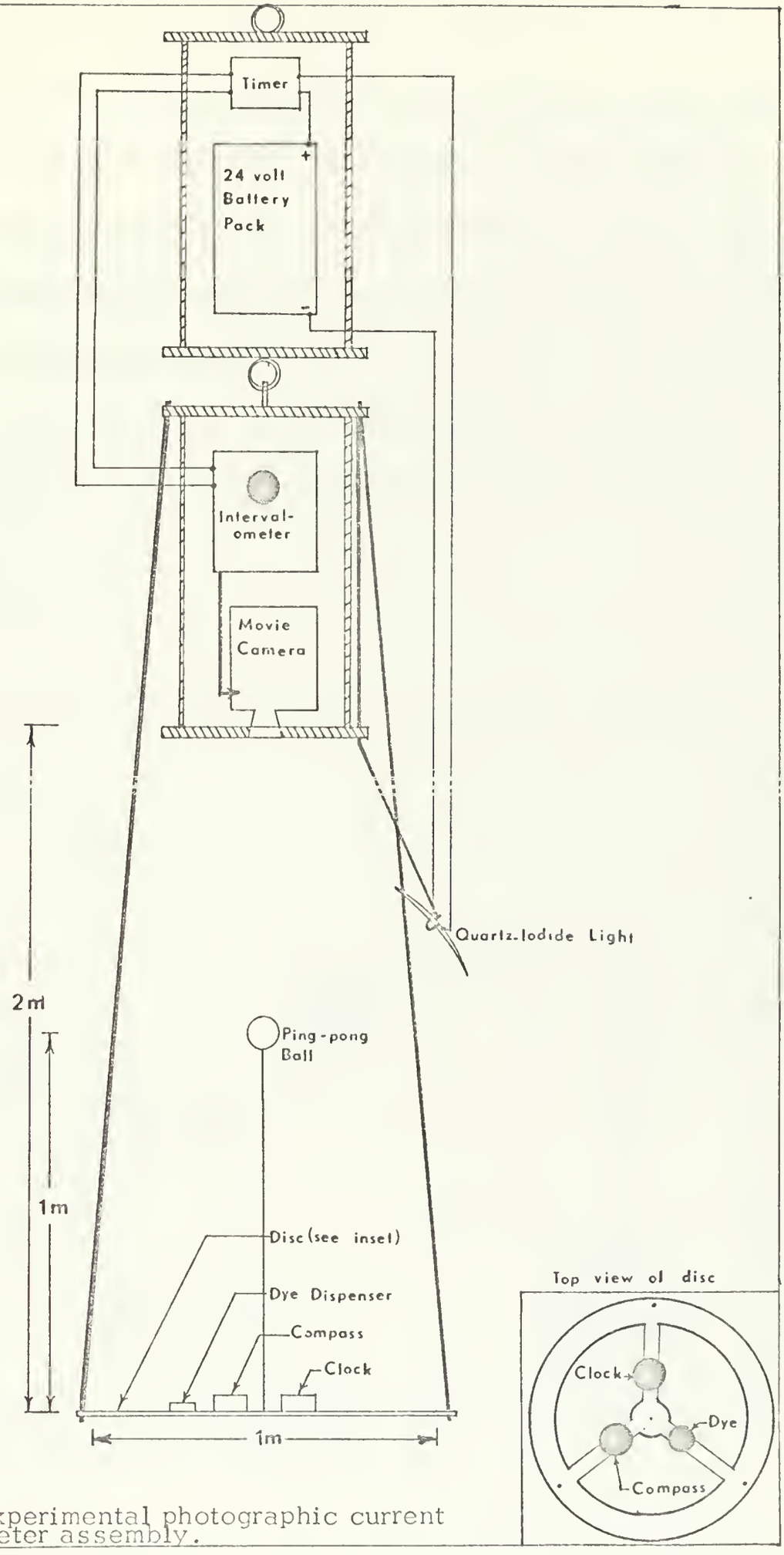

Figure 25. Experimental photographic current meter assembly.

tripped the shutter and advanced the film one frame every two seconds. This could be replaced by a timing mechanism which would allow the camera to operate continuously for five seconds each minute. A Hydro Products model LQ-2 75 watt quartz-iodide lamp, powered by four 6 V nickel-cadmium batteries, was mounted to the camera case. Operation of the light was controlled by the camera timing mechanism which consisted of a battery powered 1 rpm dc motor, a microswitch, and a relay (Figure 26). Each revolution of the motor caused the microswitch to be depressed for a short time period which activated the system.

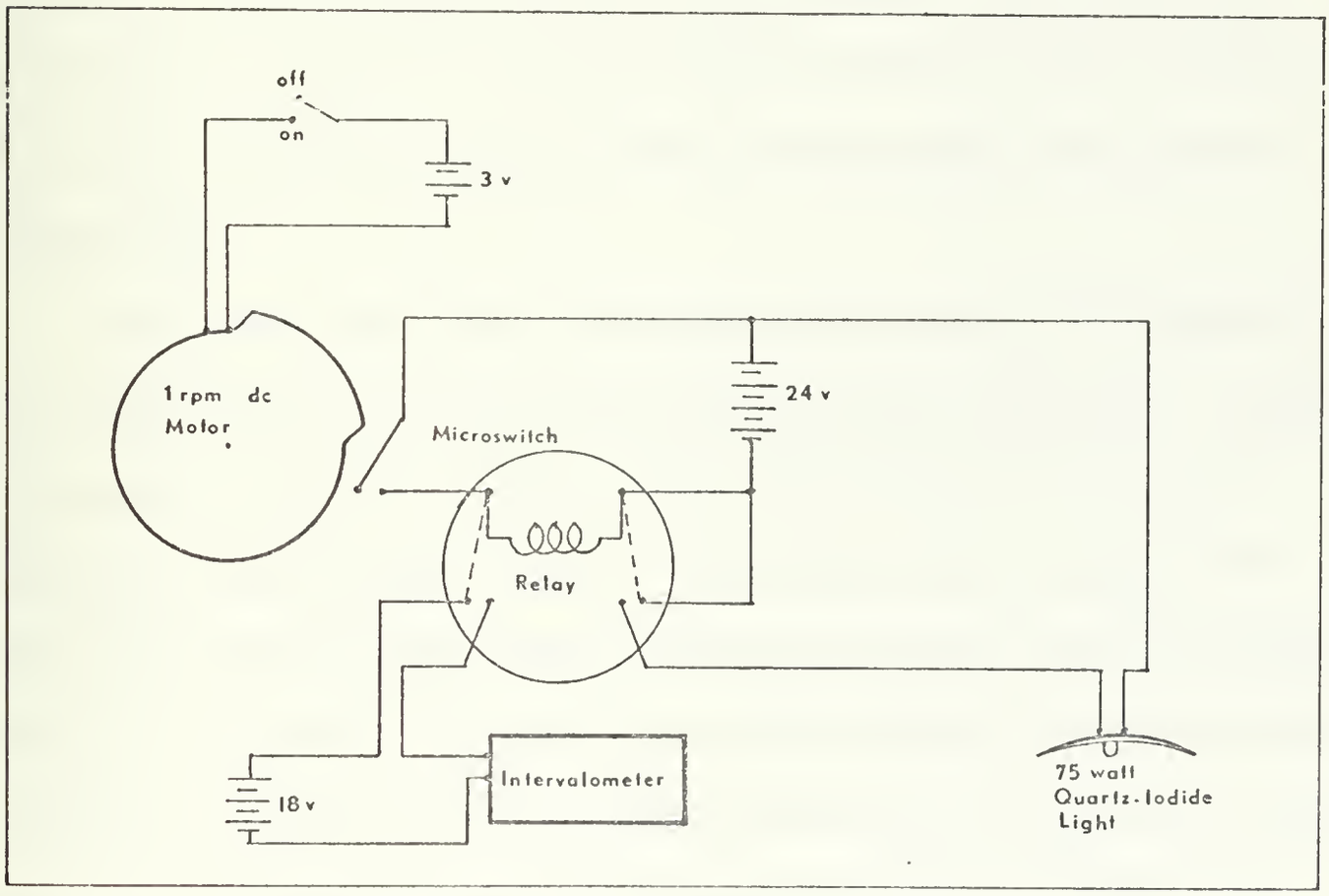

Figure 26. Current meter timing mechanism.

B. DISCUSSION OF DATA

Current measuring experiments were conducted during 14-16 March. With the temperature recording system calibrated for ten-meter depth intervals the current meter was positioned in ten discrete layers from 200 m to 219 m. The shutter was controlled directly by the timing mechanism, and the instrument remained in each layer for three minutes (15 seconds of film exposure). The resulting movie record shows the ping-pong ball in constant turbulent motion in all the layers, supporting the previous conclusion that turbulent convective overturning occurs in the layers. No current measurements were obtained within the interface sheets where laminar flow was expected. Since the basic equations from which the current meter was developed do not hold for turbulent flow, the velocity shear across the interfaces could not be calculated from the measurements within the turbulent layers.

Reasonably good current measurements were obtained by Neshyba et al [1971a] from T-3 (84-00N; 126-00W) in November 1969 with a Savonius-rotor current meter (Figure 27a). These measurements reveal a mean velocity of approximately 3 cm/sec. The vertical shear calculated from these measurements (Figure 27b) is extremely small due to the 5 m spacing. However, the range of velocities is more than sufficient to provide vertical shears of .05 cm/sec/cm if the shear occurred across a sharp density interface. High-resolution current measurements collected by Neshyba et al [op. cit.] show strong velocity shear across 15 cm intervals (Figure 28). Concurrent temperature and salinity measurements revealed significant temperature and density interfaces located at 297.8 m and 304.5 m.

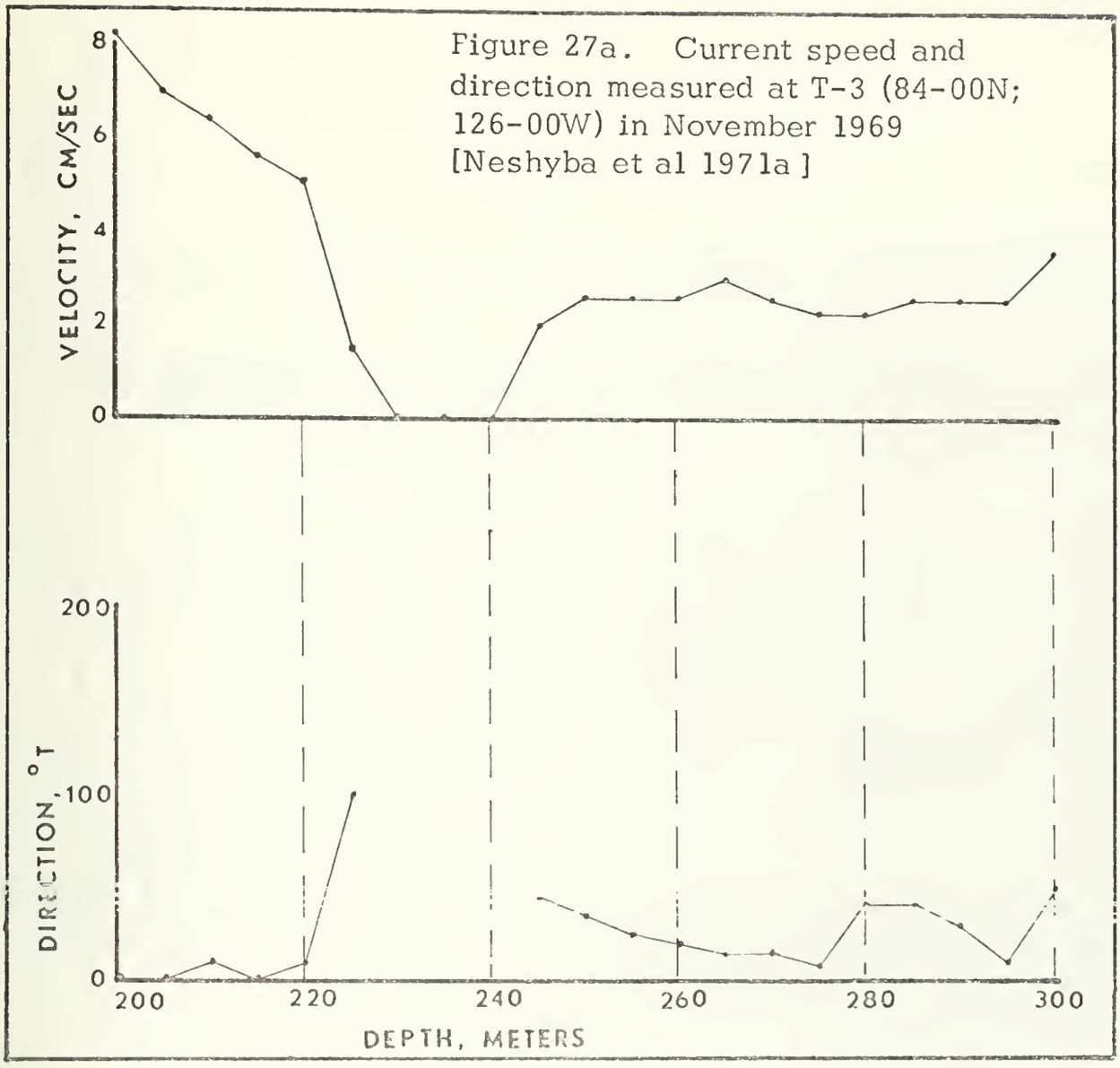

Figure 27a. Current speed and direction measured at T-3 (84-00N; 126-00W) in November 1969 [Neshyba et al 1971a]

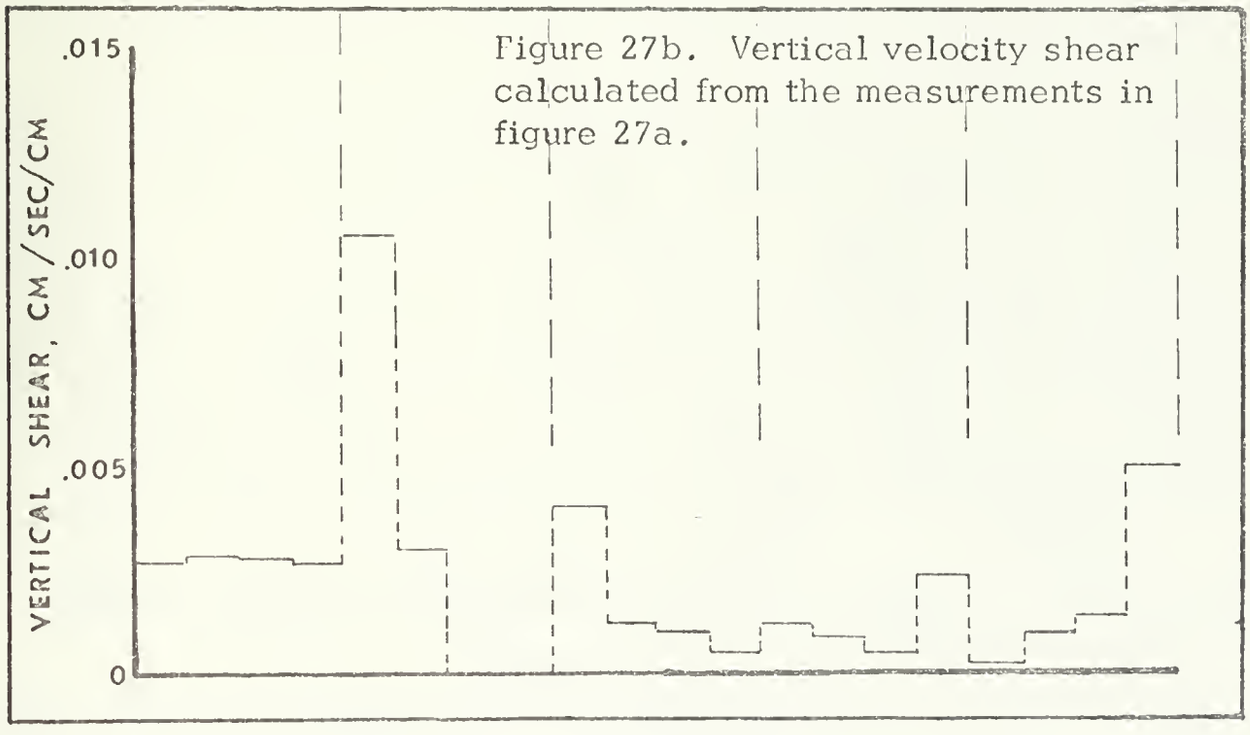

Figure 27b. Vertical velocity shear calculated from the measurements in figure 27a.

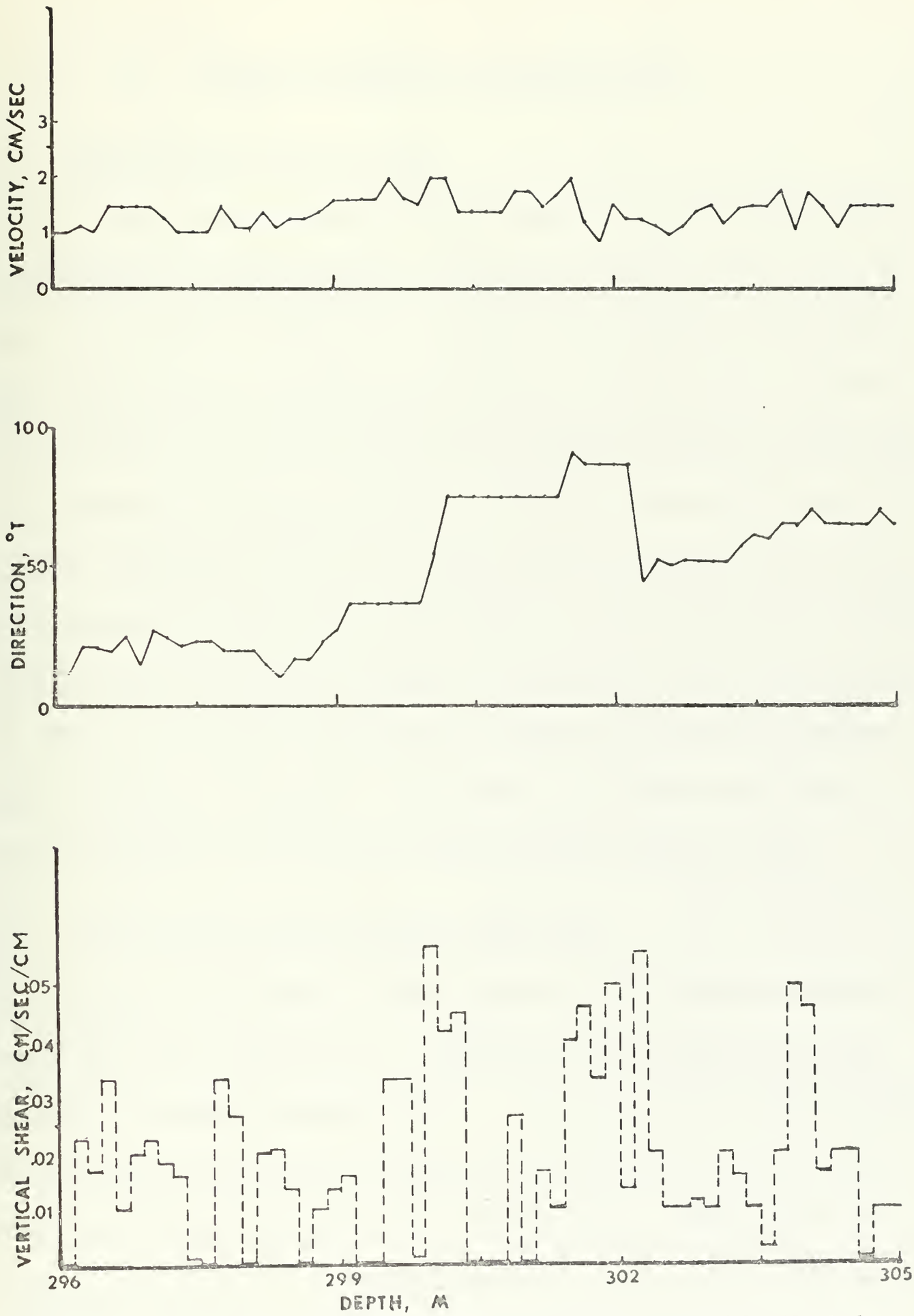

Figure 28. High-resolution current measurements obtained by Neshyba et al [1971a] , and calculated velocity shear.

IV. DENSITY DISTRIBUTION MEASUREMENTS

A. DESCRIPTION OF EQUIPMENT

A Bissett-Berman model 9070 STD recorder, an oceanographic instrument designed to measure salinity, temperature and depth, was employed from T-3 in March and April 1971. The data was recorded in digital form on a self-contained magnetic tape recorder in a pressure case. Salinity was measured by sensing conductivity and applying appropriate corrections for temperature and pressure effects by utilizing compensating networks to obtain a resolution of .001°/oo. Temperature was measured with a platinum resistance thermometer to a resolution of 0.015°C; depth was measured with a pressure transducer containing a strain-gage bridge to a resolution of .02%. The output from each sensing network was digitized, sequentially formatted for recording, and recorded as a 3-digit binary-coded decimal number at a pre-selected data sampling interval of 1 sec.

B. DESCRIPTION AND ANALYSIS OF STD DATA

Seven tapes of STD data were collected, each containing measurements from the surface to 500 m. The salinity measurements were calibrated with laboratory analyzed Nansen bottle samples that were collected from the same depth interval; temperature and depth were calibrated with the high-resolution XBT temperature profiling system. The temperature, salinity, and density (ρ_{S10}) profiles from 200-300 m are presented in Figure 29. It is observed that the density profile corresponds to the

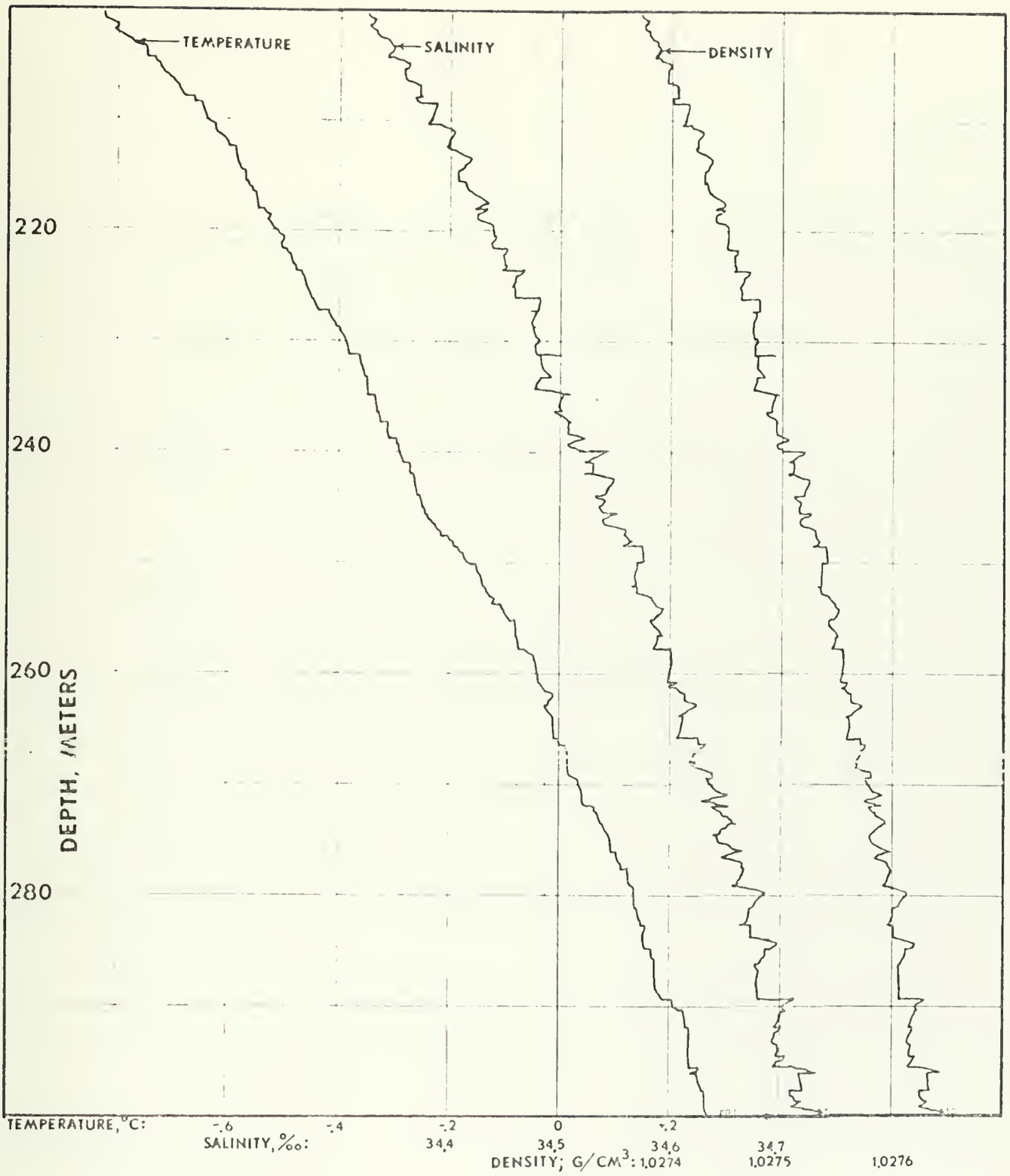

Figure 29. Temperature, Salinity, and Density profiles constructed from STD data collected in March 1971.

salinity profile. This was expected since the density ratio ($\beta\Delta S/\alpha\Delta T$) was calculated to have a nearly constant value of 7 for this water structure [Neshyba et al 1971a], where β is the coefficient of saline contraction, α is the coefficient of thermal expansion, ΔS and ΔT are the salinity

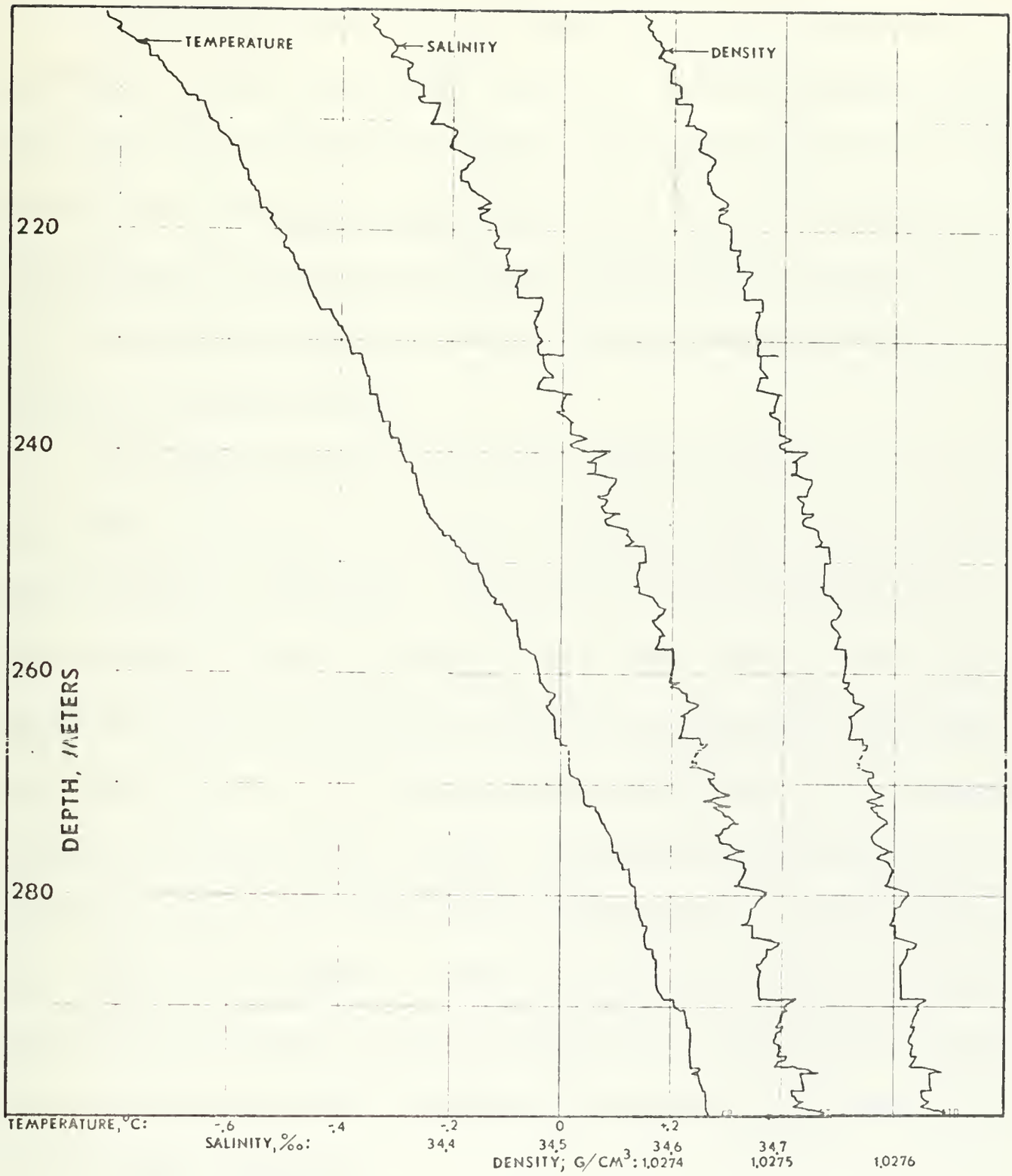

Figure 29. Temperature, Salinity, and Density profiles constructed from STD data collected in March 1971.

salinity profile. This was expected since the density ratio ($\beta\Delta S/\alpha\Delta T$) was calculated to have a nearly constant value of 7 for this water structure [Neshyba et al 1971a], where β is the coefficient of saline contraction, α is the coefficient of thermal expansion, ΔS and ΔT are the salinity

and temperature increases across an interface in parts per million and millidegrees Celsius respectively [op. cit.]. The perturbation profiles were calculated as described previously, and clearly illustrate the relation of the density and salinity profiles (Figure 30). The scale of temperature perturbations is the same as the density perturbations as expected; however it is obvious that the salinity is the controlling factor in determining the stability of the water column.

The TS-diagram (Figure 31) reveals that the water structure is generally stable, characterized by regions of extreme stability which are separated by regions of instability. Stable areas, which are illustrated by an approximate 45° slope to the right of the σ_t lines, are due to the coincidence of a temperature step and a salinity step. Extremely stable areas occur when a salinity step occurs within an isothermal layer, a phenomenon observed by Neshyba et al [op. cit.]. Relatively unstable regions are formed by a temperature step within an isohaline layer, and are illustrated by a vertical TS-distribution. Extreme instabilities occur when a salinity inversion exists within a nearly isothermal layer. These salinity inversions, which were first observed by Neshyba et al [op. cit.] , are characteristic of the salinity distribution.

Close examination of the layers containing salinity inversions reveals that the occurrence of these inversions is not necessarily dependent upon the relative positions of the salinity and temperature steps as suggested by Neshyba et al [op. cit.] . If the inversions are assumed to be permanent features, their presence contradicts the conclusion that the homogeneous

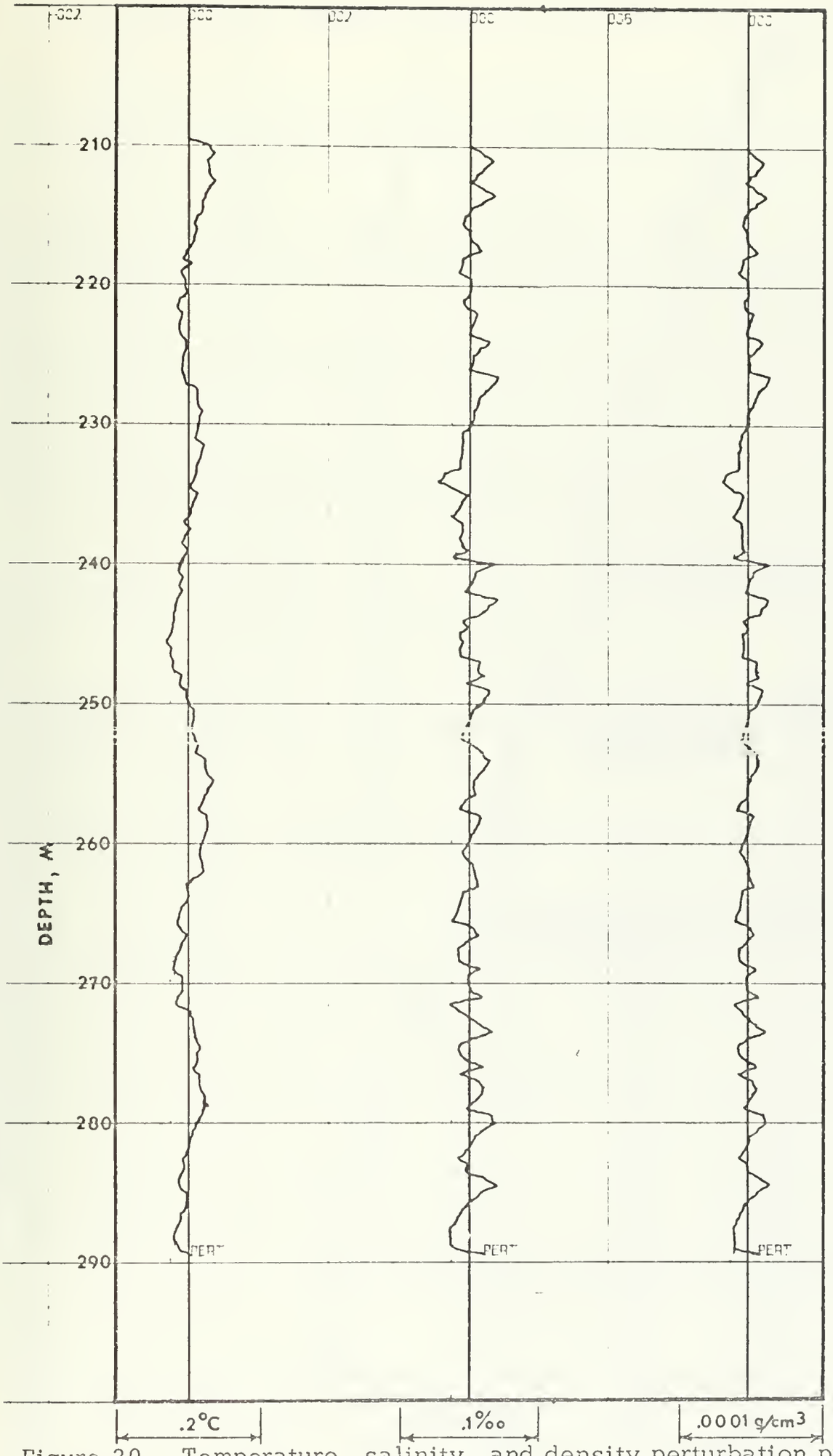

Figure 30. Temperature, salinity, and density perturbation profiles, calculated from the STD profiles illustrated in figure 29.

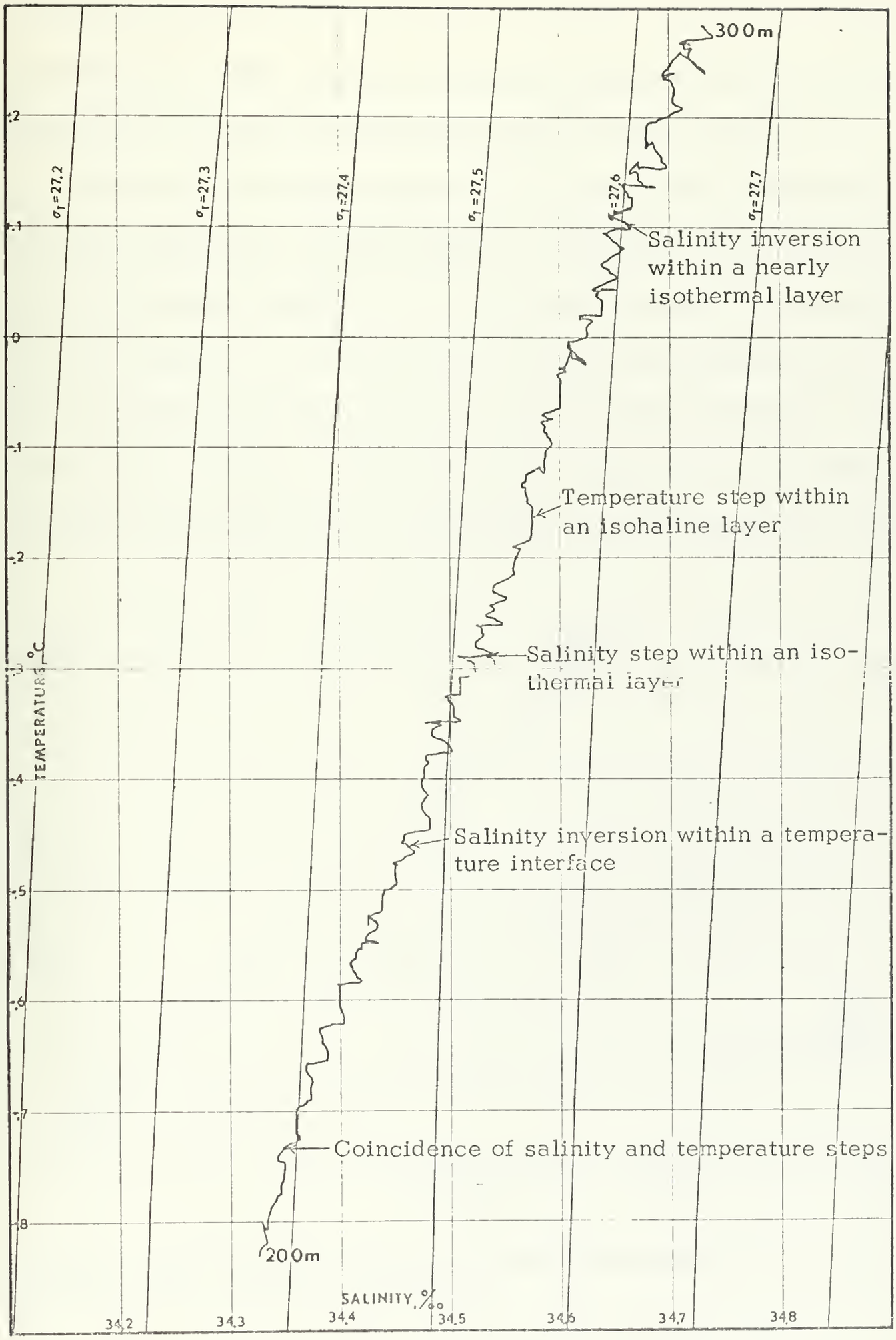

Figure 31. TS-diagram constructed from STD data collected at T-3 in March 1971.

temperature layers result from convective turbulence. However, it is certain that these salinity inversions are not permanent, but are short-lived intermediate features associated with a slow convective process.

It has been shown by Neshyba et al [op. cit.] that the distribution of salinity differences ΔS and temperature differences ΔT is bounded if dynamic equilibrium conditions exist. The scatter diagram produced from STD data collected at T-3 in November 1969 (Figure 32) illustrates the two theoretical boundaries. It has been calculated that equilibrium conditions at any level within an intermediate layer between two semi-infinite, well-mixed layers exist only if the interfaces are characterized by a density

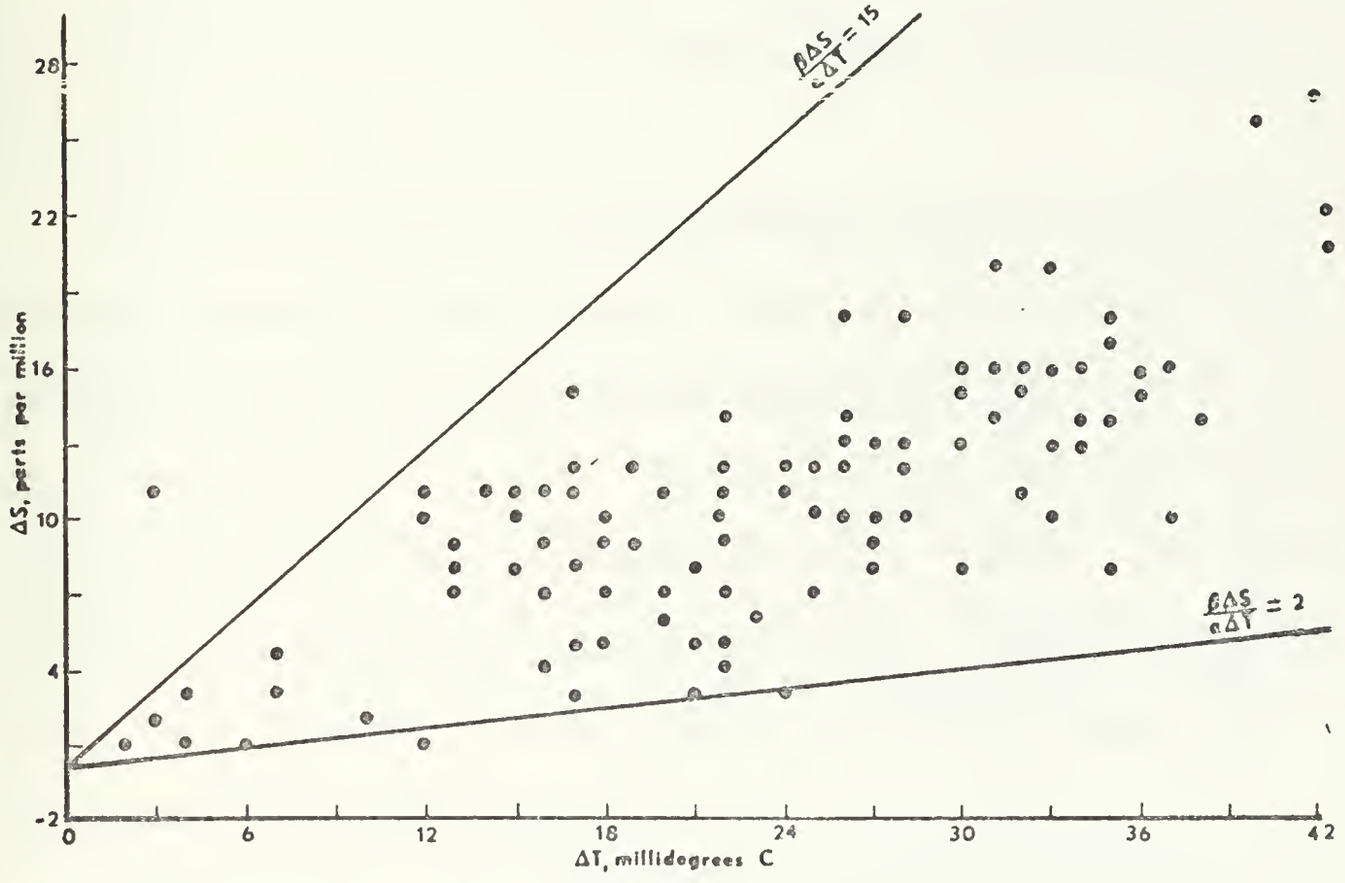

Figure 32. Scatter diagram produced from STD data collected at T-3 in November 1969 [Neshyba et al 1971a].

ratio greater than two, which forms the lower boundary. Turner [1965] showed that the ratio of the potential energy gained by salt lifted through an interface to that released by the accompanying transfer of heat has a value of 0.15 for interfaces having density ratios greater than two. An extrapolation of this relationship results in a density ratio of 15, which is the maximum allowable density ratio under diffusive conditions, and forms the upper boundary. The conclusion was reached that there was no turbulent mixing within the interfaces, but rather mixing due to the differing diffusion characteristics of heat and salt [Neshyba et al 1971a] . While the temperature resolution of the STD records obtained in March and April 1971 is not high enough to conduct a similar analysis, the same conclusion is evident from the temperature and salinity profiles, and corresponding TS-diagram.

The spectral estimates of the perturbations generated by traversing the density profile vertically (Figure 33) show a decay coefficient between -4/3 and -1. The -2 decay coefficient predicted by Phillips [1971] should also be true for this data, and it is possible that energy was added to the higher wave numbers during the Fourier analysis by "folding," as discussed in relation to the temperature perturbation spectrum. A decay coefficient between -8/3 and -3 was observed by Roden [1971] for density profile perturbations in the North Pacific.

Johns and Cross [1970] have shown that the formation of homogeneous density layers is associated with the rate of energy dissipation and dynamical stability of the various modes of propagating internal waves.

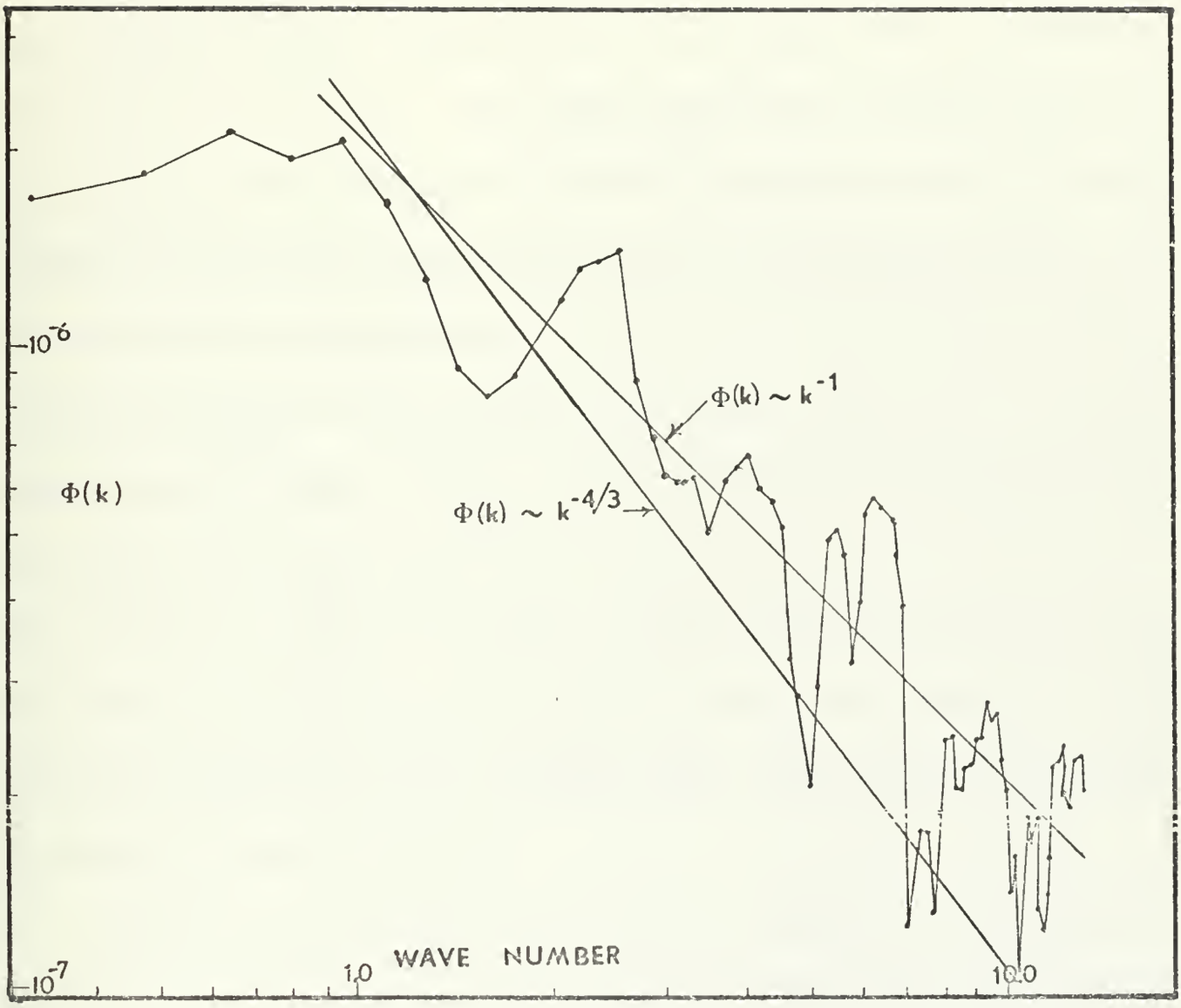

Figure 33. Spectral density for perturbations in the density profile, calculated from STD data collected at T-3 in March and April 1971.

They concluded that the dynamical stability of the internal modes is greatly increased by an increase in the number of layers. The stability criteria is based on the local Richardson's number ($Ri = \frac{\rho}{g} \frac{\partial \rho}{\partial z} / \left[\frac{\partial U}{\partial z}\right]^2$). Whenever $Ri < .25$ the internal waves become unstable, break, and lead to local turbulence causing the formation of homogeneous layers. For a specified density gradient, layers will continue to form until the stability criteria are met. Thus there are upper and lower limits on the number and

size of the layers. Generalizing, the stronger the gradient, the more layers will be formed. With a weak gradient, only a small number of relatively thick layers will be formed. The profiles discussed in Section II are in good agreement with this theory. However, considerable doubt is raised concerning the estimate of horizontal extent of the layered structure. Since the higher-order internal wave modes are heavily damped as their energy is dissipated in the formation of the layers, they cannot propagate more than a few cycles [op. cit.]. It must therefore be assumed that the deep draft of the island is the source of the internal waves which lead to layer formation. If this is the case, then the layered microstructure must be considered a phenomenon characteristic of the water under T-3 and other large ice islands or deep draft pressure ridges, and cannot be generalized to include the entire Arctic Ocean.

If the motion within the layers remained turbulent for long periods of time the layered structure would be sustained in the absence of the engendering internal waves. Since the density within the layers is nearly uniform, a very slight vertical shear in the velocity will produce a Richardson's number less than the critical value of .25. Assuming geostrophic conditions, the vertical shear can be related to the vertical density gradient ($\partial\rho/\partial z$) and the slope of the density interfaces by

$$\frac{\partial U}{\partial z} = \frac{g}{f\rho}\frac{\partial \rho}{\partial z}\tan\gamma$$

where f is the Coriolis parameter and γ is the slope of the density interfaces. The isobaric slope is assumed to be negligible [Neumann

and Pierson 1966]. The isopycnal slope can be expressed in terms of the Richardson's number Ri

$$\gamma = \tan^{-1} \frac{f^2 \rho}{Ri\ g \frac{\partial \rho}{\partial z}}$$

Using a critical Ri of .25 and observed values of ρ and $\partial\rho/\partial z$, Table I was computed showing the critical slope and velocity shear required to produce Kelvin-Helmholtz instability across density interfaces. It is significant that the critical slope decreases and the critical shear increases with increasing gradient.

Table I

ρ	$10^6 \partial\rho/\partial z$	γ	$\tan\gamma$	$\partial u/\partial z$
1.0275	0.5	0° 45.32'	.013184	.044
⋮	1.0	0° 32.05'	.009323	.062
	1.5	0° 26.17'	.007612	.076
	2.0	0° 22.66'	.006592	.088
	2.5	0° 20.27'	.005896	.099
	3.0	0° 18.50'	.005382	.108
↓	3.5	0° 17.13'	.004983	.117

The density gradient-velocity shear relationships can be organized into five distinct cases, each affecting the density interfaces in a different way. These five cases are diagrammed in Figure 34 (a-e). The first case shows a strong velocity shear associated with a relatively weak density gradient. The Richardson's number decreases below the critical value, and the resultant breaking Kelvin-Helmholtz waves produce turbulent mixing within the interface, creating an intermediate layer. The second case depicts a constant velocity shear of moderate magnitude across a strong

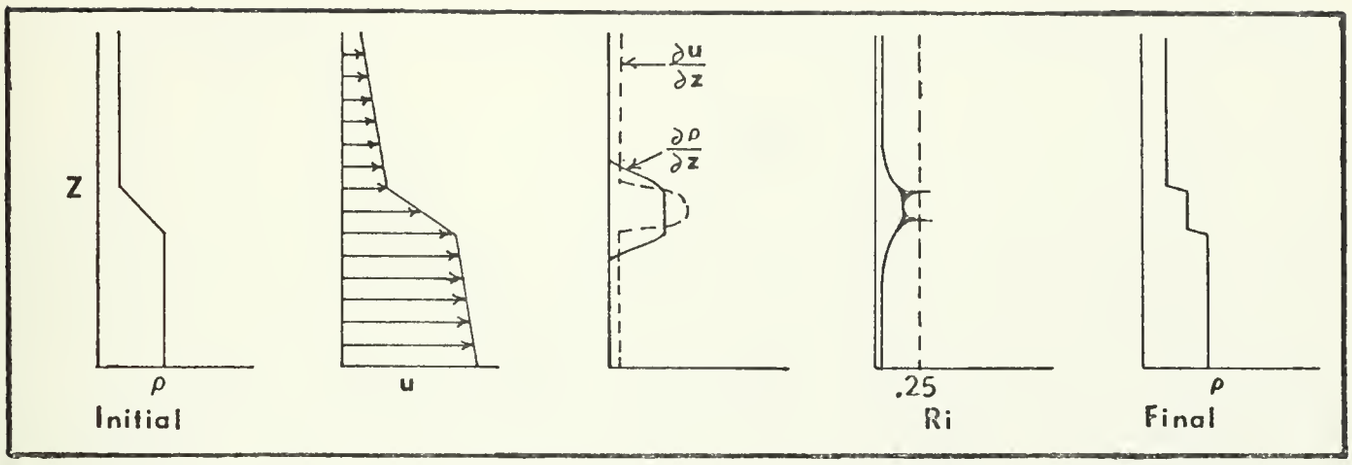

Figure 34a. Strong vertical shear across a weak density interface will produce a Richardson's number less than the critical value of .25 in the interface, resulting in the formation of a half-step. (Case 1)

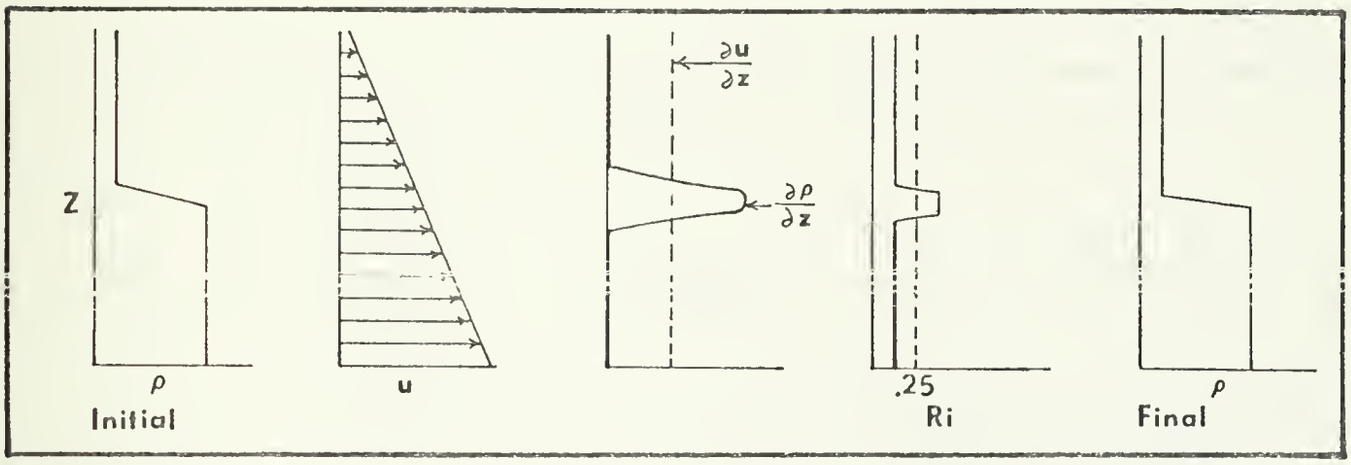

Figure 34b. Moderate vertical shear across a strong density interface will increase the turbulence in the layers, which act to increase the gradient within the interface. (Case 2)

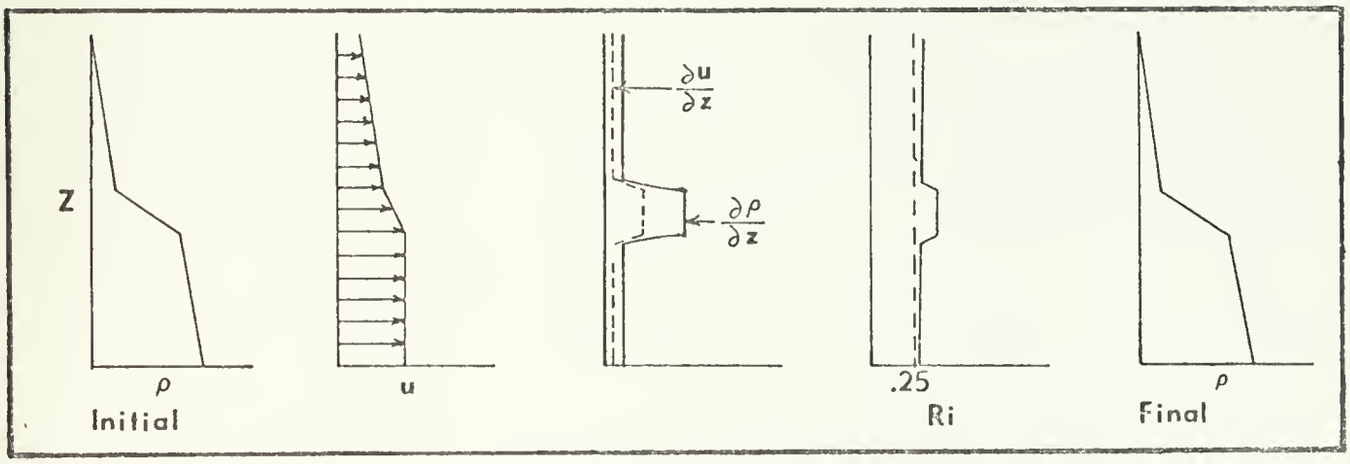

Figure 34c. Weak vertical shear across an interface will never produce the critical Richardson's number, and the structure remains unchanged. (Case 3)

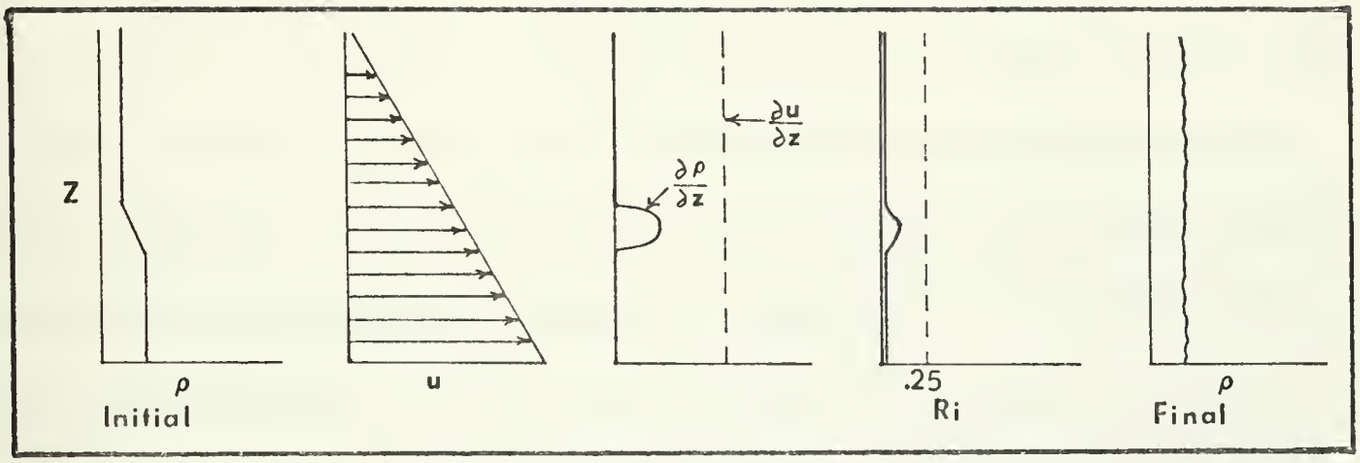

Figure 34d. Strong vertical shear across a weak interface and the adjacent layers will destroy the structure. (Case 4)

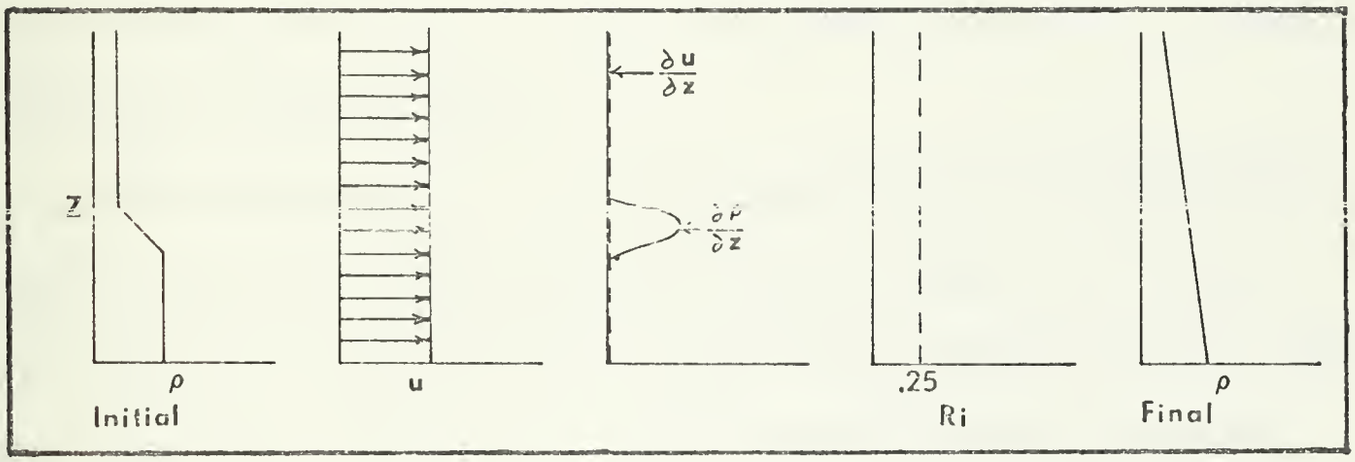

Figure 34e. In the absence of vertical shear, the double-diffusion mechanism will act to destroy the interface, resulting in a smooth gradient. (Case 5)

density gradient and into the adjacent layers. The Richardson's number is less than .25 in both layers, but is greater than .25 in the interface. The resulting turbulence in the layers will tend to increase the gradient within the interface. In the third case the weak velocity shear across a moderate density gradient never produces a critical Richardson's number and there is essentially no change to the structure. The fourth case depicts very strong shear extending through two layers separated by a weak interface gradient. The entire structure becomes turbulent, destroying the interface. The final case occurs when there is no shear. Since the flow within the layers is laminar, the interface disappears because of diffusion, resulting in a smooth gradient.

The existence of cases 1, 2, and 3 is indicated on the temperature profile records, and explains the overall general stability of the layers. Intermittent half-step formation is related to the conditions of case 1. The rapid elimination of layers, illustrated by the many small, short-lived steps at 220-230 m, may be attributed to the mechanism of case 4. Case 5 is an illustration of the gradual elimination of layers by diffusion, as proposed by Stommel and Fedorov [1967], and is not indicated on the temperature profile records. It is suggested that the dissipation of energy by decaying internal wave modes may be responsible for the initial formation of layers, and that the differing diffusion characteristics of heat and salt, coupled with weak vertical shear is the dominant combination of mechanisms responsible for sustaining the layered structure. Further research is necessary to determine if the formation of layers is confined to the vicinity of large ice islands.

Comparative profiles from T-3 obtained in March 1969 [Denner 1971], November 1969 [Neshyba et al 1971a] and March 1971, and from ARLIS V [Denner 1971] are presented in figure 35. Locations are indicated by figure 36. It is observed that the profiles collected from T-3 show nearly identical layered structure, while the profile collected from ARLIS V is anomalous in that the layered structure is several orders of magnitude smaller and not well defined. From the evidence presented in this study it appears that the necessary internal waves were absent from the ARLIS V area, providing further evidence that the internal waves are generated only under large, deep-draft ice islands or pressure ridges.

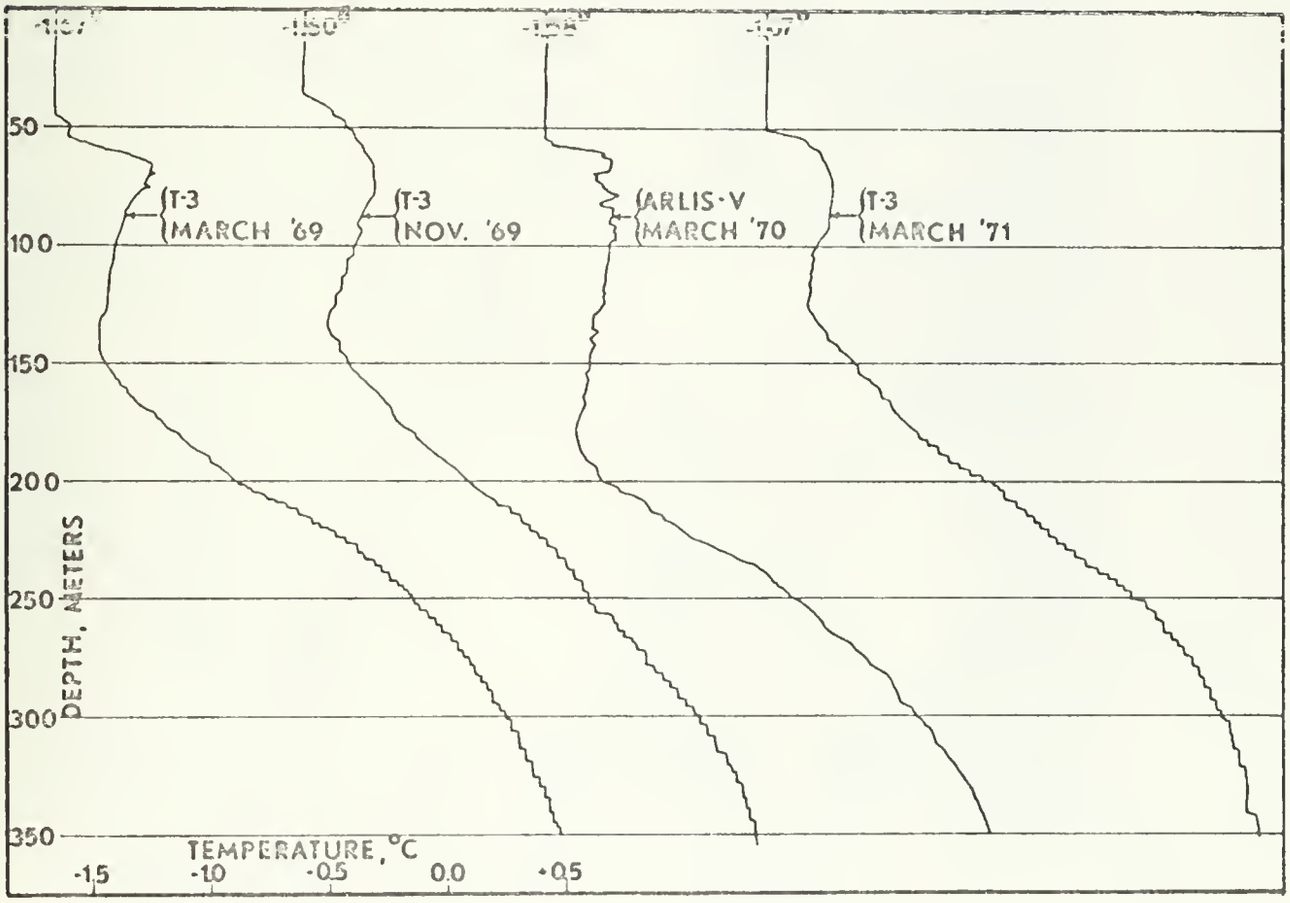

Figure 35. Comparative profiles obtained from T-3 at different times and locations, and ARLIS V.

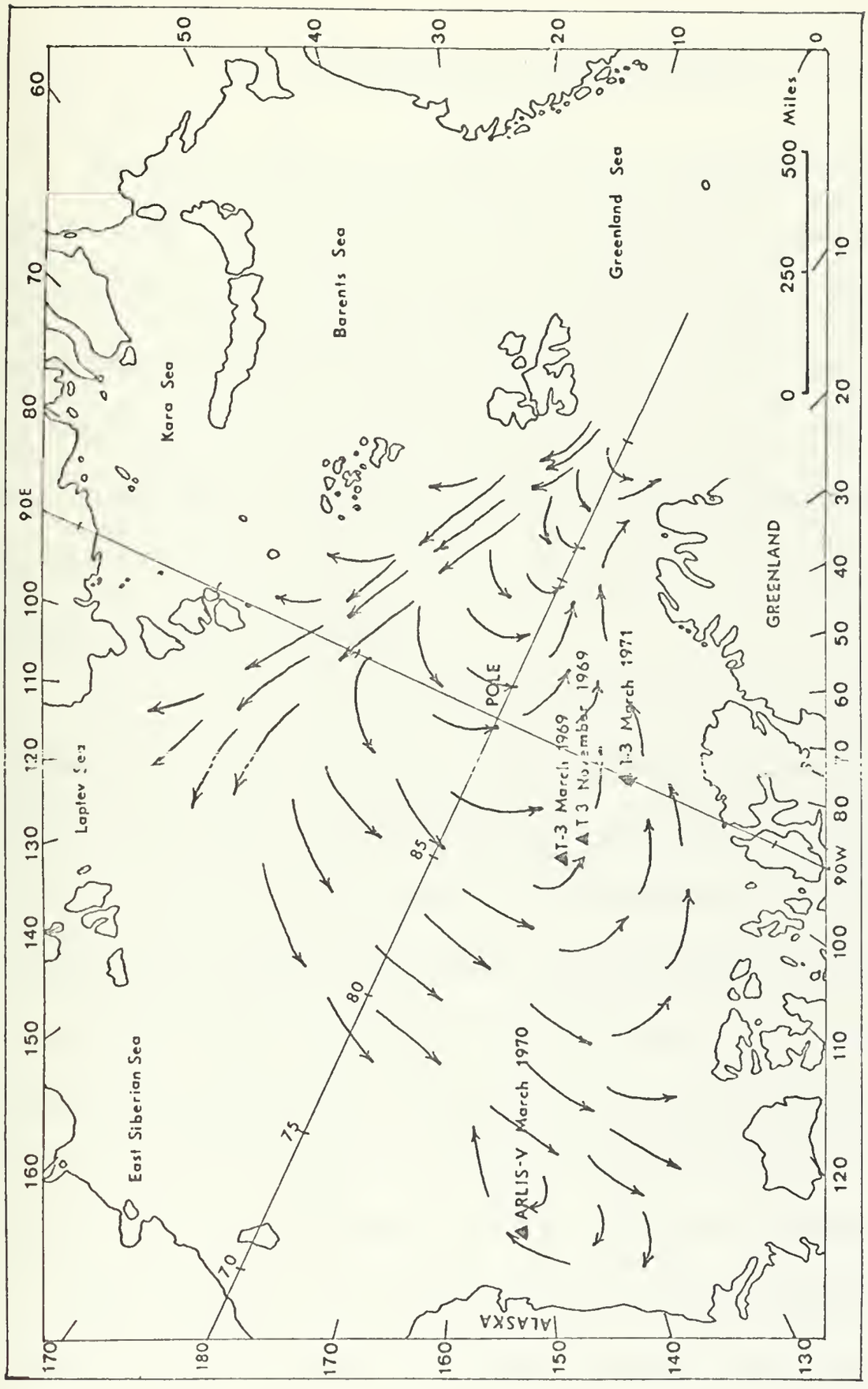

Figure 36. Locations of T-3 and ARLIS V.

VI. SUMMARY AND CONCLUSIONS

The microstructure of the upper 200 m of the Atlantic water in the Arctic Ocean beneath Ice Station T-3 is composed of discrete layers. These layers appear to have a lifetime of several weeks, and may extend some tens of nautical miles in the horizontal. The lifetime is not limited by either diffusive or turbulent transfer of heat and salt in the vicinity of T-3, and appear to be formed by locally generated internal waves. Since upward fluxes of heat and salt occur through the layers they must be in a state of dynamic equilibrium.

The flow in the interface sheets is laminar and the layers are characterized by turbulent convective mixing. The interfaces are sustained by weak vertical shear, and the formation of new layers is associated with local strong vertical shear produced by dissipating internal wave modes. Weak shear produced by geostrophic density currents may sustain the layers for long periods after the initial formation. The internal wave spectrum indicates that the energy decreases with $(\text{frequency})^{-4/3}$. However, the spectrum of temperature perturbations measured with a fixed sensor decreases with $(\text{frequency})^{-2}$ as predicted by Phillips [1971].

The thickness of the layers and the size of the temperature increase between layers are related to the mean gradient, with the ratio of the temperature increase to the layer thickness decreasing markedly with decreasing mean gradient. This relation was predicted by Johns and Cross

[1970] when considering layer formation by internal waves. The spectral density of the temperature perturbations in the vertical profile decreases proportionally as (wave number)$^{-5/3}$.

The density profile coincides exactly with the salinity profile, and is relatively unaffected by the destablizing effect of the temperature profile. Temperature interfaces do not necessarily coincide with salinity interfaces, the various combinations of interfaces creating differing stability. Salinity inversions are characteristic of the salinity profile and are suggestive of a slow convective process involving the transfer of heat and salt. The distribution of salinity and temperature differences between layers is bounded by limiting equilibrium density ratios, indicating that the transfer of heat and salt across the interface sheets is not turbulent, but is governed by the differing diffusion characteristics. The spectrum of density perturbations in the vertical profile is characterized by a decay coefficient between -4/3 and -1.

APPENDIX A

CALCULATION OF CURRENT VELOCITY

The Reynolds number ($Re = \frac{uD}{\nu}$) was calculated to be 2114 where:

u = current velocity = 10 cm/sec

D = diameter of ball = 3.81 cm

ν = kinematic viscosity of sea water = 1.80×10^{-2} cm^2/sec.

The corresponding coefficient of drag C_D is .4 [Schlichting 1960]. Assuming horizontal, irrotational laminar flow, and negligible drag on the anchor line, the velocity can be related to the drag force by:

$$F = \frac{1}{2} C_D \rho_w A u^2 \text{ (dynes)} \qquad (1)$$

where:

F = force on ball due to the velocity field

ρ_w = density of sea water

A = cross-sectional area of ball

The tension of the anchor line balances the horizontal current force and the vertical buoyancy force, B (Figure 37)

$$B = (\rho_w - \rho_B) V g \text{ (dynes)} \qquad (2)$$

where g is the acceleration of gravity (cm/sec^2).

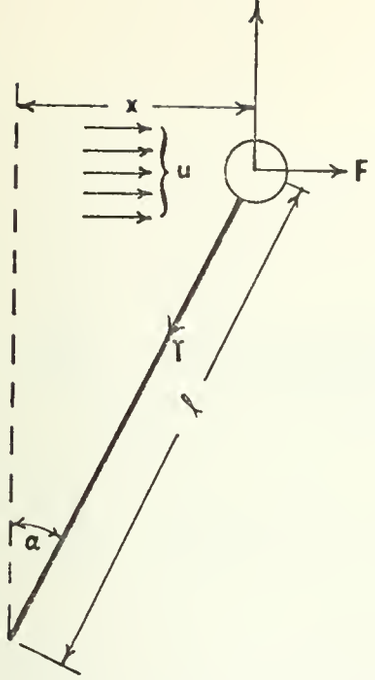

α = displacement angle

l = anchor line length

x = horizontal displacement

Figure 37

From figure 37 it is seen that:

$$\alpha = \tan^{-1}\left(\frac{F}{B}\right) = \tan^{-1}\left[\frac{C_D \rho_w A u^2}{\rho_w - \rho_B V g}\right] \qquad (3)$$

and: $x = l \sin \alpha$. (4)

The horizontal displacement x is measured with the current meter, and the magnitude of the current velocity is calculated from (3) and (4):

$$u = \left[\frac{2Vgx(\rho_w - \rho_B)}{C_D \rho_w A l \sqrt{1 - (x/l)^2}}\right]^{\frac{1}{2}} \text{ (cm/sec)} \qquad (5)$$

Figure 38 shows the current meter response based upon the following values:

ρ_w = 1.02737 g/cm^3

$V = \frac{1}{6} D^3 = 28.96$ cm^3

g = 997 cm/sec^2 (average for 85°N latitude)

C_D = 0.4

$A = (\frac{D}{2})^2 = 11.4$ cm^2

l = 100 cm

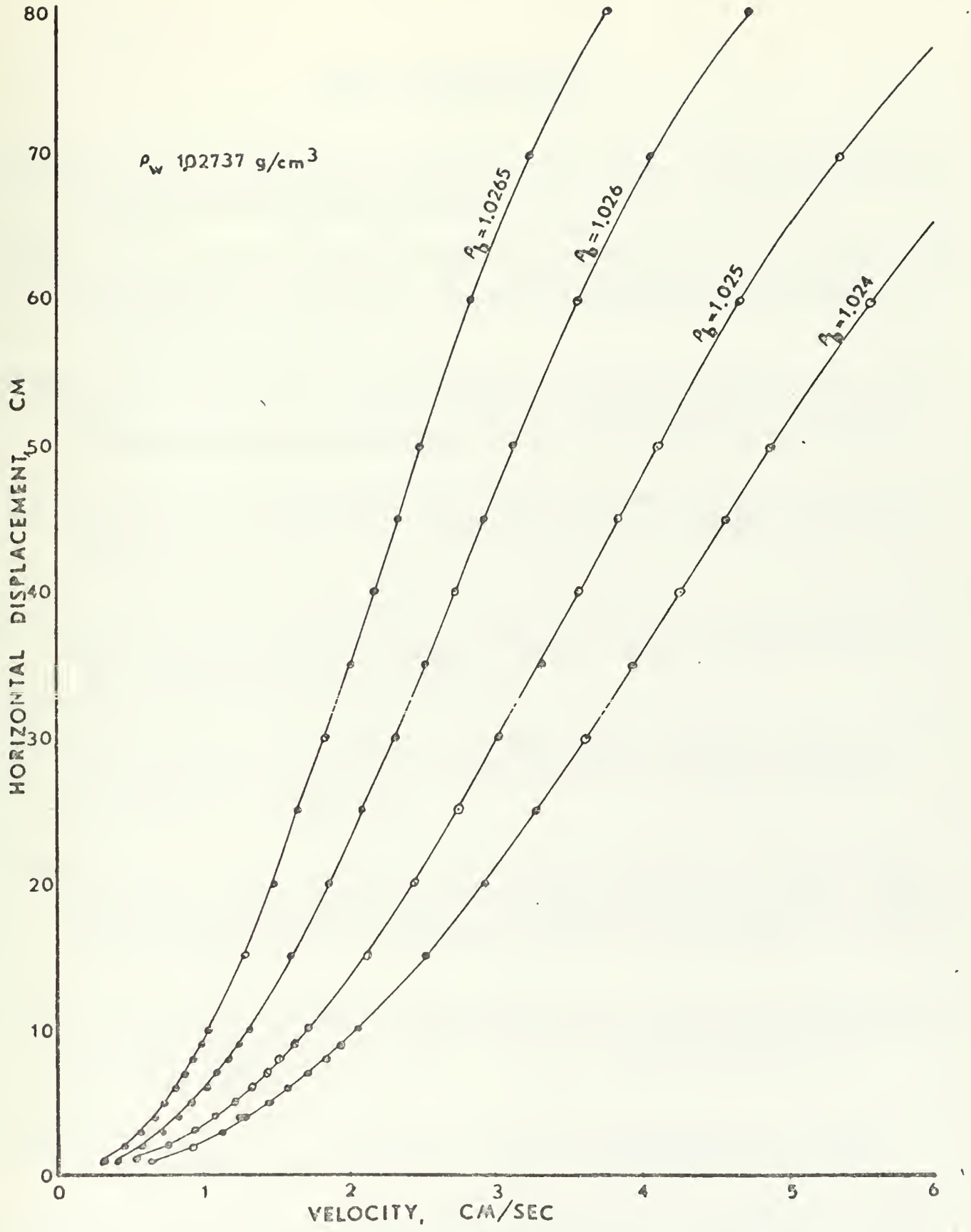

Figure 38. Experimental Photographic Current Meter Calibration Curve.

LIST OF REFERENCES

Coachman, L.K (1962): Water Masses of the Arctic, Proc. of the Arctic Basin Symposium October 1962, Hershey, Pa., 143-167.

Cooper, J.W. and H. Stommel (1968): Regularly Spaced Steps in the Main Thermocline Near Bermuda. Journal of Geophysical Research, 73: 5849-5854.

Denner, W.W. (1969): The Significance of Layered Stratification in the Arctic Ocean to Acoustic Propagation. Paper presented to the American Geophysical Union, San Francisco, Cal., 17 Dec 1969.

_____ (1971): The Layered Microstructure and Acoustic Propagation in the Arctic Ocean. U. S. Navy Journal of Underwater Acoustics, 39: 45-51.

_____ , V. T. Neal, and S. J. Neshyba (1971): A Modification of the Expendable Bathythermograph for Thermal Microstructure Studies, Deep Sea Research, 18: 375-378.

Johns B. and M. J. Cross (1970): The Decay and Stability of Internal Wave Modes in a Multisheeted Thermocline, Journal of Marine Research, 28: 215-224.

Neshyba, S. J., V. T. Neal and W.W. Denner (1971a): Measurements In-Situ of a Salt Stabilized Ocean Water Heated from Below. Proc. of 8th U. S. Navy Symposium on Military Oceanography, Monterey, Cal., 18 May 1971.

_____ (1971b): Spectra of Internal Waves: In-Situ Measurements in a Multiple-Layered Structure. In press (Journal of Physical Oceanography).

Neumann, G. and W. J. Pierson, Jr. (1966): Principles of Physical Oceanography, pp. 161-164. Prentice-Hall, Inc.

Phillips, O. M. (1971): On Spectra Measured in an Undulating Layered Medium. Journal of Physical Oceanography, 1: 1-6.

Roden, G. I. (1971): Spectra of North Pacific Temperature and Salinity Perturbations in the Depth Domain. Journal of Physical Oceanography, 1: 25-33.

Schlichting, H. (1960): Boundary Layer Theory, 4th ed. p. 21, McGraw-Hill.

Stommel, H. and K. N. Fedorov (1967): Small Scale Structure in Temperature and Salinity Near Timor and Mindanao. Tellus, 19: 306-325.

Tait, R. I. and M. R. Howe (1968): Some Observations of Thermohaline Stratification in the Deep Ocean. Deep Sea Research, 15: 275-280.

Turner, J. S. (1965): The Coupled Turbulent Transports of Salt and Heat Across a Sharp Density Interface. International Journal of Heat Mass Transfer, 8: 759-767.

_____ (1967): Salt Fingers Across a Density Interface. Deep Sea Research, 14: 599-611.

Woods, J. D. (1968): Wave-Induced Shear Instability in the Summer Thermocline. Journal of Fluid Mechanics, 32: 791-800.

_____ and G. G. Fosberry (1966): Observations of the Thermocline and Transient Stratifications Made Visible by Dye. Proc. 1965 Malta Symposium Underwater Assn., London, p. 31.

Woods Hole Oceanographic Institution (1967): Response Characteristics of a Savonius Rotor Current Meter. Tech. Report 67-33 (Unpublished Manuscript).

INITIAL DISTRIBUTION LIST

		No. Copies
1.	Defense Documentation Center Cameron Station Alexandria, Virginia 22314	2
2.	Library, Code 0212 Naval Postgraduate School Monterey, California 93940	2
3.	Associate Professor W.W. Denner, Code 58Dw Department of Oceanography Naval Postgraduate School Monterey, California 93940	5
4.	Assistant Professor J.A. Galt, Code 58Gl Department of Oceanography Naval Postgraduate School Monterey, California 93940	1
5.	Department of Oceanography Naval Postgraduate School Monterey, California 93940	3
6.	Dr. Ned A. Ostenso Office of Naval Research, Code 480D Arlington, Virginia 22217	3
7.	Lieutenant Commander William C. Barney HQ MACV Box 38 APO San Francisco, California 96222	3
8.	The Oceanographer of the Navy The Madison Building 732 North Washington Street Alexandria, Virginia 22314	1
9.	Director Naval Arctic Research Laboratory Barrow, Alaska 99723	1
10.	Captain Austen M. Oake Box 66 Fogo, Newfoundland, Canada	1

Security Classification

DOCUMENT CONTROL DATA - R & D

(Security classification of title, body of abstract and indexing annotation must be entered when the overall report is classified)

1. ORIGINATING ACTIVITY (Corporate author)

Naval Postgraduate School
Monterey, California 93940

2a. REPORT SECURITY CLASSIFICATION

Unclassified

2b. GROUP

3. REPORT TITLE

Properties of the Discretely Stratified Microstructure in the Arctic Ocean

4. DESCRIPTIVE NOTES (Type of report and, inclusive dates)

Master's Thesis; September 1971

5. AUTHOR(S) (First name, middle initial, last name)

William Clifford Barney

6. REPORT DATE	7a. TOTAL NO. OF PAGES	7b. NO. OF REFS
September 1971	90	19

8a. CONTRACT OR GRANT NO.	9a. ORIGINATOR'S REPORT NUMBER(S)
b. PROJECT NO.	
c.	9b. OTHER REPORT NO(S) (Any other numbers that may be assigned this report)
d.	

10. DISTRIBUTION STATEMENT

Approved for public release; distribution unlimited.

11. SUPPLEMENTARY NOTES	12. SPONSORING MILITARY ACTIVITY
	Naval Postgraduate School Monterey, California 93940

13. ABSTRACT

The layered microstructure in the Arctic Ocean is examined from long time-series of high-resolution temperature profiles and concurrent digital salinity data. The motion within the layers is found to be turbulent, while the flow within the interface sheets is laminar. The structure is stable for long periods of time, and is coherent for a considerable horizontal extent. It is suggested that the initial formation of the layers is due to the energy dissipation of higher modes of locally generated internal waves. The layers may be sustained for long periods by weak shear produced by geostrophic density currents. The distribution of salinity and temperature differences between layers indicates that the layers are in a state of dynamic equilibrium, the differing diffusion characteristics of heat and salt accounting for the transfer of these properties across the interface sheets.

DD FORM 1 NOV 68 1473 (PAGE 1)

S/N 0101-807-6811

Security Classification

A-31408

KEY WORDS	LINK A		LINK B		LINK C	
	ROLE	WT	ROLE	WT	ROLE	WT
Arctic Ocean						
Stratified Microstructure						
Internal Waves						

Thesis
B2334
c.1

Barney
Properties of the discretely stratified microstructure in the Arctic Ocean.

4 OCT 72
27 JUL 73
27 SEP 82
22213
21290
28340

Thesis
B2334 Barney
c.1 Properties of the discretely stratified microstructure in the Arctic Ocean.
130805